

Chapter 3: Oxygen Projections for the Future

Matthew C. Long ¹, Takamitsu Ito ², Curtis Deutsch ³

¹Climate and Global Dynamics Laboratory, National Center for Atmospheric Research, Boulder, Colorado, USA.

²Georgia Institute of Technology, Atlanta, Georgia, USA.

³School of Oceanography, University of Washington, Seattle, Washington, USA.

Summary

The loss of oxygen from the ocean, termed “deoxygenation”, is a consequence of climate warming. As the ocean warms, it loses oxygen due to the direct effect of temperature on gas solubility: warmer waters hold less oxygen. Additionally, reductions in vertical mixing associated with enhanced upper-ocean buoyancy stratification cause respiration-driven oxygen depletion at depth. The ocean as a whole is expected to lose about 3–4% of its oxygen inventory by the year 2100 under a “business-as-usual” scenario (RCP8.5) with most of this loss concentrated in the upper 1000 m where species richness and abundance is highest. There will be distinct regional differences in the intensity of oxygen loss as well as variations in ecological and biogeochemical impacts. There is consensus across models that oxygen loss at mid and high-latitudes will be strong and driven by both solubility reductions and increased respiration effects. Projections are more ambiguous in the tropics, where models suggest that there will be compensation between oxygen decline due to reduced solubility and oxygen increase caused by reductions in cumulative respiration. Thus, oxygen concentrations in the core of present-day oxygen minimum zones may increase; however, the total volume of waters classified as “suboxic” and “hypoxic” is still likely to grow substantially. Low oxygen conditions and increased temperature jointly limit the viable habitat for marine macroorganisms; warming accompanied by deoxygenation will drive habitat contraction and fragmentation in regions where oxygen levels decline below metabolic requirements. Expansion of suboxic zones will likely disrupt the cycling of nitrogen in the ocean; denitrification may increase, yielding greater rates of fixed nitrogen loss from the ocean. Perturbations to the nitrogen cycle may include substantial changes to nitrous oxide production, though this is highly uncertain. Warming-driven deoxygenation cannot be easily reversed; indeed, the ocean oxygen inventory is likely to take centuries to recover from warming projected under “business-as-usual” emissions scenarios. Deoxygenation is intrinsically linked to climate warming; reduction of human-driven warming

is the only means of preventing widespread ocean oxygen loss. Stabilization of climate-changing emissions, however, can enable ocean ventilation to recover to some degree, thereby mitigating oxygen loss. Given the long persistence timescales of climate drivers, earlier mitigation action will yield maximum benefit.

1 Introduction

Warming of the climate system is driving declines in ocean oxygen content at a rate that is expected to rapidly accelerate over coming decades. Global warming leads to ocean oxygen loss because O₂ is less soluble in warmer waters and warming increases upper ocean stratification, curtailing the supply of oxygen to the ocean interior [Keeling *et al.*, 2010]. Model projections of deoxygenation under the recent Couple Model Intercomparison Project Phase 5 (CMIP5) [Taylor *et al.*, 2012], suggest that by the year 2100, the ocean will have lost 3–4% of its O₂ inventory, with much of this loss concentrated in the upper ocean (above 1000 m) [Bopp *et al.*, 2013; Cocco *et al.*, 2013]. This is a significant perturbation that is very likely to have widespread consequences for marine life and biogeochemical cycles.

1.1 Animals

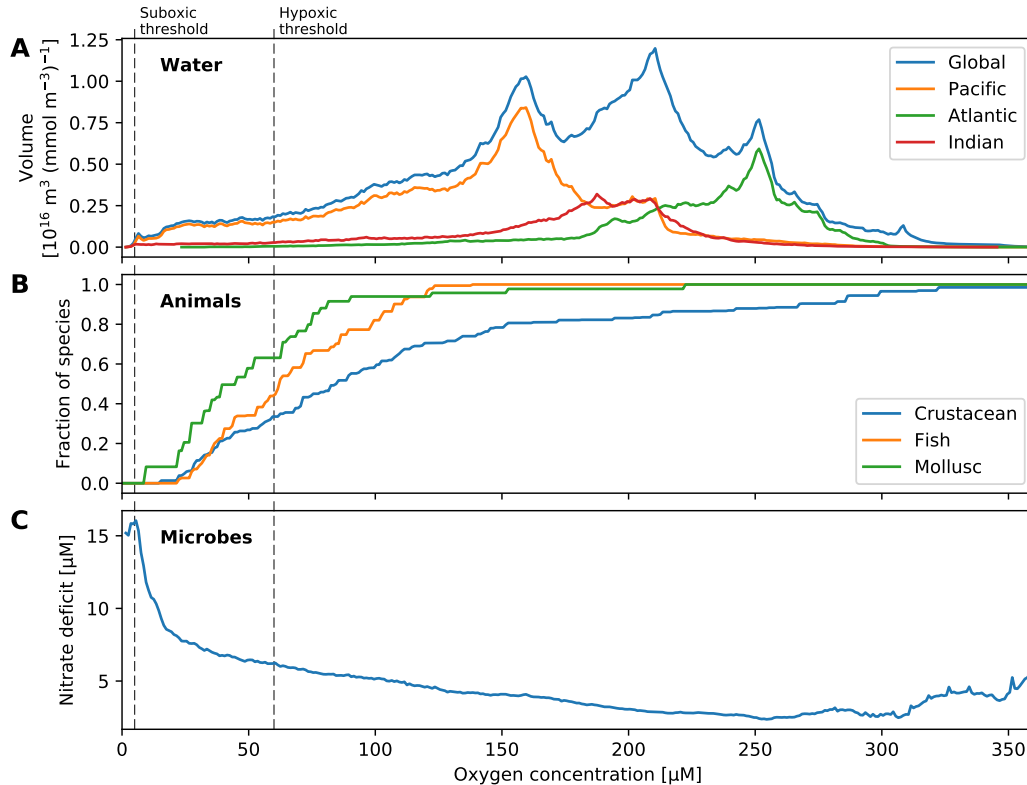
Dissolved oxygen (O₂) is a fundamental control on marine habitat. Animals require oxygen and, except for marine mammals, animals in the sea depend on the oxygen dissolved in seawater for their supply. Typically, animals are not sensitive to oxygen distributions as long as concentrations remain sufficiently high; as O₂ levels drop, however, organisms are unable to sustain aerobic metabolism and will eventually die. Concentrations of oxygen below about 60 mmol m⁻³ (1 mmol m⁻³ = 1 µM) are termed “hypoxic”; regions with oxygen persistently below this threshold are referred to as “dead zones”: normal respiration is severely limited in these regions and animals cannot function. Dead zones are found in many coastal systems, caused by nutrient pollution that drives eutrophication and oxygen depletion, though global ocean deoxygenation is also expected to exacerbate these effects [Diaz and Rosenberg, 2008; Rabalais *et al.*, 2002]. Hypoxic tolerances vary considerably across taxonomic groups and lethal thresholds have been found well above the conventional definition of hypoxia (Figure 1b) [Vaquer-Sunyer and Duarte, 2008]. Furthermore, hypoxic tolerances can change as a function of temperature and body size, requiring

62 consideration of multiple life stages and environmental factors when projecting the ecological
63 impacts of deoxygenation [Deutsch *et al.*, 2015; Pörtner and Farrell, 2008].

70 While dead zones may expand under climate warming, the impacts of ocean de-
71 oxygenation on marine macroorganisms may be more profound and widespread than sug-
72 gested by projected changes in hypoxic volumes. Indeed, the large-scale biogeographic
73 distributions of ectothermic organisms in the contemporary ocean are limited in part by
74 the combined effects of temperature and oxygen [Deutsch *et al.*, 2015]. Metabolic rates in-
75 crease in proportion to temperature; thus, an aerobic organism’s demand for oxygen also
76 increases in warmer waters. Viable habitat is bounded by the need for a sufficient supply
77 of oxygen to meet temperature-dependent metabolic demand. Concomitant warming and
78 ocean deoxygenation, therefore, can be expected to result in a contraction of metabolically
79 viable habitat [Deutsch *et al.*, 2015]. Organisms are likely to be forced poleward, where
80 cooler waters temper oxygen demand; additionally, since oxygen concentrations typically
81 decline with depth, we can expect a vertical habitat compression as the region of the near-
82 surface ocean with sufficient oxygen shrinks [Koslow *et al.*, 2011].

83 1.2 Microbes

84 Just as higher animals are physiologically constrained when oxygen concentrations
85 become low, oxygen also exerts a strong control on microbial metabolism. When oxygen
86 in the ocean falls below “suboxic” concentrations ($O_2 < 5 \text{ mmol m}^{-3}$), aerobic metabolism
87 becomes inefficient and microbes that use alternate electron acceptors to oxidize organic
88 matter begin to dominate. It may initially seem strange to worry about impinging on mi-
89 crobes; much of our familiarity with microbes stems from disease. Microbes, however,
90 play a fundamental role in sustaining all life on Earth by enabling nutrient cycling. The
91 importance of nutrient cycles can be appreciated by considering that the energy that pow-
92 ers virtually all life on Earth is harvested from the Sun during photosynthesis. Life is
93 carbon based—but nutrient elements such as nitrogen and phosphorus, are also funda-
94 mental building blocks required to make organic materials. Plants and algae use sunlight
95 to make organic matter from carbon dioxide and nutrients; they split water, use the hy-
96 drogen energy to make biomass and release O_2 as waste. The organic matter created by
97 photosynthesis enters the food chain; primary producers are eaten by secondary produc-
98 ers and so on, supporting complex ecosystems. In this manner, primary production in the
99 ocean is the ultimate constraint on the biomass of the whole marine ecosystem. Secondary



64 **Figure 1.** Distributions as a function of oxygen concentration: (A) the volume of water in the global ocean,
65 and in each major basin; (B) the fraction of species in three groups of organisms that survive at a given oxy-
66 gen concentration; and (C) the nitrate deficit relative to phosphorus, defined as $-N^* = N - r_{N:P}P$ [Gruber
67 and Sarmiento, 1997], where $r_{N:P}$ is the stoichiometric ratio of remineralization of organic matter (we as-
68 sume $r_{N:P} = 16$) [Anderson and Sarmiento, 1994]. Mortality thresholds are from a compilation of empirical
69 studies [Vaquer-Sunyer and Duarte, 2008].

producers have fundamentally different metabolisms than the photosynthesizers they eat; rather than producing oxygen as waste, they require oxygen to oxidize organic matter during respiration; the resulting energy is harnessed, supporting synthesis of organic matter and functional activities such as acquisition of food, growth, predator avoidance, and reproduction. The inorganic nutrients incorporated during photosynthesis are carried up the food chain; ultimately, however, as organisms die, the organic material of which they are comprised is decomposed: microbes oxidize this material, converting its constituents back to their inorganic forms, returning nutrients to the pools upon which photosynthesis relies. Since the ocean is a single volume of fluid, interconnected by circulation, the marine cycles of nutrients like nitrogen and phosphorus are coupled on a global scale—entering the food chain during photosynthesis, returning to dissolved inorganic forms when organic matter is “remineralized” via microbially-mediated oxidation.

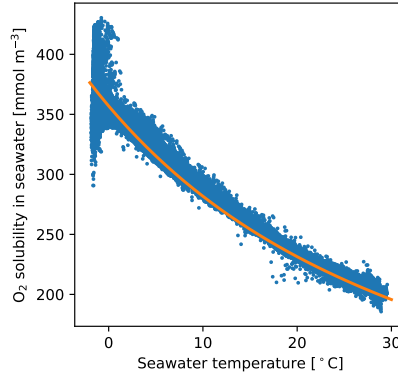
Oxygen plays a fundamental role in these global nutrient cycles. To illustrate this, we need to consider the fact that the cycles of nitrogen and phosphorus are regulated by fundamentally difference processes—yet organic matter is composed of nitrogen and phosphorus in specific relative amounts: more nitrogen is useless with insufficient phosphorus and vice versa. Phosphorus is supplied to the ocean from the land via weathering and runoff; it is removed from the ocean when organic material sinks and is buried in sediments. Nitrogen, by contrast, is sourced primarily from the atmosphere, which consists of about 78% dinitrogen gas (N_2). Most photosynthetic organisms cannot use N_2 directly, however; rather, only certain types of cyanobacteria (diazotrophs) can “fix nitrogen,” converting N_2 gas into forms available to other organisms. Thus, microbes determine the rate at which fixed nitrogen enters the ocean—and, as it turns out, microbes also determine the rates of removal. As oxygen concentrations decline to suboxic levels, aerobic processes become increasingly inefficient; ultimately, when oxygen is too scarce, microbes use other compounds as the electron acceptor needed to oxidize organic matter and make a living. In the ocean, nitrate (NO_3^-) is a widespread form of fixed nitrogen; nitrate is used to oxidize organic matter in suboxic regions, converting the nitrogen to N_2 , which is lost to the atmosphere. This process is termed “denitrification” and it accounts for the majority of fixed nitrogen loss from the ocean [Gruber, 2004; Gruber and Galloway, 2008]. The signature of denitrification is evident as a “deficit” of nitrate relative to phosphate in suboxic regions of the global ocean (Figure 1c). As suboxic zones grow, the loss of fixed nitrogen to denitrification can increase, ultimately feeding back to limit primary productivity. As ocean

133 ecosystems are built on photosynthesis, climate-driven perturbations to oxygen that im-
134 pact nutrient cycles can ultimately feedback to higher trophic levels. Microbially-mediated
135 processes involved in the nitrogen cycle can also have direct impacts on climate. Den-
136itrification and nitrification (the oxidation of ammonium to nitrate) can produce nitrous
137 oxide (N_2O), which is an important greenhouse gas [Bange *et al.*, 2010]. Expansion of hy-
138 poxic and suboxic volumes in the ocean may change the production and release of N_2O
139 [Martinez-Rey *et al.*, 2015; Nevison *et al.*, 2003], though this projection involves substantial
140 uncertainty.

141 1.3 Paleo-perspective

142 The history of oxygen on Earth provides an important perspective on the future of
143 oxygen in the ocean. Indeed, for roughly the first half of Earth’s 4.5 billion-year history,
144 oxygen was not plentiful in the atmosphere; rather, significant concentrations of oxygen
145 arose between 2.4 and 2.1 billion years ago [Lyons *et al.*, 2014]. Photosynthesis is the
146 primary source of oxygen in the atmosphere, illustrating how the evolution of life is in-
147 tertwined with the character of Earth’s environment: the accumulation of oxygen in the
148 atmosphere enabled animal life, whereas prior to the evolution of photosynthesis, aerobic
149 metabolisms were not viable.

150 Earth’s history has been punctuated by five major extinctions, catastrophic events
151 when more than 65% of extant species rapidly disappeared. The present era has been
152 characterized as Earth’s sixth mass extinction event, caused by humans and leading to ir-
153 reversible changes in ecosystems [Barnosky *et al.*, 2011]. Some of the mechanisms driv-
154 ing present extinction rates are unique to the global expansion of humans—for instance,
155 habitat fragmentation, the spread of invasive species and disease. However, the libera-
156 tion of massive amounts of geologically-sequestered carbon has happened before; thus,
157 climate warming and the loss of ocean oxygen have well-documented analogs in the geo-
158 logic record. The end-Permian extinction, for instance, which occurred ~252 million years
159 ago, is the largest extinction event in Earth’s history; nearly 95% of terrestrial and ma-
160 rine species perished [Erwin, 1993; Raup, 1979]. Notably, the end-Permian extinction was
161 coincident with massive volcanism, which led to elevated CO_2 and climate change; extinc-
162 tions in the ocean during this event can be explained by changes in oxygen levels, CO_2 ,
163 and temperature [Song *et al.*, 2014], making this catastrophic event a compelling analog
164 for the ocean of the 21st century [Payne and Clapham, 2012].



165 **Figure 2.** Relationship between dissolved oxygen and temperature for surface data in the World Ocean
 166 Atlas 2013 [Garcia *et al.*, 2014]. The orange line shows the saturation concentration of oxygen at equilibrium
 167 with the atmosphere [Garcia and Gordon, 1992]. Strong deviations from saturation are evident at near-
 168 freezing temperatures, which is partially a function of sea-ice inhibition of gas exchange [Ito *et al.*, 2004].

1.4 Climate-driven deoxygenation

170 Our understanding of the basic mechanisms driving ocean deoxygenation is robust
 171 [Bopp *et al.*, 2002; Gruber, 2011; Keeling *et al.*, 2010; Matear and Hirst, 2003; Najjar
 172 and Keeling, 2000; Plattner *et al.*, 2002]. Increasing concentrations of greenhouse gases,
 173 primarily carbon dioxide, trap heat in the atmosphere, leading to a planetary energy imbal-
 174 ance [Trenberth *et al.*, 2014]. The ocean is the dominant thermal reservoir in the climate
 175 system and it is estimated that the ocean has absorbed more than 90% of the excess heat
 176 accumulating in the Earth system since the beginning of the industrial revolution [Cheng
 177 *et al.*, 2016; Loeb *et al.*, 2012; Rhein *et al.*, 2013]. As the planet has warmed, this extra
 178 heat has accumulated in the near-surface ocean [Abraham *et al.*, 2013; Balmaseda *et al.*,
 179 2013; Levitus *et al.*, 2012]. Warmer waters hold less oxygen due to the temperature de-
 180 pendence of solubility; thus, as the surface ocean warms, oxygen concentrations can be
 181 expected to decline according to the solubility relationship with temperature (Figure 2).
 182 Reductions in solubility are compounded by an additional mechanism driving deoxygenation,
 183 which involves changes to ocean circulation in response to warming. The density
 184 of seawater is strongly temperature dependent; warmer waters are less dense or, equiva-
 185 lently, more buoyant. As extra heat is absorbed by the ocean, it tends to warm the surface
 186 ocean at a greater rate than warming at depth, increasing the density difference between
 187 surface and deep water. This enhanced density stratification inhibits exchange between

the oxygen-rich surface ocean and waters in the interior where oxygen is consumed by respiration. Diminished surface-to-depth exchange reduces the quantity of oxygen supplied to the ocean interior, shifting the balance maintaining oxygen concentrations: consumption exceeds supply, oxygen concentrations decline. This reinforcing mechanism, wherein temperature-related solubility effects are amplified by the effect of density stratification, makes oxygen exceptionally sensitive to variations in climate. However, the enhanced stratification and slower circulation of the upper ocean has a countervailing effect: it simultaneously reduces the supply of nutrients from deep waters to the photic zone, reducing productivity at the surface and ultimately the respiration of organic matter below. The reduced oxygen demand offsets part of the reduced supply. This compensating mechanism, in concert with the reinforcing mechanism noted above, creates the potential for complex regional and time-scale dependent behavior in the O₂ changes. Indeed, as we shall see below, dissolved oxygen is highly dynamic in the present-day climate, exhibiting dramatic variations on annual to multi-decadal timescales [Deutsch *et al.*, 2011; Ito and Deutsch, 2010]. These natural fluctuations in oxygen drive important shifts in marine ecology and biogeochemistry [e.g., Deutsch *et al.*, 2014; Rabalais *et al.*, 2010; Yang *et al.*, 2016; Zamora *et al.*, 2012]—and yet over the next century, the amplitude of oxygen changes is likely to be much greater, far exceeding the range of natural variability [Henson *et al.*, 2017; Long *et al.*, 2016; Rodgers *et al.*, 2015].

1.5 Earth system models

While the basic mechanisms controlling deoxygenation are well-understood in principle, details of ocean circulation and biological productivity lead to regional differences in the rate and magnitude of oxygen loss. In this chapter, we discuss projections of ocean oxygen under future emissions scenarios. Our most sophisticated tools in this enterprise are Earth system models (ESMs); these consist of coupled atmosphere and ocean general circulation models (GCMs) and include representations of processes relevant to ocean biogeochemistry. Our objectives are to review the state of knowledge regarding the rate, magnitude and geographic distribution of expected deoxygenation trends, relying primarily on ESM projections.

To illustrate both the robust and uncertain projections for future ocean oxygen, we will present results from two primary collections of model solutions. First, we make use of a large ensemble of a single, fully-coupled ESM: the Community Earth System Model

(CESM). The CESM Large Ensemble (CESM-LE) has more than 30 independent realizations of the historical period from 1920–2005 and future projections out to 2100 under the CMIP5 “business-as-usual” RCP8.5 forcing scenario [Kay *et al.*, 2015]. Second, we show results from a subset of the CMIP5 multi-model ensemble, enabling perspective on the degree to which CESM is representative of this broader collection of independently developed models. The models are from the Geophysical Fluid Dynamics Laboratory (GFDL) [Dunne *et al.*, 2012, 2013]; the UK Met Office Hadley Centre (HadGEM) [Collins *et al.*, 2011; HadGEM2 Development Team, 2011]; the Max Planck Institute (MPI) [Giorgetta *et al.*, 2013]; and the Institut Pierre Simon Laplace (IPSL) [Dufresne *et al.*, 2013]. We also include CESM’s CMIP5 solutions [Hurrell *et al.*, 2013]; this model is similar to the CESM-LE in many respects, but has a different atmospheric model so does display distinct behavior.

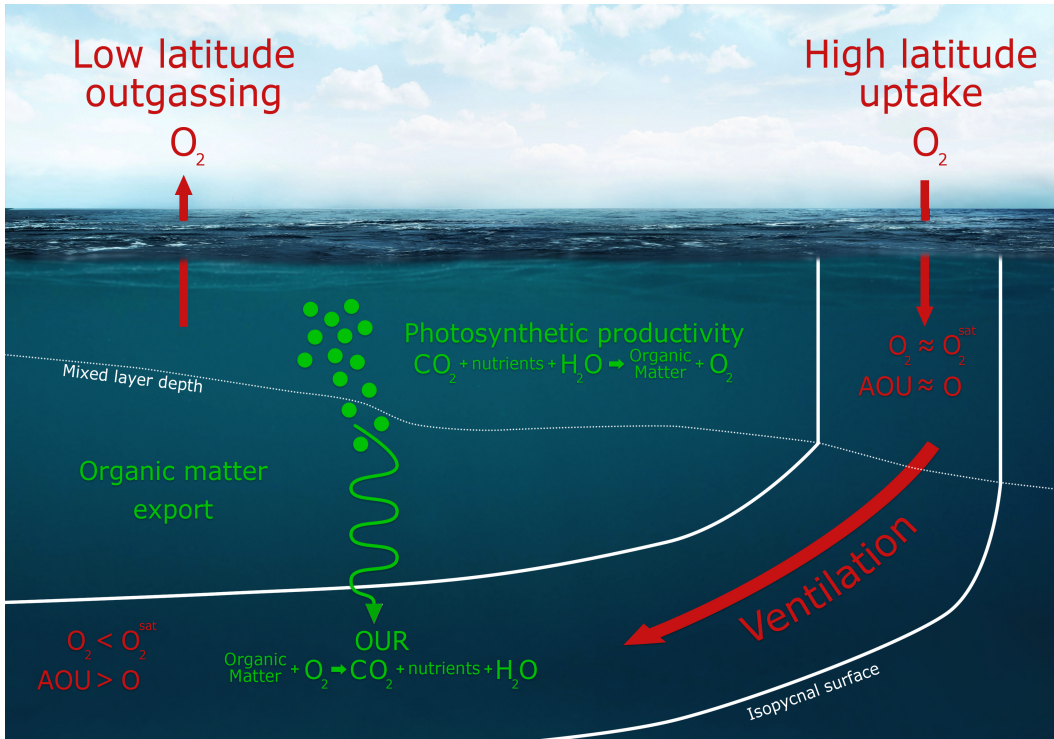
The “spread” across the CESM-LE and the CMIP5 ensembles reflects different sources of uncertainty [Hawkins and Sutton, 2009]. Internal variability is an intrinsic feature of the climate system, arising from nonlinear dynamical processes and interactions between the ocean, atmosphere and land surface that each integrate forcing over different timescales [Hasselmann, 1976]. Earth system models generate internal climate variability representative of that in nature, thus the ensemble spread of the CESM-LE can be used to assess the contribution of natural variability to uncertainty in future projections, which is particularly important on regional scales [Deser *et al.*, 2012; Lovenduski *et al.*, 2016; McKinley *et al.*, 2016]. While internal climate variability contributes to the spread in the CMIP5 ensemble, each of the models in this collection has distinct behavior reflecting differences in underlying formulations. Thus, spread across the CMIP5 models reflects a minimum bound on the contribution of “structural uncertainty” to future projections [Hawkins and Sutton, 2009; Lovenduski *et al.*, 2016]. Finally, human activity introduces substantial uncertainty into future projections. Indeed, the magnitude of surface warming during the next century is strongly dependent on the amount of greenhouse gases emitted over the next several decades [Collins *et al.*, 2013]. To account for this source of uncertainty, CMIP5 included four “Representative Concentration Pathway” scenarios intended to span a range of total radiative forcing at 2100 from 2.6 W m^{-2} (RCP2.6) to 8.5 W m^{-2} (RCP8.5) [Meinshausen *et al.*, 2011]. The differences in these scenarios illustrate the contribution of “scenario uncertainty” to future projections. Our primary focus will be on the RCP8.5 scenario, but we include limited results from RCP4.5 and discuss the benefits of

253 climate change mitigation activities to the ocean deoxygenation problem [Henson *et al.*,
254 2017].

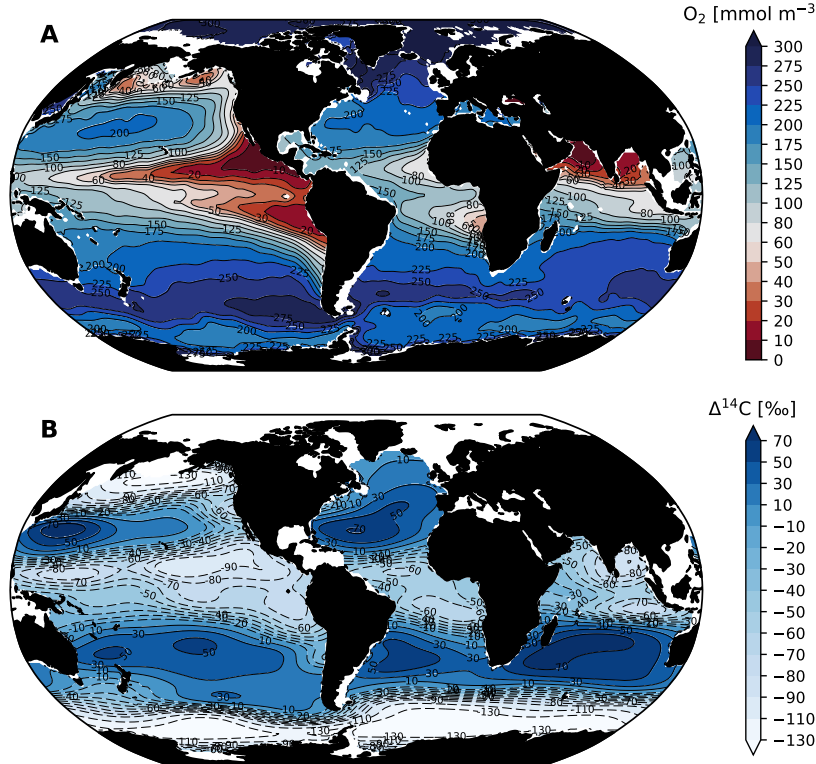
255 **2 Understanding dissolved oxygen**

263 Several concepts are required to understand the mechanisms driving ocean deoxy-
264 genation. To review these, we first examine the large-scale structure of present-day oxy-
265 gen distributions. An understanding of the basic physical and biological controls on these
266 distributions provides perspective on the mechanisms by which climate warming drives
267 oxygen loss. Our primary resource for understanding the global scale ocean oxygen dis-
268 tributions come from the World Ocean Atlas (WOA), produced by the National Oceano-
269 graphic Data Center (United States). WOA is a compilation of observations that have been
270 objectively-analyzed to produce gridded fields at a spatial resolution of $1^\circ \times 1^\circ$. While we
271 only consider annual-mean distributions here, WOA includes monthly data, enabling evalua-
272 tion of the seasonal cycle. The observations upon which WOA is based, however, do not
273 have sufficient coverage to enable a globally gridded-product with temporal resolution be-
274 yond the monthly mean annual cycle. Thus, efforts to evaluate global-scale trends in O_2
275 based on observations (section 2.1) have relied on independently-developed compilations
276 of observations [e.g., Helm *et al.*, 2011; Ito *et al.*, 2017; Schmidtko *et al.*, 2017].

277 As discussed in section 1, oxygen is supplied to the ocean via exchange with the
278 atmosphere and photosynthetic oxygen production at the surface. The ocean surface, there-
279 fore, tends to be well-oxygenated—which is to say the concentration of oxygen remains
280 near the saturation concentration (O_2^{sat}) with respect to the atmosphere. Photosynthesis in
281 the surface ocean produces organic matter; detrital remnants of this material sink to depth
282 where they are broken down by microbial respiration, consuming oxygen (Figure 3). Thus,
283 oxygen concentrations are elevated where freshly subducted surface waters flow into the
284 interior, but concentrations decline downstream of these regions as a respiration signal
285 accumulates. Large-scale patterns are set by the global overturning circulation, wherein
286 oxygen is supplied to the ocean in ventilation regions, and is subsequently depleted as wa-
287 ters circulate in the interior. In the upper ocean thermocline, where respiration rates are
288 relatively fast, oxygen concentrations span a range from full saturation at the surface to
289 near zero at the tropical terminus (Figure 4). In the abyssal ocean, where respiration rates
290 are very slow, the high O_2 values obtained in polar surface waters decline to intermediate
291 values at the end of the great ocean conveyor in the Pacific [Broecker, 1991].

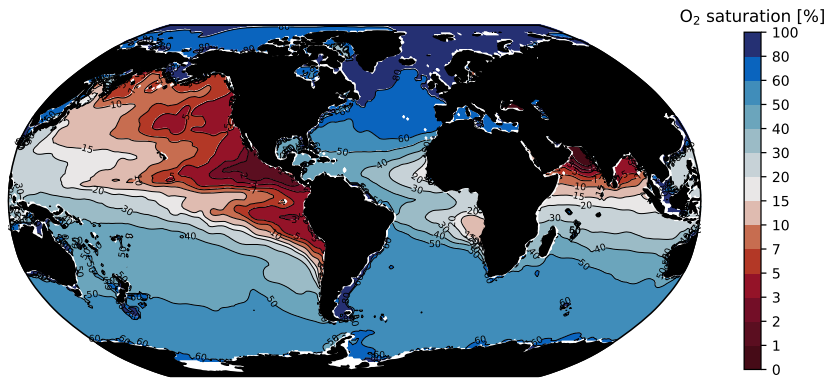


256 **Figure 3.** Schematic illustration of the mechanisms controlling oxygen distributions in the ocean. Oxygen
 257 is produced in the surface ocean by biological productivity, which generates organic matter. Air-sea exchange
 258 keeps oxygen in the surface ocean near saturation concentrations with the atmosphere (O_2^{sat}). Oxygen is
 259 consumed in the interior as organic matter is respired; the rate of oxygen consumption is termed the “oxy-
 260 gen utilization rate” (OUR). “Apparent oxygen utilization” ($AOU = O_2^{\text{sat}} - O_2$) provides an estimate of the
 261 amount of oxygen that has been consumed by respiration as a water parcel circulates in the ocean interior.
 262 Illustration by Matthew Long and Ryan Johnson (NCAR).



292 **Figure 4.** Oxygen distributions and a metric of water mass age averaged over 200–600 m depth based on
 293 observations. (A) The average dissolved oxygen concentration from the World Ocean Atlas, 2013, version
 294 2 [Garcia *et al.*, 2014]; regions plotted in red are below 60 mmol m^{-3} , which is a common definition for an
 295 hypoxic threshold. (B) Total radiocarbon concentrations ($\Delta^{14}\text{C}$) from the Global Data Analysis Project (GLO-
 296 DAP) data synthesis [Key *et al.*, 2004]. Low $\Delta^{14}\text{C}$ is indicative of older waters; since these waters have been
 297 isolated from the atmosphere for longer, they are depleted in natural ^{14}C and contain limited anthropogenic
 298 ^{14}C . Most of the spatial structure in the total radiocarbon field at these depths is from the anthropogenic or
 299 “bomb” component [Key *et al.*, 2004].

300 The “age” of waters in the ocean interior is a useful metric to consider in the con-
 301 text of ocean ventilation; age can be defined as the time since waters last contacted the
 302 surface. As waters grow older in the ocean interior, oxygen is continually depleted by res-
 303piration; the accumulated impact of this consumption is termed Apparent Oxygen Utiliza-
 304 tion and is estimated based on the difference from saturation ($AOU = O_2^{sat} - O_2$), assum-
 305 ing that the oxygen concentration was close to O_2^{sat} at the time of subduction [Ito *et al.*,
 306 2004]. Thus, AOU is an estimate of the amount of respiration integrated along the path
 307 waters take as they circulate in the ocean interior. Older waters can be expected to have



323 **Figure 5.** Oxygen saturation at the point in the vertical column where oxygen saturation is minimum; com-
324 puted from the World Ocean Atlas, 2013, version 2 [Garcia *et al.*, 2014]. Saturation values less than 15% are
325 colored in red.

308 greater *AOU*, and hence lower oxygen, because they have spent a longer time accumulat-
309 ing a respiration signal. This explains the contrast between dissolved oxygen concentra-
310 tions in the thermocline of the North Pacific versus North Atlantic, for instance (Figure 4).
311 Freshly formed deep water fills the North Atlantic basin; this water is rich in oxygen from
312 recent surface exchange and, as there is only modest accumulation of a respiration signal,
313 it remains relatively close to saturation concentrations (low *AOU*). The North Pacific, by
314 contrast, is the last stop on the great ocean conveyor and as a result, deep water in this
315 basin is substantially depleted in oxygen (Figure 5). Mode water ventilation in the western
316 North Pacific supplies oxygen to the subtropical thermocline, but the thermocline on the
317 eastern side of the basin is characterized by strong oxygen depletion (Figure 4). An exam-
318 ination of the global distributions of radiocarbon ($\Delta^{14}\text{C}$) in the thermocline depth range
319 confirms that water mass age is a dominate control on oxygen: old waters are highly de-
320 pleted in ^{14}C since they have been isolated from the atmosphere for longer; these waters
321 have had longer to accumulate *AOU*, and thus tend to be more depleted in oxygen (Fig-
322 ure 4).

326 The age of water dictates the time available to accumulate a respiration signal in the
327 form of oxygen depletion; however, the rate at which oxygen is depleted by respiration—
328 or, equivalently, the rate at which *AOU* increases—can also vary. In particular, *AOU* in-
329 creases at a rate that is largely proportional to the quantity of organic matter being respired.
330 Regions with greater inputs of organic matter will have higher oxygen utilization rates

(331) (OUR), which drive faster increases in *AOU*. Depth is a dominant control on *OUR* be-
332 cause the downward flux of organic matter decreases approximately exponentially with
333 depth. Most sinking organic matter is resired in the upper 1,000 m of the ocean, lead-
334 ing to higher *OUR* there; oxygen demand in deep waters is relatively low. This reminer-
335 alization profile is an important driver of “oxygen minimum zones” (OMZs), which are
336 regions of very low oxygen found on the eastern side of the ocean basins in the tropics
337 (highlighted in red on Figure 4a). Oxygen concentrations approach zero in the core of the
338 OMZs because the rate of fresh oxygen supply via mixing and advection cannot match
339 the rate of organic matter consumption. As discussed above, oxygen minimum zones play
340 an important role in global biogeochemical cycles of nutrients; in particular, nitrogen. As
341 oxygen declines, a larger fraction of the oxidation of nitrogen in organic matter is shunted
342 to N_2O , increasing the concentrations of this greenhouse gas in hypoxic waters. As O_2
343 is depleted to near zero concentrations, nitrate becomes the dominant electron acceptor
344 used to oxidize organic matter, resulting in a loss of fixed nitrogen from the ocean; micro-
345 bial communities also switch from N_2O production to consumption when O_2 is very low
346 [Codispoti, 2010].

347 As we have already said, climate warming drives deoxygenation via two pathways.
348 The first is straightforward and involves reductions in thermal solubility of gases. The sec-
349 ond is less straightforward; it includes the role of diminished ventilation (Figure 3) that
350 results from density stratification. As ventilation declines, the age of waters in the ocean
351 interior increase, leading to an increase in *AOU*. Notably, the same processes involved
352 with ventilation play a role in sustaining surface ocean primary productivity. Primary pro-
353 ductivity operates in the sunlit-surface layer of the ocean (the euphotic zone); nutrients are
354 consumed in the process of carbon fixation, and ultimately exported to depth where they
355 are remineralized; this collection of processes is referred to as the “biological pump”: it
356 “pumps” carbon into the deep ocean in spite of the homogenizing influence of circulation
357 [Volk and Hoffert, 1985]. The biological pump is dependent on vertical mixing and advec-
358 tion to return nutrients from depth back into the surface layer; warming-driven stratifica-
359 tion will curtail this nutrient supply, just as it does for the delivery of fresh oxygen to the
360 interior ocean. Stratification, therefore, is expected to lead to a reduction in surface ocean
361 primary production [Bopp *et al.*, 2013; Steinacher *et al.*, 2010], which will very likely have
362 significant consequences for marine ecosystems and the fisheries they support [Stock *et al.*,
363 2017]. A reduction in the biological pump alleviates some demand for oxygen in the in-

terior via reducing *OUR*; this effect, however, is not expected to fully compensate for the reduced ventilation because in regions with unused surface nutrients, a slower circulation need not slow the rate of organic matter production. Since stratification increases the residence time of surface waters, primary productivity is able to effect a more complete utilization of nutrients in the surface layer. It is useful to consider the partitioning of nutrients, such as phosphate, into preformed and regenerated pool. The “preformed” phosphate, for instance, refers to the phosphate concentration at the time of water mass formation—when the water first subducts in the ocean interior. In contrast, “regenerated” phosphate is closely related to *AOU* as it accounts for the cumulative (or path-integrated) amount of phosphate released by the microbial decomposition of organic matter since the water mass entered the interior. As nutrient utilization in the surface ocean becomes more complete, “preformed” concentrations of nutrients in waters sinking into the ocean interior decline. Practically, the oceanic inventory of phosphate can be treated as constant on timescale of tens of thousands of years, so the global sum of preformed and regenerated phosphate must be conserved; therefore, the decline in preformed phosphate must be compensated by an increase in remineralized (or regenerated) phosphate. On this basis, stratification can be expected to yield an increase in *AOU* and an associated decrease in oxygen.

2.1 Observed trends

A few studies have examined oxygen distributions on a global scale and found declines that appear consistent with expectations based on model simulations. *Helm et al.* [2011] found a globally-averaged decrease in upper-ocean (100–1000 m) oxygen an inventory trend of -55 ± 13 Tmol yr^{-1} (1 Tmol = 10^{12} mol). This is consistent with *Manning and Keeling* [2006], who found a net oxygen outgassing from the ocean over the period 1993–2003 of -45 Tmol yr^{-1} . *Schmidtko et al.* [2017] reported somewhat larger numbers analyzing data from full depth over the period 1960–2015, finding trends in the oxygen inventory of -96.1 ± 42.9 Tmol yr^{-1} . *Ito et al.* [2017], using a different compilation of similar datasets, found a trend of -24.3 ± 12.4 Tmol yr^{-1} over the upper 1000 m. Data coverage is a major limitation in assessing global trends; however, the observed changes are not inconsistent with the changes expected from anthropogenic warming. Notably, observationally-based studies have found that direct solubility effect can account for about 15% of oxygen declines [*Helm et al.*, 2011; *Schmidtko et al.*, 2017], which is significantly less than modeling studies have found [e.g., *Bopp et al.*, 2002].

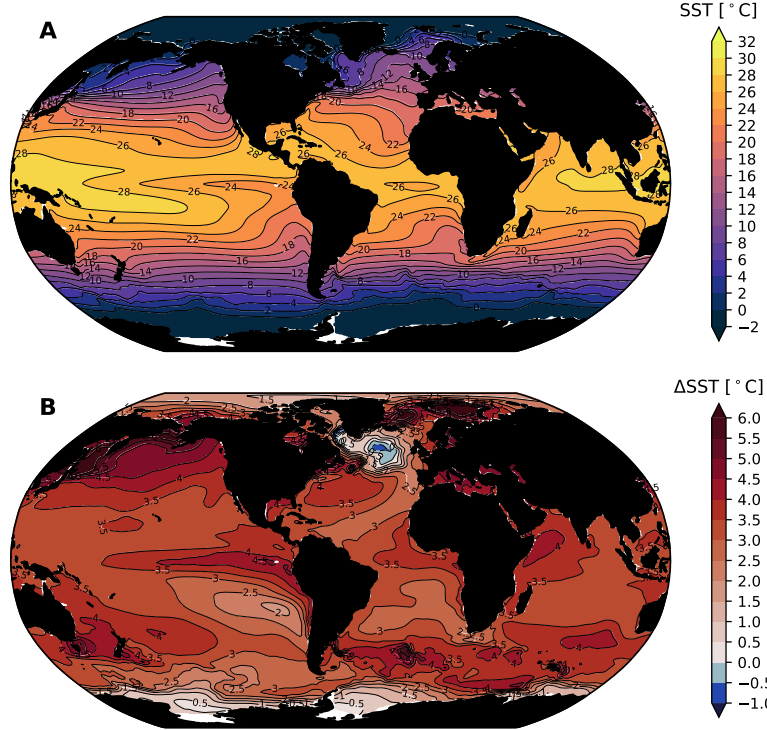
While global data coverage is difficult to achieve, one might imagine that sufficiently long time series exist in particular oceanic regions, thereby enabling detection and attribution of forced trends. Indeed, many studies have evaluated low-frequency variability and long-term trends in local to regional scale O₂ observations, including at ocean time series sites [e.g., *Andreev and Baturina*, 2006; *McClatchie et al.*, 2010; *Ono et al.*, 2001; *Whitney et al.*, 2007], repeat hydrographic sections [e.g., *Emerson et al.*, 2004; *Johnson and Gruber*, 2007; *Mecking et al.*, 2008; *Sasano et al.*, 2015; *van Aken et al.*, 2011] or compilation and optimal interpolation of historic observations [e.g., *Helm et al.*, 2011; *Stendardo and Gruber*, 2012; *Stramma et al.*, 2008]. While statistically significant trends in interior oxygen distributions have been observed in specific oceanic regions, and in some cases over long time periods (50 years) [*Stendardo and Gruber*, 2012], definitive attribution of these trends to externally-forced climate change is challenged by the presence of significant background ‘noise’ associated with internally-driven, low-frequency climate variability [*Garcia et al.*, 2005; *Ito and Deutsch*, 2010].

3 Future projections

Just as the distribution of oxygen in the modern ocean can be understood on the basis of the combined influences of temperature, ventilation rates, and patterns of oxygen consumption, the future of dissolved oxygen can be predicted on the basis of expected perturbations in these factors. The proximal driver of these perturbations is the warming of the ocean, thus we first examine expected changes in ocean heat content and its impact on stratification.

3.1 Ocean heat uptake

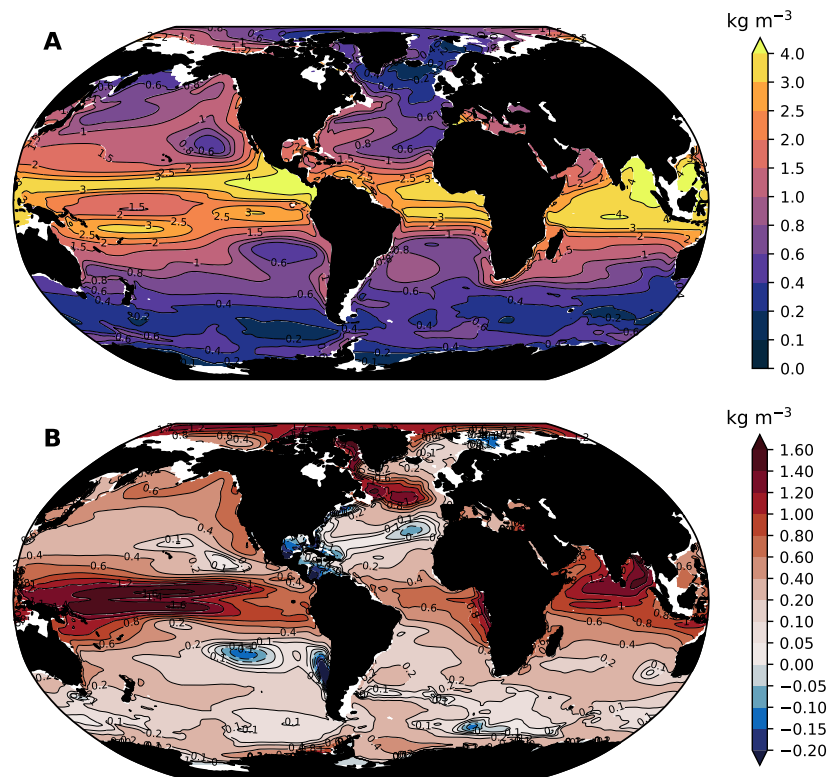
In each of the CMIP5 scenarios (RCP2.6, RCP4.5, RCP6.0 and RCP8.5), increasing atmospheric carbon dioxide (CO₂) concentrations is the dominant driver of changes in radiative forcing, accounting for about 80–90% of the total anthropogenic influence on climate [*Collins et al.*, 2013]. All scenarios result in substantial warming of the ocean, which moderates the effect of climate change on land, but results in impacts on sea level rise and ocean circulation [*Gattuso et al.*, 2015]. The CMIP5 collection of models suggests that at 2100, the top 100 m of the ocean will have warmed by about 0.6°C under RCP2.6 and up to 2.0°C under RCP8.5 relative to preindustrial [*Collins et al.*, 2013]. Figure 6 illustrates the distribution of sea surface temperature (SST) change in the CESM-LE under RCP8.5;



417 **Figure 6.** (A) Ensemble-mean sea surface temperature (SST) in the mean climate and
 418 (B) the change in SST at the year 2100 as simulated by the CESM-LE [Kay *et al.*, 2015].

431 there is a near-ubiquitous increase in tropical and subtropical SSTs by 3–4°C and very
 432 strong warming in the Subarctic North Pacific. A “warming hole” appears in the North
 433 Atlantic, a feature associated with reduced meridional overturning circulation that limits
 434 northward heat transport [Drijfhout *et al.*, 2012].

435 The distribution of warming in future projections is consistent with an amplification
 436 of observed patterns of temperature change [Levitus *et al.*, 2012] and manifests in
 437 part from ocean circulation. Low latitude oceans are relatively well-stratified (Figure 7a),
 438 which inhibits mixing and advection of heat away from the surface and into the ocean
 439 interior; heat trapped in surface waters drives large temperature increases. High-latitude
 440 regions tend to be weakly stratified, by contrast, leading to smaller changes in tempera-
 441 ture as heat is mixed over a larger volume of ocean. The Southern Ocean is exceptional
 442 in this regard; recent decades have been marked by little surface warming in this region,
 443 explained by upwelling and subsequent northward advection of deep water [Armour *et al.*,
 444 2016].



420

Figure 7. Upper ocean stratification: (A) Density difference between the upper-ocean (0–50 m) and upper-

421

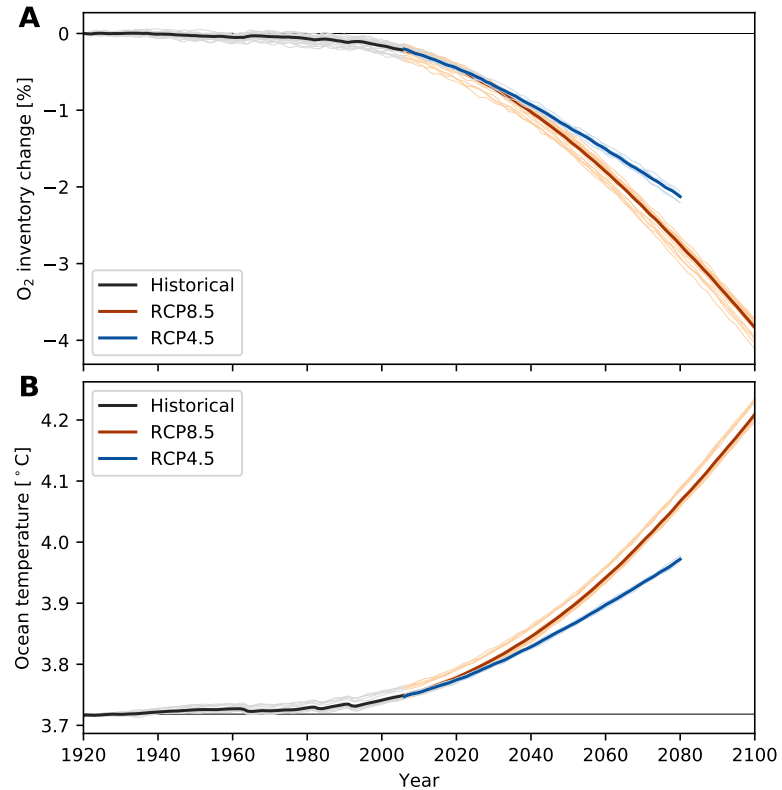
thermocline (100–200 m) in the mean climate from the CESM-LE; (B) changes in stratification at 2100.

A key feature of the ocean warming expected under future scenarios is that it is strongly surface intensified. Half of the excess heat absorbed by the ocean at 2100 under RCP4.5, for instance, is expected to be confined to the upper 700 m of the water column [Collins *et al.*, 2013]. This is expected on the basis of theoretical understanding of ocean response timescales to transient forcing [Held *et al.*, 2010; Stouffer, 2004]. The mixed layer in the surface ocean responds rapidly to changes in radiative forcing in the atmosphere, but the deep ocean requires millennia to equilibrate [Hansen *et al.*, 2011; Li *et al.*, 2013]. A consequence of this vertical progression of warming is a strong increase in upper ocean stratification, particularly while transient forcing remains in effect [Xu *et al.*, 2012, 2013]. Figure 7b shows the change in upper ocean stratification simulated by the CESM-LE. The change in stratification is strongest in the tropics and in the Arctic Ocean; there are widespread increases in stratification at mid- to high-latitudes, with some localized and weak reductions in stratification. Stratification in the Subarctic North Pacific is expected to increase dramatically. The “warming hole” in the North Atlantic is associated with a strong increase in stratification, confirming that this feature involves substantial changes in freshwater content that accompanies cooling.

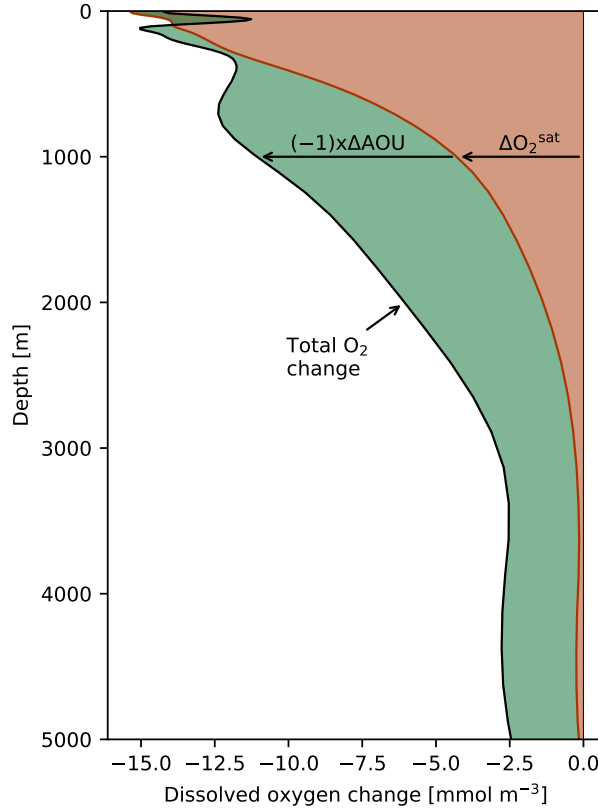
3.2 Global oxygen declines

Earth system model simulations indicate that the global ocean will begin to lose oxygen at an accelerating rate in the early 21st century, with a tight correspondence to increases in ocean heat content [Bopp *et al.*, 2013]. This phenomenon is illustrated in Figure 8, which shows results from the CESM-LE, including RCP8.5 and RCP4.5 scenarios. In these simulations, oxygen declines are evident in the late 20th century, but rates of change strongly increase in the early to mid 21st century. Notably, ensemble spread is limited at the global scale; this is because spatial averaging reduces the contribution of natural variability to trends, leaving a signal that is mostly driven by external forcing. Differences between RCP8.5 and RCP4.5 start to become evident for global ocean temperature around 2040, but manifest somewhat later for global O₂, reflecting, in part, the greater variability (ensemble spread) in the simulated O₂ inventory relative to temperature.

The acceleration in the rate of oxygen depletion is a common feature across the CMIP5 models [Bopp *et al.*, 2013; Cocco *et al.*, 2013]. In the CESM-LE under RCP8.5 (Figure 8a), the ensemble mean trend in the global-ocean oxygen inventory during the first two decades of the 21st century increased in magnitude from about –20 Tmol yr^{–1} to



462 **Figure 8.** Change in global-mean ocean properties as simulated in the Community Earth System Model
463 Large Ensemble (CESM-LE): (A) percent change the ocean oxygen inventory relative to the “control” climate;
464 and (B) ocean temperature. Red lines show results from RCP8.5, blue lines show results from RCP4.5 (blue).
465 We use the ensemble mean over the period 1920–1939 to define the “control” climate.



489 **Figure 9.** Mechanisms driving global oxygen change in the CESM-LE. The total oxygen decline (black)
 490 and the contribution of reduced solubility (orange area) and increase respiration (ΔAOU , green area). We use
 491 the ensemble mean over the period 1920–1939 to define the “control” climate.

481 nearly -60 Tmol yr^{-1} . By mid-century (2050s), the model suggests that the ocean will be
 482 losing about 100 Tmol of oxygen per year and this rate of loss will continue to increase
 483 to more than 130 Tmol yr^{-1} by the end of the century. Notably, however, Schmidtko *et al.*
 484 [2017] reported an observationally-based estimate of the rate of oxygen loss between 1960–
 485 2015 that was about $-100 \text{ Tmol yr}^{-1}$. This suggests that models may underestimate the
 486 true deoxygenation rates. The reasons for this discrepancy are not fully understood, but
 487 there are indications that strong trends observed in the tropical oceans [Stramma *et al.*,
 488 2008, 2012] are not replicated in many simulations [Oschlies *et al.*, 2017].

492 The global-scale O_2 declines depicted in Figure 8 result from a combination of the
 493 direct warming-induced reduction in solubility and changes cumulative respiration brought
 494 about by stratification. Changes in respiration can be quantified by changes in AOU , pre-
 495 suming that oxygen in the surface ocean remains relatively close to saturation. As ex-

496 plained above, an increase in AOU indicates greater path-integrated respiration, which
 497 corresponds to a decrease in the oxygen concentration. Therefore, the total change in oxy-
 498 gen concentrations under climate warming, ΔO_2 , can be written as the sum of changes due
 499 to warming effects on saturation concentrations (ΔO_2^{sat}) and respiration effects quantified
 500 by the negative of changes in AOU ($-\Delta AOU$):

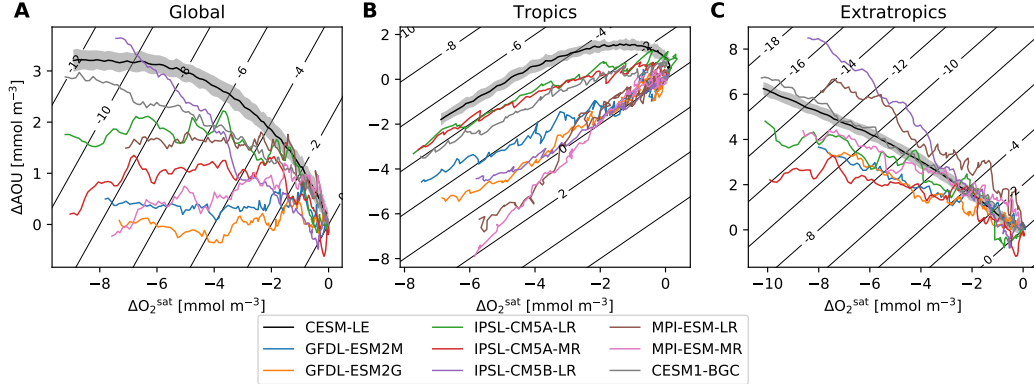
$$\Delta O_2 = \Delta O_2^{sat} - \Delta AOU. \quad (1)$$

501 Figure 9 illustrates this interplay of mechanisms driving oxygen loss for a global-
 502 mean vertical profile computed from the CESM-LE. The total global O_2 change at 2100
 503 (ΔO_2) is shown as a black line; the contribution of changes in oxygen solubility (ΔO_2^{sat})
 504 and respiration ($-\Delta AOU$) are highlighted with orange and green shading, respectively.
 505 Oxygen depletion is strongest in the upper 1000 m, exceeding -10 mmol m^{-3} over this
 506 depth range. Solubility-driven declines in oxygen decay rapidly with depth, consistent
 507 with our expectation of a vertical progression of ocean warming (section 3.1). In the near-
 508 surface ocean, the direct effect of warming on solubility is the dominant driver of oxygen
 509 loss, accounting for global-mean reduction of near 15 mmol m^{-3} at the surface; below
 510 about 3000 m depth, the solubility effect is negligible. The respiration-driven component
 511 of oxygen change ($-\Delta AOU$), by contrast, is actually weakly negative in the near-surface
 512 ocean. Recall that AOU is the difference between the oxygen concentration and the sat-
 513 uration concentration; thus, this decline in the absolute magnitude of surface AOU sug-
 514 gests that, although saturation concentrations are lower due to warming, surface oxygen
 515 is closer to saturation in the future climate. This effect can be understood as a result of
 516 shoaling mixed layer depths and reduced sea ice concentrations; these factors enable oxy-
 517 gen in the surface ocean to more effectively reach equilibrium with the atmosphere [Ito
 518 et al., 2004]. In spite of reductions in surface AOU , respiration-driven declines in oxygen
 519 rapidly become substantial below about 500 m depth and dominate oxygen depletion in
 520 the deep ocean (Figure 9). These changes in respiration are indicative of reduced ventila-
 521 tion due to increases in surface stratification. At the global-scale, increased stratification
 522 limits surface-to-depth exchange, cutting off the supply of oxygen to waters in the ocean
 523 interior.

524 Figure 10 presents another perspective on deoxygenation in the upper ocean (above
 525 1000 m) and includes simulations from the CMIP5 models as well as the CESM-LE.
 526 These plots show a phase-space defined by changes in cumulative respiration (ΔAOU)

and changes in solubility (ΔO_2^{sat}); total oxygen change is directly proportional to changes in both these factors (equation 1), which we illustrate with contour lines: a trajectory perpendicular to these contour lines is consistent with reinforcing changes in respiration and solubility; trajectories following a particular contour line indicate exact compensation between changes in respiration and solubility (i.e., no change in oxygen). Each colored line on this plot shows the evolution of a CMIP5 model simulation from 1970 to 2100; the lines begin at the origin ($\Delta O_2^{sat} = 0$, $\Delta AOU = 0$) at 1970 and their trajectory demonstrates the degree to which AOU and solubility change over the 21st century. The CESM-LE is shown as a black line with gray shading to represent the ensemble spread. All models simulate substantial changes in upper ocean oxygen concentrations, spanning a range from about -7 to -12 mmol m $^{-3}$ averaged over the upper 1000 m. While deoxygenation is universal, the models show widely divergent behavior with respect to the relative balance of ΔO_2^{sat} and ΔAOU driving oxygen change. The global oxygen changes in the CESM-LE, for instance, are initially dominated by increases in AOU (upward trajectory), but are later dominated by solubility (Figure 10a). Global oxygen change in the GFDL models, by contrast, is strongly dominated by changes in solubility out to 2100, with very little change in AOU ; the IPSL-CM5B-LR model behaves more like the CESM-LE, with substantial changes in both solubility and AOU (Figure 10a). Oxygen loss in the CESM-LE is more strongly dominated by changes in AOU than most of the models in the CMIP5 collection (Figure 10a).

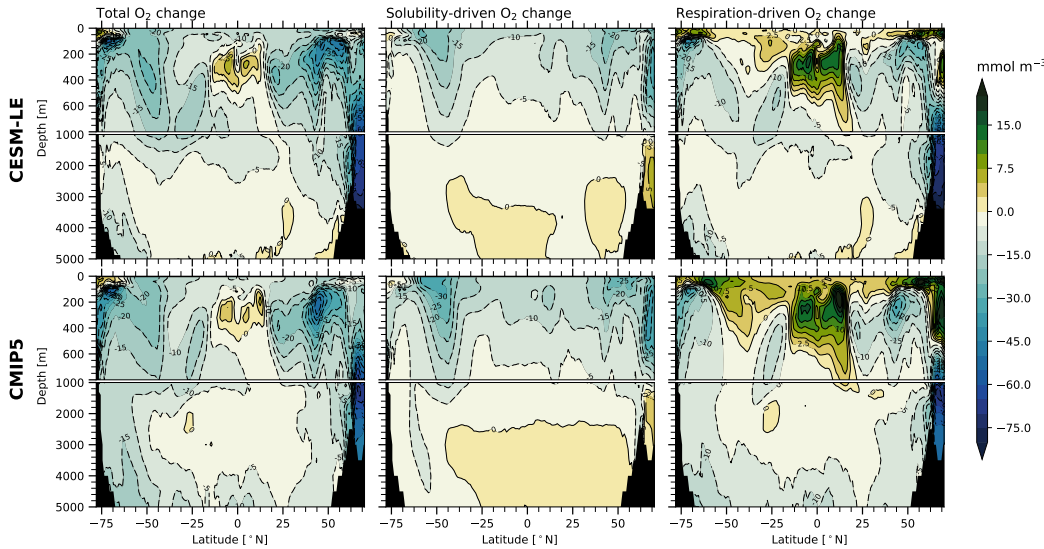
The divergent behavior within the CMIP5 models in the mechanisms driving upper ocean deoxygenation globally is partially a result of fundamentally different dynamics in the tropics versus high latitude regions; the models show more consistent behavior when these regions are considered separately (Figure 10bc). Deoxygenation in the extratropics (poleward of 20° latitude) is more intense than in the tropics and involves a combination of strong solubility and respiration effects; most models show trajectories near-perpendicular to the oxygen-change contours (Figure 10c). The CESM-LE simulates high latitude changes near the center of the CMIP5 model spread. In contrast to AOU increases in the extratropics, all CMIP5 models considered simulate decreasing AOU in the upper ocean within the tropics (equatorward of 20° latitude; Figure 10b). Decreasing AOU means less respiratory consumption of oxygen; therefore, while the models simulate warming-driven solubility declines in the tropics, reductions in AOU compensate, tempering oxygen declines such that in some models, tropical oxygen is actually projected to



547 **Figure 10.** Simulated relationships between upper ocean (above 1000 m depth) (ΔAO_U) and ΔO_2^{sat}
 548 changes: (A) globally, (B) in the “tropics” ($20^\circ S$ – $20^\circ N$), and (C) in the “extratropics” (poleward of 20°
 549 latitude). The black line show results from the CESM-LE (shading shows the region within one standard
 550 deviation of the ensemble spread). The colored lines show a subset of the CMIP5 models. Contours show the
 551 total oxygen depletion.

565 increase by 2100 (Figure 10b). The CESM-LE is an end-member model in the simula-
 566 tion of tropical oxygen change; its initial trajectory includes modest oxygen decline driven
 567 by increased respiration (positive ΔAO_U); AO_U subsequently declines, however, at a rate
 568 that largely compensates for warming (Figure 10b). It is this initial reinforcing behavior in
 569 tropical and extratropical AO_U and subsequent cancellation that leads to the global trajec-
 570 tory for CESM-LE shown on Figure 10a.

574 Figure 11 shows the change in dissolved oxygen along a zonal-mean, depth sec-
 575 tion; the left column shows the total simulated oxygen change at 2100, while the middle
 576 and right columns shows the contribution of solubility and respiration to oxygen change.
 577 This figure presents a picture consistent with that shown in Figure 10: oxygen declines are
 578 most intense at high latitudes due to the reinforcing effects of solubility and respiration-
 579 driven change. Opposing solubility and respiration effects mean that oxygen declines in
 580 the tropics are more modest—there is even a local oxygen increase in the low latitude
 581 thermocline. The imprint of ocean ventilation pathways is evident on Figure 11 as regions
 582 of strong deoxygenation extending from surface to depth at mid-latitudes; these features
 583 are similar to those found in observations of oxygen declines [Helm *et al.*, 2011]. Reduc-
 584 tions in AO_U are evident at the surface globally (as we saw in Figure 9), however, while
 585 the CMIP5 ensemble mean shows some weak AO_U declines in the extratropical southern

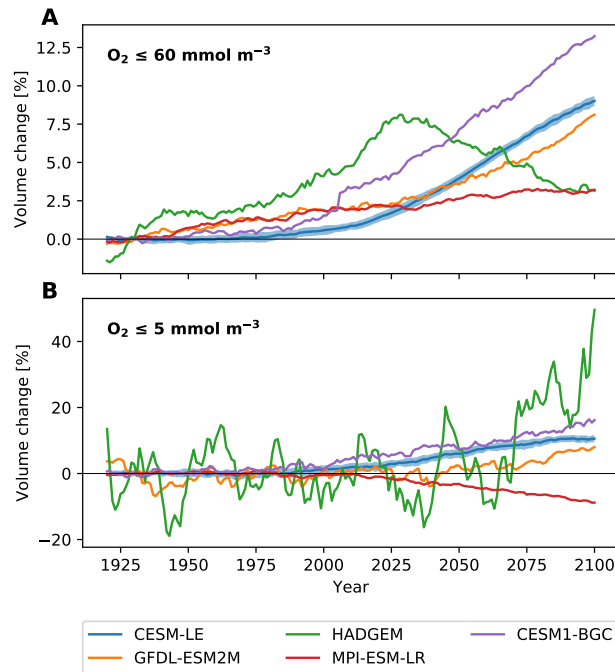


571 **Figure 11.** Zonal-mean, ensemble-mean change in the concentration of dissolved oxygen in the ocean
 572 simulated by the (top row) Community Earth System Model Large Ensemble (CESM-LE) and the CMIP5
 573 multi-model collection under RCP8.5.

586 hemisphere, the tropics are where pronounced *AOU* declines above about 600 m depth
 587 compensate for solubility, leading to weak oxygen increases.

593 Figure 12 shows the projected time-evolution of hypoxic ($O_2 \leq 60 \text{ mmol m}^{-3}$) and
 594 suboxic ($O_2 \leq 5 \text{ mmol m}^{-3}$) volumes in the CESM-LE and a subset of the CMIP5 ensem-
 595 ble. All of the models show an increase in hypoxic volume by 2100, though hypoxic vol-
 596 umes actually peaks mid-century in the HadGEM model. Suboxic volume increases in all
 597 but one model, though the range of increase is large. The coarse resolution of the ESMs
 598 precludes adequate representation of complex coastal processes; thus, these increases in
 599 hypoxic volumes do not properly reflect changes in coastal hypoxia. They predominantly
 600 reflects changes to open-ocean regions in the tropics.

601 The distribution of O_2 in the current ocean implies that suboxic zones are particu-
 602 larly sensitive to changes in regional oxygen concentrations. A decline in mean O_2 of the
 603 tropical upper ocean of only $\sim 2 \text{ mmol m}^{-3}$, substantially smaller than the global average,
 604 is enough to double the current volume of suboxia globally [Deutsch *et al.*, 2014]. This
 605 expansion of suboxic zones would be associated with enhanced denitrification. Assuming
 606 a constant volumetric rate of nitrogen loss in suboxic zones, integrated rates of denitri-
 607 fication would rise in proportion to the volume of suboxic waters, and may therefore also



588 **Figure 12.** Change in the volume of (A) hypoxic ($O_2 \leq 60 \text{ mmol m}^{-3}$) and (B) suboxic ($O_2 \leq 5 \text{ mmol m}^{-3}$)
589 waters in the CESM-LE (blue) and a subset of the CMIP5 models relative to a 1920–1939 baseline. The
590 CESM-LE has a average hypoxic volume of $1.1 \times 10^{17} \text{ m}^3$ over the period 1920–1939, whereas the CMIP5
591 ensemble mean hypoxic volume is $9.2 \times 10^{16} \text{ m}^3$. The suboxic volumes are $1.6 \times 10^{16} \text{ m}^3$ and $2.5 \times 10^{16} \text{ m}^3$
592 for the CESM-LE and CMIP5 ensemble mean, respectively.

be exceptionally sensitive to deoxygenation. Models of microbial nitrogen cycling in these regions indicate that the efficiency of nitrogen removal also increases as the volume of suboxic zones increases, so that the sensitivity of nitrogen loss to deoxygenation is further enhanced [Penn *et al.*, 2016]. Historical reconstructions of nitrogen loss from the North Pacific based on sedimentary records and model hindcasts support a high sensitivity of denitrification, implying a 3-fold change in the integrated rate of denitrification in recent decades [Deutsch *et al.*, 2014; Yang *et al.*, 2016]. The impacts of historical changes in nitrogen loss can be seen in the nitrate deficit (N^* ; see Figure 1 caption) well outside the suboxic zone, in the productive California Current System [Deutsch *et al.*, 2011], with presumed impacts on the N-limited net primary production in that upwelling zone. Large uncertainties still surround the future projections in the impacts of deoxygenation on nitrogen cycling and its effects on remote productivity. Resolving these uncertainties will require models that better reproduce the mean state of the suboxic zones, the microbial dynamics in these regions, and the rates and pathways by which their nitrate deficits are transported to nitrogen limited surface regions, all of which are crudely represented in ESMs.

3.3 Relationships with heat content

We have just seen that deoxygenation is driven by the direct impact of temperature on solubility and the secondary effect of changes in circulation that lead to changes in respiration as estimated by *AOU*. The CMIP5 models and the CESM-LE show that deoxygenation in the extratropics results from a synergy between these factors, which drive reinforcing changes in oxygen (Figure 10c). In the tropics, by contrast, the models suggest that solubility and respiration effects work in opposition; reductions in respiration tend to win-out slightly in some models, leading to modest increases in tropical oxygen (Figure 10b). While the models are relatively consistent with regard to these tendencies when the tropics and extratropics considered independently, divergent behavior results at the global scale due to averaging over regions with opposing tendencies. Additionally, the opposing respiration-driven changes at high-latitude and in the tropics lead to cancelation, such that global deoxygenation in the multi-model mean is mostly solubility driven (Figure 10a). Another reason why the models might show different relative amounts of deoxygenation relates to the physical climate simulation: the models simulate different amounts of warming over the 21st century [Bopp *et al.*, 2013]. This motivates us to consider the relationship between changes in oxygen with simulated changes in ocean heat content.

640 Figure 13 shows the change in upper-ocean oxygen in each model plotted against
 641 the concomitant change in temperature; the top row of plots shows the period 1970–2014
 642 and includes observational estimates; the bottom row shows 1970–2100. Observational
 643 estimates of oxygen variability are from the data compilation of *Ito et al.* [2017] and the
 644 ocean heat content estimates are from the European Centre for Medium-Range Weather
 645 Forecasts Ocean Reanalysis (ORAS4) [*Balmaseda et al.*, 2013]. While the models were
 646 shown to have substantial differences in the mechanisms driving simulated oxygen decline,
 647 there is a fairly tight correspondence across the models between oxygen and temperature
 648 at the global scale (Figure 13ab); indeed, the relationship between the global mean O₂
 649 and global mean temperature above 1000 m depth tends to collapse into a quasi-linear
 650 relationship. The dashed line in each panel of Figure 13 shows the O₂-heat relationships
 651 that would arise if changes in O₂ were purely solubility-driven. Declines in O₂ that exceed
 652 the solubility slope are due to the effect of respiration.

653 Notably, the observations indicate a much stronger O₂-heat relationship than is ev-
 654 ident in any of the models. Over recent decades, the global scale simulated O₂-heat re-
 655 lationship (Figure 13a) is in the range of -7 to -13 mmol m⁻³ K⁻¹; the observations,
 656 by contrast, show much more O₂ loss for a given temperature increase, with a relation-
 657 ship of -33.6 ± 2.98 mmol m⁻³ K⁻¹. The observational estimates of O₂-heat relation-
 658 ships in the extratropics (-32.2 ± 2.47 mmol m⁻³ K⁻¹; Figure 13e) and tropics ($-25.5 \pm$
 659 5.53 mmol m⁻³ K⁻¹; Figure 13c) are also stronger than simulated. The average slope of
 660 the simulated O₂-heat relationship is -11.7 mmol m⁻³ K⁻¹ in the extratropics, which is
 661 only slightly stronger than pure-solubility (Figure 13e), and the slope is very close to solu-
 662 bility (-3.27 mmol m⁻³ K⁻¹; Figure 13c) in the tropics.

663 Ocean warming between 1970 and 2014 is quite modest in comparison to the changes
 664 projected by 2100 (Figure 13ab). Over the full 1970–2100 time period, the models show
 665 distinct behavior in the tropics and extratropics. At the global scale and in the extratrop-
 666 ics, deoxygenation is tightly coupled to temperature, with a slope that exceeds solubility
 667 in most models (Figure 13bf). In the tropics, by contrast, all the models show less deoxy-
 668 genation than would be predicted on the basis of solubility changes alone and the spread
 669 across the models in simulated oxygen change is wide (Figure 13d). Tropical oxygen loss
 670 in the CESM-LE, for instance, begins with a temperature relationship much stronger than
 671 solubility, but the rate of decline with respect to temperature diminishes, ultimately yield-

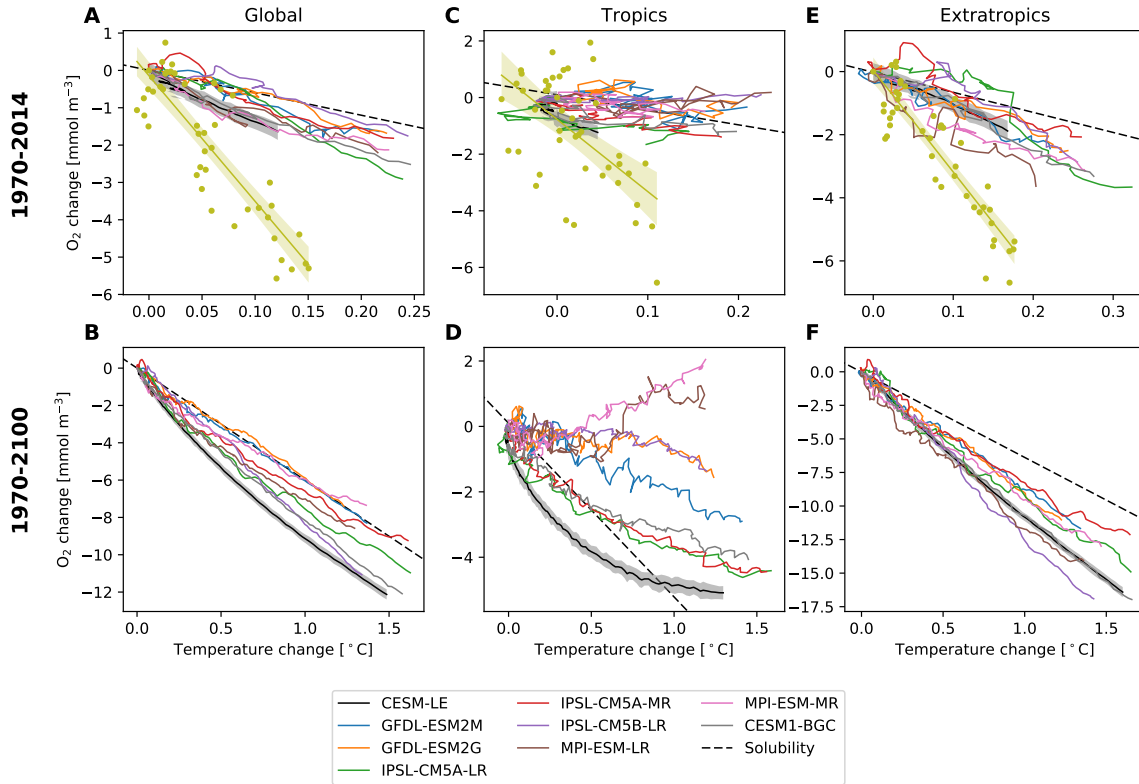
672 ing a relationship integrated out to 2100 that is less than would be predicted from pure
673 solubility-driven changes (Figure 13d).

674 It is not clear what causes these large differences in the sensitivity of ocean oxygen
675 content to the heat uptake. The observations themselves involve substantial uncertainty,
676 much of which arises from the fact that oxygen measurements are relatively sparse in
677 space and time—and particularly sparse in the tropics. Furthermore, as we lack long-term
678 records of oxygen trends on the global scale, it is possible that the observations include
679 periods or regions strongly influenced by natural variability, which may involve a different
680 mix of solubility and respiratory (*AOU*) changes. It is also possible that the models are
681 missing a mechanism that is actually driving O₂ declines in nature. For instance, *Ito et al.*
682 [2016] showed that polluted aerosol deposition has driven substantial declines in tropi-
683 cal Pacific oxygen concentration over recent decades. If ESMs lack such forcing, which
684 may be strongly correlated temporally with ocean heat content, they should predict an
685 O₂-temperature relationship that is too weak. Similarly, the models may omit important
686 changes due to ocean acidification, stoichiometry and specifics of tropical wind forcing
687 [*Oschlies et al.*, 2017, and references therein].

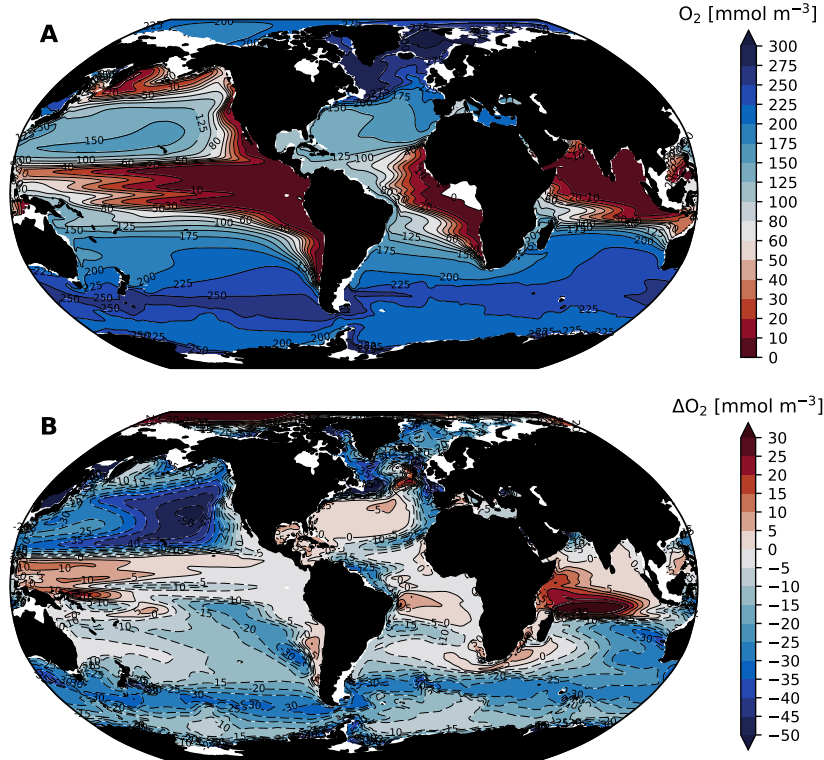
688 In summary, the collection of CMIP5 models and the CESM-LE are relatively con-
689 sistent in their simulation of O₂-heat relationships in the extratropics; however, there is
690 little agreement on this relationship in simulations of the tropics. Observations indicate a
691 stronger O₂-heat relationship than is simulated by any of the models, which suggests that
692 the models underestimate the amount of respiration-driven deoxygenation. If we believe
693 that the observations provide an accurate assessment of the true O₂-heat relationship, the
694 implication is that the simulated deoxygenation is a substantial underestimate of the oxy-
695 gen loss that will be realized for a given warming scenario.

704 3.4 Oxygen change in the thermocline

705 While the global trends in oxygen are characterized by consistent secular declines
706 (Figure 8), regional patterns of change, as we have just seen, are more complicated; thus,
707 we next examine patterns in oxygen over the thermocline, which we take to be over the
708 200–600 m depth range. Our focus on the thermocline depth is motivated by relevance to
709 ecological impacts. As the base of the oxygenated surface layer, oxygen declines in this



696 **Figure 13.** Modeled and simulated relationships between upper ocean (above 1000 m depth) mean O₂ and
 697 temperature changes. Top row shows model and observational data over the period 1970–2014; the bottom
 698 row shows the models from 1970–2100; annual means are plotted and all change is relative to the year 1970.
 699 The left column shows data averaged globally; the middle column shows data averaged in the tropics (20°S–
 700 20°N); and the right column shows the extratropics (poleward of 20° latitude). Simulation data is taken from
 701 a subset of the CMIP5 models (noted in legend) and the CESM-LE. Observational data is taken from *Ito*
 702 *et al.* [2017]. The dashed line in the each panel indicates the expected relationship if all change in oxygen was
 703 solubility-driven.



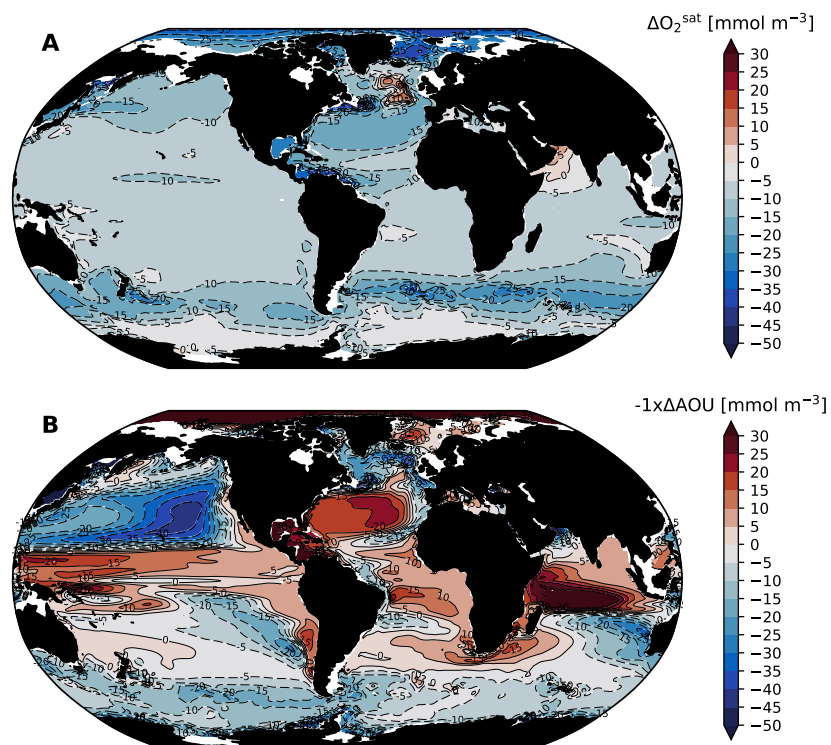
712 **Figure 14.** Thermocline (mean over the 200–600 m depth range) oxygen distributions simulated by the
 713 CESM-LE: (A) O_2 concentration in the control climate; (B) change in O_2 concentration at 2100. We use the
 714 ensemble mean over the period 1920–1939 to define the “control” climate.

710 depth range might drive vertical habitat compression, impacting marine organisms that are
 711 concentrated in the near surface [Deutsch *et al.*, 2015; Stramma *et al.*, 2011].

715 Figure 14a shows the distribution of oxygen in the “control” climate of the CESM-
 716 LE. It is important to note the discrepancies between this simulated oxygen distribution
 717 and that inferred from observations (Figure 4a): oxygen concentrations in CESM-LE tend
 718 to be too low and hypoxic regions are too extensive. These biases, a well-known and com-
 719 mon feature of coarse-resolution ESMs, are partially attributable to sluggish circulation
 720 yielding weak ventilation and are discussed further in section 4.1. In spite of the biases in
 721 simulated oxygen distributions, however, the basic spatial structure of the oxygen field is
 722 well represented (i.e., the pattern correlation with observations is relatively high); thus, we
 723 are confident that this model (and other ESMs) can provide some insight into the mech-
 724 anisms driving deoxygenation—though projections for oxygen variability and trends in
 725 tropical OMZs are to be treated with particular caution.

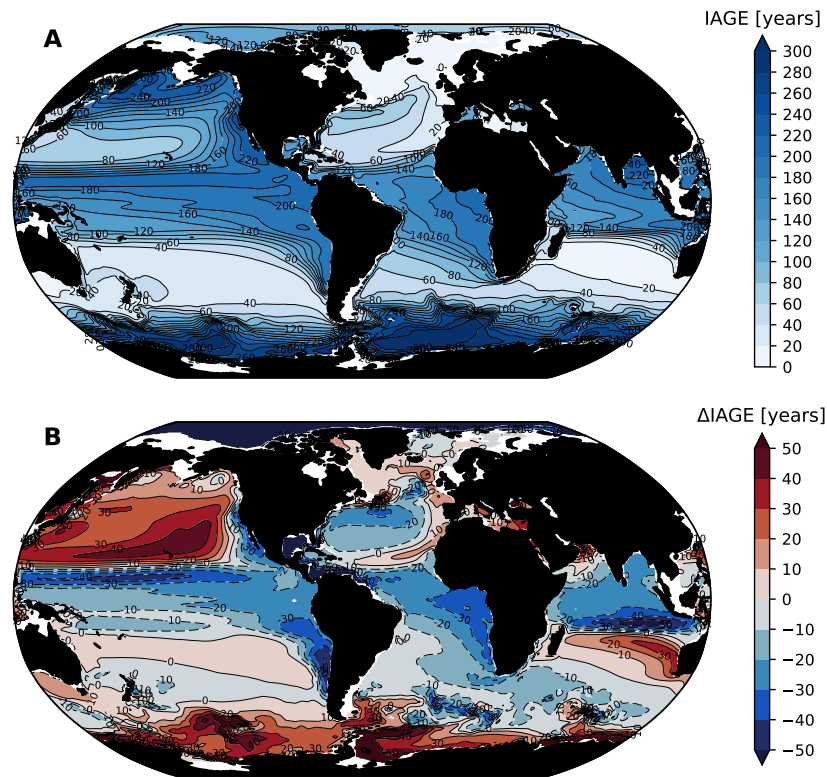
Thermocline oxygen depletion at 2100 is most pronounced in extratropical regions, with particularly strong changes in the North Pacific (Figure 4b). Consistent with what we have already seen, there are modest increases in oxygen in the tropics in all ocean basins, with moderately strong increases in the western equatorial Pacific and Indian Oceans. In order to understand the mechanisms modulating the intensity of deoxygenation and its spatial structure, it is instructive, once again, to examine the direct temperature effects on oxygen decline (ΔO_2^{sat}) and respiration-driven declines (ΔAOU). These fields are shown in Figure 15, noting that, as in Figure 9, we plot the negative of the ΔAOU , which can be directly interpreted as the change in oxygen due to changes in respiration, presuming that surface waters remain close to equilibrium with atmospheric O₂. The structure in ΔO_2^{sat} is a direct reflection of changes in ocean temperature in the thermocline depth range; ΔO_2^{sat} is strongly negative in the Southern Ocean, the Arctic, and parts of the North Atlantic. The Southern Ocean dominates ocean heat uptake in the present-day climate [Talley *et al.*, 2015] and is expected to persist in this role under future warming scenarios [Frölicher *et al.*, 2015]. The North Atlantic, as a site of substantial deepwater formation, also plays a strong role in ocean heat uptake; however, the patterns associated with the “warming hole” lead to localized cooling where solubility-driven changes in oxygen are positive (Figure 15a). There is no substantial deepwater formation in the Arctic basin; however, this region is subject to strong sea ice declines and warming associated with polar amplification [Screen and Simmonds, 2010] leading to widespread reductions in solubility in this region.

While the direct effect of temperature on oxygen is almost universally negative (driving declines), changes associated with respiration are more complicated (Figure 15b). By examining the changes in AOU , we can see that strong oxygen depletion in the thermocline of the North Pacific is a result of increases in respiration-driven oxygen depletion (increased AOU) that reinforce temperature effects. This contrasts with the North Atlantic, where respiration-driven declines in oxygen (increased AOU) are confined to the subpolar gyre; AOU in the mid-latitude North Atlantic thermocline decreases, which mitigates solubility driven oxygen declines there. Tropical regions are characterized by widespread declines in AOU , indicative of reduced oxygen consumption by respiration, consistent with the picture gleaned from our analysis of the ΔAOU - ΔO_2^{sat} phase space for the tropics (Figure 10b).



747
748
749

Figure 15. Solubility and respiration-driven changes in thermocline (200–600 m mean) oxygen at the year 2100; computed from the CESM-LE ensemble mean: (A) Solubility-driven oxygen change (ΔO_2^{sat}). (B) Respiration-driven oxygen change (the negative of ΔAOU).



761

Figure 16. Thermocline (mean over the 200–600 m depth range) ideal age (IAGE) distributions simulated

762

by the CESM-LE: (A) IAGE in the control climate; (B) change in IAGE at 2100.

763 Why are there decreases in cumulative respiration (*AOU*) in the tropical thermocline
764 under climate warming? Our first clue to answering this question come from looking at
765 the distibution of water mass age in the CESM-LE simulation. Figure 16 shows the mean
766 distribution and change in a tracer called “ideal age” (IAGE) in the CESM-LE. Ideal age
767 is transported by the OGCM; it is set to zero in the surface layer and increases at a rate of
768 1 year per year in the ocean interior—thus providing a direct estimate of the average time
769 since a water-mass was last in contact with the atmosphere. Just as we saw in section 2,
770 there is a tight correspondence between the age of waters in the thermocline (Figure 16a)
771 and their oxygen content (Figure 14a); older waters tend to have lower O₂ concentrations.
772 Similarly, the change in the age of thermocline waters at 2100 is a relatively good predic-
773 tor of changes in oxygen; waters that become older show O₂ declines, whereas waters that
774 become younger have modest increases in oxygen. As discussed above, water mass age
775 controls *AOU* by determining the time available for a respiration signal to accumulate. If
776 we imagine the flow in the ocean interior as consisting of a one-dimensional pipe, a re-
777 duction in age is akin to moving upstream in that pipe, where water mass properties are
778 closer to those of the inlet at the ocean surface. The reduction in ideal age with the tropi-
779 cal thermocline is likely due to a shift in the relative balance of water masses contributing
780 to these regions [Gnanadesikan *et al.*, 2007]. In particular, as upwelling in the tropics is
781 diminished under climate warming, the contribution of old deep waters to the thermocline
782 is reduced, leading to a local reduction in age.

783 Another mechanisms that might lead to local increases in oxygen is a reduction
784 in *OUR*; indeed, changes in *AOU* can be thought of as originating from changes in age
785 and/or changes in *OUR*. As we noted in section 2, net primary productivity in the surface
786 ocean is expected to decline under climate warming, which will drive diminished export
787 of organic matter, thereby alleviating the demand for oxygen in ocean interior. Most of
788 the CMIP5 models do indeed simulate declines in net primary productivity under climate
789 warming, though there is substantial differences between the models and some simulate
790 an increase [Laufkötter *et al.*, 2015]. A reduction of *OUR* was found to be the dominant
791 mechanism driving multi-decadal changes in suboxic zone volume and denitrification in
792 retrospective model simulations of the tropical Pacific that reproduce observed changes
793 in nitrogen cycle tracers [Deutsch *et al.*, 2011; Deutsch *et al.*, 2014]. Figure 17 shows the
794 change in carbon export in the CESM-LE. There is a global reduction in export produc-
795 tion, with the strongest reductions in the North Atlantic; export production increases, how-

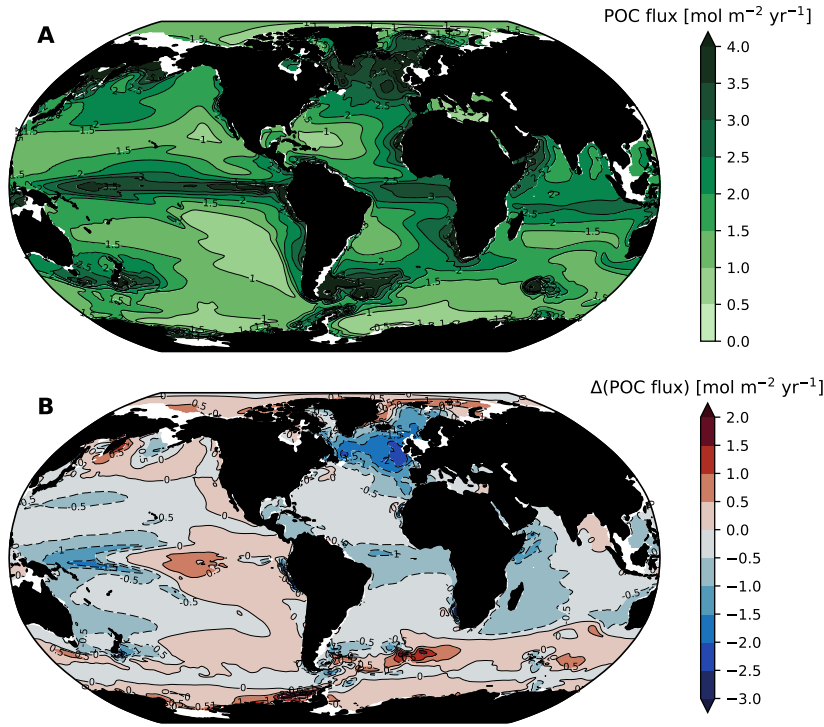
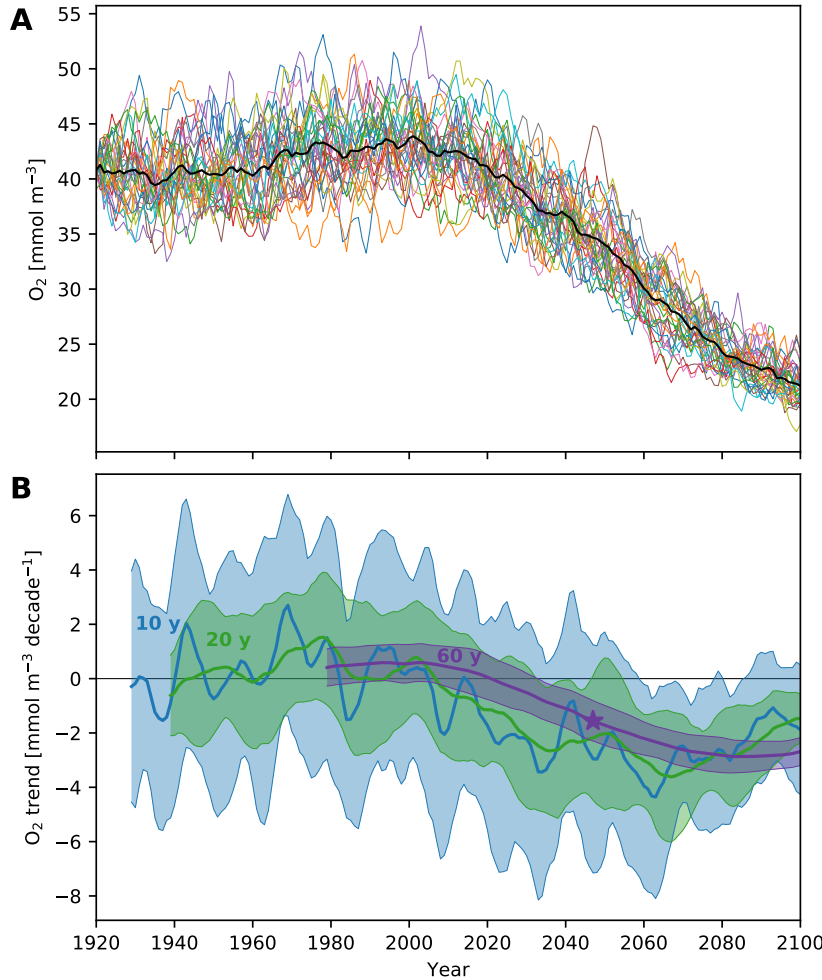


Figure 17. Carbon export at 100 m in the CESM-LE.

ever, over broad regions of the Southern Ocean and tropical Pacific. The widespread reduction in export production in the North Atlantic might be expected to temper oxygen declines in that basin, consistent with the reduction in *AOU* (Figure 14b). The changes in *OUR* in the tropical Pacific, however, are more complicated and further analysis is necessary to assess the role of changes in *OUR* in driving oxygen change there.

3.5 Time of emergence

One question that arises in the context of interpreting observations is whether trends are attributable to human-driven climate change. A key challenge in making definitive assessments of attribution is the role of natural climate variability, which has the potential to drive long-term trends in ocean oxygen. Indeed, variations in weather from year-to-year can produce thermally-driven surface O₂ anomalies, modulate surface-to-depth exchange, and alter the structure of the upper ocean environment, thereby impacting organic matter production and *OUR* in the interior [Deutsch *et al.*, 2011; Ito and Deutsch, 2010]. Observations collected in the Labrador Sea, for instance, have linked regional variations in O₂ to changes in deep convection on decadal or shorter timescales [van Aken *et al.*, 2011]. In



817 **Figure 18.** Oxygen concentrations and trends in the thermocline of the California Current System (CCS)
 818 simulated by the CESM-LE. (A) Oxygen concentrations in the CCS; colored lines show individual ensemble
 819 members; black line is the ensemble mean. (B) Retrospective trends computed from the data displayed in
 820 panel (A).

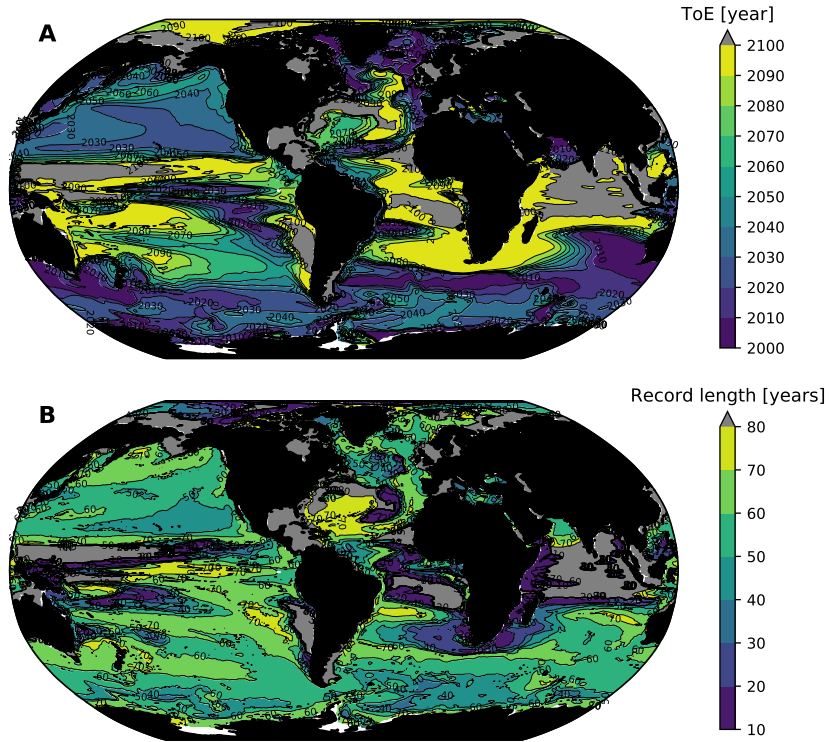
812 the subpolar North Pacific, oxygen displays significant variability [Deutsch *et al.*, 2006],
 813 which has been linked to fluctuations in the winter-time atmospheric forcing of the ocean
 814 [Andreev and Baturina, 2006]. Variability of thermocline O_2 ventilation in the North Pa-
 815 cific is mainly controlled by the areal extent of winter mixed layer water intersecting the
 816 density layers through which atmospheric O_2 is supplied to the ocean [Kwon *et al.*, 2016].

817 Our view of global-scale changes in ocean oxygen leaves an impression of smooth
 818 changes and clear trends (Figure 8a). Indeed, at the global-scale, spatial averaging reduces
 819 the contribution of natural variability to fluctuations in oxygen concentrations, which is re-

flected in relatively little ensemble spread. The case is different moving to regional scales; here, natural variability crops up as major driver of trends. Figure 18a, for instance, shows oxygen concentrations simulated by the CESM-LE in thermocline depth range in the California Current System (CCS; 33–46°N, within ~800 km of the coast). Notably, there is substantial variability in oxygen at this regional scale. Each colored line in Figure 18a shows the oxygen concentration in the CCS for a particular ensemble member; these lines can each be considered equally plausible realizations of the historical period. There is substantial spread because the timing of modes of natural climate variability are out of phase across the ensemble; the fluctuations amount to weather-like noise and are entirely natural. Changes driven by increasing greenhouse gas concentrations, however, are superimposed on the natural variability; this “forced” signal is evident most clearly in the ensemble mean. Just as spatial averaging to the global-scale decreases noise, averaging across the ensemble tends to cancel out the effects of natural variability, leaving only the forced signal.

Given the role of natural variability in driving random fluctuation, detection and attribution of human-driven climate change amounts to a signal-to-noise problem. For detection to be possible, forced signals must develop magnitude and persistence sufficient to transcend the noise, which is characterized by the envelop of background variability [Hasselmann, 1993; Santer *et al.*, 1994, 2011]. In this context, internally-generated variability inherently limits detection of climate-change signals regardless of practical observing capabilities; inferring trends from sparse observations is an obvious additional complication.

To illustrate the issues associated with detection and attribution of human-forced climate change, we consider the “time of emergence” (ToE) of the forced signal in the CCS region. We use a relatively narrow definition of ToE, in which we compare the magnitude of trends in oxygen to the variability of similar trends across the ensemble. We compute retrospective trends in each ensemble member starting at the year 2000 and continuing through the year 2100. For each year, we compute trends over record lengths from 10 to 100 years. We normalize the trends computed at each year and record length by the standard deviation of trends within the full CESM-LE, yielding a signal-to-noise ratio estimate. We then diagnose ToE as the earliest year in which a trend of any length is more than two standard deviations (2σ) outside the variability in trends across the ensemble and does not return to within 2σ for all remaining years in the simulation.



867 **Figure 19.** Time of emergence for trends in thermocline (mean over the 200–600 m depth range) oxygen, as
 868 simulated by the CESM-LE: (A) the year at which a significant trend is detected on average across the ensemble;
 869 and (B) the length of record required to detect a significant trend. Gray areas are regions where detection
 870 was not possible by 2100; in some cases these are regions where oxygen increased.

856 The results of this computation for thermocline oxygen in the CCS are illustrated
 857 in Figure 18b. Each line shows the ensemble mean trend and the shaded region shows
 858 the range within one standard deviation of the mean; blue shows 10 year trends, green
 859 shows 20 year trends and purple shows 60 year trends. As is evident from the 10 year
 860 trends, there is substantial decadal variability in oxygen in the CCS within the CESM-
 861 LE simulation; trends span a wide range from strongly increasing to strongly decreasing
 862 O₂. As the trend length moves to 20 years in duration, the spread across the ensemble is
 863 diminished and the variability in the ensemble mean trend is reduced. However, even with
 864 20 year trends, it is not possible to identify a ToE for forced O₂ change in the CCS in
 865 this simulation—even out to 2100. Trends of 60 years in length further reduce the noise,
 866 however, and detection of anomalous trends is possible around 2050 (the purple star).

871 Figure 19 shows the results of this same computation applied to thermocline oxygen
872 globally. Interestingly, while the North Pacific has some of the strongest deoxygenation
873 signals at 2100 (Figure 14), the detection of ToE on the basis of trends in this region is
874 delayed until the 2030s and 2040s. Broad region of the Southern Ocean and high latitude
875 North Atlantic, by contrast, show relatively advanced detection times: in the early 2000s.
876 Figure 19b illustrates, however, that detection of the forced signal can require fairly long
877 observational records. Indeed, over much of the areas where early detection is possible,
878 identifying ToE requires records of 40–60 years in length.

879 In addition to trends, there are other elements of the time-evolving signal-to-noise
880 relationship that can facilitate identifying ToE [Santer *et al.*, 1994]. First, changes in the
881 mean value of dissolved oxygen concentrations may be compared to the variability over
882 a period known to have little influence from external forcing. In this context, as concen-
883 trations pass outside the range of unforced variability, these changes might be classified
884 as externally forced [Christian, 2014]. Second, the large-scale spatial structure associated
885 with the forced signal can be evaluated relative to the dominant spatial structures associ-
886 ated with natural oxygen variability. Detection in this context relies on the extent to which
887 the pattern associated with a forced signal is distinct from the patterns associated with nat-
888 ural variability. We considered these methods in Long *et al.* [2016]; a key point from all
889 approaches is that high quality, sustained observing systems are critical to enabling early
890 detection.

891 This discussion is not meant to cast doubt on the notion that the ocean is losing
892 oxygen due to anthropogenic forcing. Rather, it is important to emphasize that natural cli-
893 mate variability can make substantial contributions to oxygen trends at local to regional
894 scales—and this must be considered in the interpretation of observations. It is scientif-
895 ically useful to understand the mechanisms driving O₂ fluctuations, and ideally be able
896 to attribute variability to natural versus human-driven causes. Ultimately, with sufficient
897 investments in observing and modeling capabilities, it may be possible to forecast large-
898 scale oxygen anomalies years in advance. Improvements in our understanding of oxygen
899 variability and trends could reduce uncertainty in the nature, magnitude, and impact of cli-
900 mate change on marine ecosystems, thereby providing a more reliable basis for adaptation
901 strategies and understanding cost/benefit trade-offs associated with climate change mitiga-
902 tion.

903 4 Implications and uncertainties

904 Our focus in this chapter thus far has been to describe how large-scale oxygen distri-
905 butions are expected to change. We have relied on ESMs because these provide a compre-
906 hensive basis for assessing interactions between climate and ocean biogeochemistry under
907 future forcing scenarios. As has been alluded to many times above, however, ESMs are
908 far from perfect; their deficiencies merit additional attention, which we will apply here,
909 with a focus on characterizing the structural uncertainty in model projections. In addi-
910 tion to uncertainty, there are several implications of deoxygenation that are not directly
911 simulated by the ESMs discussed above. These include the impacts on N₂O production
912 as a result of hypoxic and suboxic zone expansion. Additionally, the deoxygenation prob-
913 lem is likely to manifest at spatial scales smaller than those easily amenable to study with
914 global ESMs. In particular, it is very likely that coastal marine systems will be impacted
915 by ocean deoxygenation, so we include some discussion of this below. Finally, our ability
916 to understand how the structure and function of ecosystems will change in response to de-
917 oxygenation is a major challenge. We discuss an approach to characterizing the projected
918 future environmental change directly in ecophysiological terms.

919 4.1 Structural uncertainty

920 The ESM projections discussed above suggest that the ocean will lose substantial
921 oxygen over the 21st century. Deoxygenation will be most intense at high latitudes due to
922 the combined effects of solubility and respiration-driven reductions. Oxygen loss in the
923 tropics is more ambiguous; the models project modest increases in oxygen within the trop-
924 ical thermocline, where declines in solubility are offset by declines in respiration that are
925 largely driven by changes in circulation (Figure 11). Most models show an increase in hy-
926 poxic and suboxic volumes, indicating that while the intensity of oxygen depletion in the
927 core of oxygen minimum zones is diminished, these zones will expand in future. However,
928 while the models provide a relatively consistent picture in their projections of high latitude
929 deoxygenation, there is limited consensus on the balance of mechanisms driving projected
930 tropical oxygen change (i.e., Figures 10b and 13b). We will discuss the implications of
931 this uncertainty in this section and attempt to provide perspective on why models solutions
932 might be biased.

933 First, it is well recognized that the state-of-the-art ESMs struggle to accurately re-
 934 produce the observed mean state of oxygen distributions and biases are most pronounced
 935 in the tropics, where oxygen levels are very low [Bopp *et al.*, 2013]. Common biases are
 936 characterized by oxygen distributions that are generally too low and oxygen minimum
 937 zones that are (vastly) too extensive, though not all models have this combination of bi-
 938 ases [Bopp *et al.*, 2013]. The distribution of very low oxygen involves a subtle interplay
 939 of physical and biological mechanisms; getting the balance of these correct is clearly chal-
 940 lenging. For instance, the derivative of the oxygen solubility relation with respect to tem-
 941 perature (Figure 2) is approximately -5 mmol m^{-3} per degree. This suggests that a 1°C
 942 bias in sea surface temperatures can make a substantial difference in downstream waters
 943 near the suboxic threshold of 5 mmol m^{-3} .

944 ESMs are also limited by their relatively coarse spatial resolution, which is con-
 945 strained by computational cost. Ocean dynamics are characterized by motions on scales
 946 ranging from sub-meter to planetary; most of the kinetic energy in the ocean is contained
 947 within currents that have spatial scales ranging from 10 to 100 km; this range of spatial
 948 scales is defined as the ocean mesoscale [Stammer, 1997]. The resolution of the OGCMs
 949 used by ESM is too coarse to explicitly represent mesoscale dynamics; thus, these motions
 950 must be approximated with subgrid-scale parameterizations [e.g., Gent and McWilliams,
 951 1990]. These approximations, however, do not represent certain mesoscale features known
 952 to be present in equatorial current systems. Indeed, observations indicate that circulation
 953 in the tropics is characterized by zonally-coherent, zonal jets that alternate in direction
 954 with latitude [Cravatte *et al.*, 2012]. These jets contribute to OMZ ventilation but are not
 955 well-simulated at coarse resolution [Brandt *et al.*, 2008, 2012; Dietze and Loepfien, 2013;
 956 Duteil *et al.*, 2014; Getzlaff and Dietze, 2013]. Lacking a primary physical mechanism me-
 957 diating delivery of oxygen to the eastern side of tropical basins, OMZs in coarse resolu-
 958 tion models grow too large; moreover, omitting these processes may preclude representing
 959 important drivers of change. The situation is similar for other unresolved physical pro-
 960 cesses, such as vertical mixing, which is mediated by fine-scale turbulence. Mixing over
 961 rough topography is particularly challenging to represent accurately in models; insuffi-
 962 ciently accurate parameterization of this process may contribute to low oxygen biases in
 963 the Subarctic North Pacific, for instance [Nakamura *et al.*, 2006].

964 Finally, in addition to physical processes, the extent of simulated OMZs is sensi-
 965 tive to biogeochemical parameterizations used in the models. The biological pump begins

966 with net primary productivity and ends as organic matter sinks and is remineralization
 967 at depth. Many opportunities arise for inaccurate simulation in the complex collection
 968 of processes mediating this production and transit. Models include simplified represen-
 969 tations of phytoplankton physiology, for instance; they often simulate growth with fixed
 970 stoichiometric ratios between carbon and nutrients, whereas natural phytoplankton assem-
 971 blages are known to display systematic geographic variation [Devries and Deutsch, 2014].
 972 Changes in nutrient ratios (stoichiometry) impact *OUR* and thus OMZs by modulating
 973 oxygen demand: for a given nutrient supply rate, a surface ecosystem will generate more
 974 carbon export and hence more oxygen demand if carbon-to-nutrient ratios are greater. In
 975 addition to phytoplankton physiology, carbon export is controlled by a range of ecological
 976 and biogeochemical processes, including grazing and packaging of carbon by zooplankton
 977 [e.g., Wilson and Steinberg, 2010], physical and chemical aggregation mechanisms [Burd
 978 and Jackson, 2009; Passow, 2002], and ballasting of organic matter by biogenic or min-
 979 eral materials [Armstrong *et al.*, 2002; Klaas and Archer, 2002]. Variations in these factors
 980 drive geographic variability export production, as well as in the efficiency with which car-
 981 bon is transferred from the base of the sunlit surface layer to depth [Buesseler and Boyd,
 982 2009; Weber *et al.*, 2016]. These variations result in variation in the depth distribution of
 983 *OUR* that may not be captured by models. Ultimately, accurate simulation of oxygen dis-
 984 tributions depends on correctly representing *AOU* in the context of the model’s circulation
 985 field. Most of the models considered here have a reasonable simulation of the large-scale
 986 structure in oxygen distribution patterns; it is not surprising, however, that they struggle
 987 to exactly match simulated oxygen supply with simulated demand; indeed, this a delicate
 988 balance in nature [Watson *et al.*, 2017].

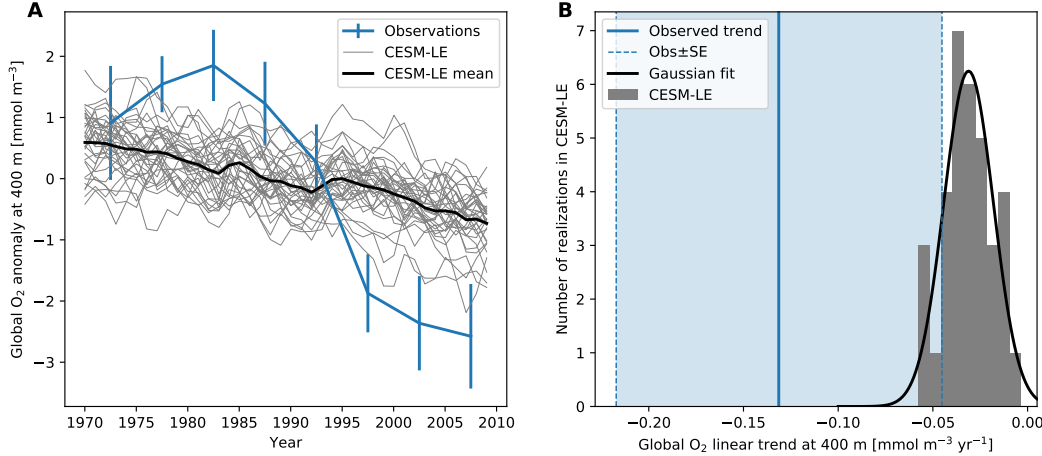
989 The ability to capture mean states does not necessarily guarantee convergence of fu-
 990 ture productions [Tagklis *et al.*, 2017], but it does provide important perspectives on the
 991 uncertainties of model-based projections. The negative bias in the simulated mean state of
 992 tropical thermocline oxygen is problematic if one anticipates a decreasing O₂ trend, for in-
 993 stance. Since the models start with much lower O₂ levels than the real ocean, they simply
 994 lack the O₂ to lose. A key question arising from our presentation of the observationally-
 995 based relationship between oxygen loss and ocean heat content anomaly (Figure 13) is
 996 whether model projections of oxygen loss are too conservative. The observations suggest
 997 a greater rate of oxygen loss for a given heat content anomaly than simulated by the mod-
 998 els. The solubility-driven line for oxygen loss (Figure 13) is a fixed thermodynamic refer-

999 ence in the O₂-temperature phase space; departures from this line can only be achieved by
1000 changes in the respiration, *AOU*, driven component of oxygen change. Thus, the fact that
1001 models underestimate oxygen loss relative to observations suggests that their simulation of
1002 *AOU* is insufficiently sensitive to changes in temperature.

1003 It is important to keep in mind that natural variability exerts substantial influence
1004 on oxygen trends (section 3.5). While we do not expect natural variability to be a domi-
1005 nant driver of decadal-scale variability on the global scale (i.e., Figure 8), observations do
1006 not provide comprehensive global coverage, introducing the possibility that inferred global
1007 trends arise from a peculiarity of the sampling distribution. As discussed earlier, the his-
1008 toric O₂ datasets include large data gaps and irregular sampling frequencies, which makes
1009 the quantification of the long term trends difficult. Trends arising in model simulations,
1010 therefore, can only be evaluated in the context of large observational uncertainty.

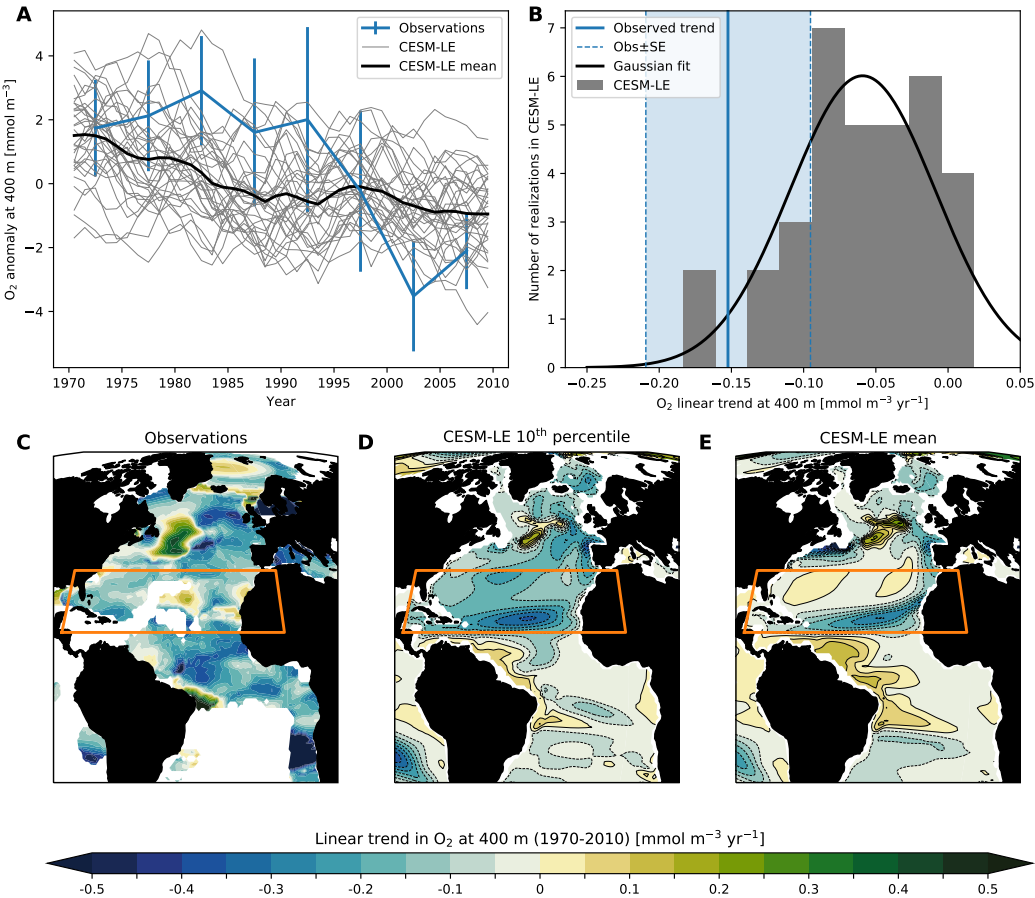
1011 Earth system model generate their own natural variability that is representative of
1012 that in nature—but does not necessarily evolve according to the temporal sequence fol-
1013 lowed in the real world. A large number of simulations with randomized initial conditions,
1014 therefore, can provide a means of quantifying uncertainty due to natural variability. For
1015 instance, if we had a perfect model, we might expect individual realizations of the histori-
1016 cal period in that model to have trends weaker or stronger than those observed, depending
1017 on the particular evolution of natural variability in each case. However, while individual
1018 realizations may not match observations, the observed trends will fall within the ensem-
1019 ble spread of a sufficiently large ensemble of a perfect model. So we now consider the
1020 following question: To what extent are O₂ trends within the CESM-LE consistent with
1021 observationally-estimated trends?

1029 Figure 20a shows the comparison of the global O₂ time series from the objectively-
1030 mapped historic O₂ dataset [Ito *et al.*, 2017] and CESM-LE. They are both evaluated at
1031 400 m depth for the period of 1970 to 2010. The model and observations both show de-
1032 clining global O₂ trends but the model appears to underestimate the global O₂ trend evi-
1033 dent in the observations. The objectively mapped historic O₂ dataset indicates a trend of
1034 $-0.13 \pm 0.09 \text{ mmol m}^{-3} \text{ yr}^{-1}$, where the uncertainty is the standard error of the regression
1035 coefficient. The significant uncertainty arises because the observed time series substan-
1036 tially departs from a linear trend [Santer *et al.*, 2011], which is due to the superposition
1037 of large, decadal-scale change evident as an apparently sinusoidal variation on Figure 20a.



1022 **Figure 20.** Global O₂ trends from observations and CESM-LE. (A) Globally average O₂ concentration
 1023 at the depth of 400m from 1970 to 2010. The thin solid lines represent individual ensemble members of the
 1024 CESM-LE, and the thick solid line is the ensemble mean. Blue line is the pentad time series of objectively
 1025 mapped O₂ dataset based on the World Ocean Database [Ito *et al.*, 2017]. Error bars indicates one standard
 1026 deviation of the pentad data. (B) Histogram of linear O₂ trend at 400 m. The black line is a gaussian fit, and
 1027 the blue solid is the observed trend; the dashed lines and shaded region show its uncertainty as measured by
 1028 one standard error.

1038 Figure 20b contrasts the observed and simulated linear trends of O₂. The overlap between
 1039 observations and the model is quite marginal. The model underestimates the magnitude of
 1040 the global O₂ decline, as no single ensemble member reproduces the observed trend. The
 1041 ensemble mean trend ($-0.03 \text{ mmol m}^{-3} \text{ yr}^{-1}$) is a factor of 4 smaller in magnitude than
 1042 the observationally-based estimate, but—due to the large uncertainty in the observations—the
 1043 lower quartile trend ($-0.04 \text{ mmol m}^{-3} \text{ yr}^{-1}$) still overlaps with the upper bound of the
 1044 observational uncertainty range (blue dashed line in Fig 20b). The effect of natural vari-
 1045 ability, as represented by the spread of histogram in Figure 20b, provides some sense of
 1046 an expected range in the simulated trend, but there is a strikingly large difference between
 1047 the spread in the ensemble members and the standard error of observed trend. This in-
 1048 dicates that the model may be severely underestimating the natural variability, and/or the
 1049 existing observations lacks the spatial coverage to accurately determine the decadal fluctu-
 1050 ation of global O₂ time series. Considering the poor data coverage in the historic observa-
 1051 tions, consistent and accurate monitoring of global O₂ fields is a primary challenge.



1052 **Figure 21.** O₂ trends in the Subtropical North Atlantic (STNA; 15–35°N) from observations and CESM-
 1053 LE. (A) STNA average O₂ concentration at the depth of 400 m from 1970 to 2010. The thin solid lines
 1054 represent individual ensemble members of the CESM-LE, and the thick solid line is the ensemble mean. The
 1055 blue line is the pentad time series of objectively mapped O₂ dataset based on the World Ocean Database [Ito
 1056 et al., 2017]. Error bar indicates one standard deviation of the pentad data. (B) Histogram of linear O₂ trend
 1057 at 400 m. The black line is a gaussian fit, and the blue solid is the observed trend; the dashed lines and shaded
 1058 region show its uncertainty as measured by one standard error. (C) Observed pattern of linear trend at 400 m
 1059 depth from 1970 to 2010. The trend is plotted for 1° × 1° grid cells within which at least 20-years of obser-
 1060 vations are available. (D,E) 10th percentile and ensemble mean trend from the CESM-LE for the same depth
 1061 and time period. The orange box on the maps shows the region for which time series and trends are presented
 1062 in panels (A) and (B).

Assessing global trends places significant demands on observations for comprehensive coverage. We might expect to be able to assess model behavior more robustly at regional scales. Unfortunately, however, regions of intense interest, such as the thermocline of the Eastern Tropical Pacific, have been poorly sampled in the historical dataset, making the model-observation comparison difficult. Even with the large observational uncertainty, *Oschlies et al.* [2017] showed a persistent discrepancy in observed and simulated trends of O₂ at the depth of 300 m, wherein the observations show trends that are consistently stronger than the models. The subtropical North Atlantic, in contrast, has relatively high sampling density. This is also a region where the models and observations agree relatively well (Figure 21). Comparing the observed and simulated time series of O₂ in the subtropical North Atlantic (15–35°N), however, the ensemble mean again underestimates the long-term trend of O₂. The observed linear trend (1970–2010) is $-0.15 \pm 0.06 \text{ mmol m}^{-3} \text{ yr}^{-1}$, where the uncertainty again is a standard error of the regression coefficient [*Santer et al.*, 2011]. The ensemble mean trend ($-0.06 \text{ mmol m}^{-3} \text{ yr}^{-1}$) is a factor of 2.5 smaller than the observed trend. However, a few ensemble members exceed the magnitude of observed deoxygenation in this region (as measured by the linear trend; Figure 21b). Figures 21c–e compare the pattern of deoxygenation in the North Atlantic between observations, the 10th percentile composite from the CESM-LE, and the ensemble mean. The ensemble mean clearly lacks the strong deoxygenation of the central subtropical gyre; however, there are a subset of ensemble members that exhibited trends nearly as intense as observed. Further investigation is required to partition the roles of natural variability versus external forcing in driving observed O₂ trends in this region; however, while this analysis emphasizes that natural variability can indeed play a substantial role in modulating trends, it also suggests that the CESM-LE and other CMIP5 models may underestimate deoxygenation.

4.2 Nitrous oxide production

Nitrous oxide (N₂O) affects climate in two distinct ways. First, it is a strong greenhouse gas; thus, increasing N₂O concentrations in the troposphere have a strong effect on radiative forcing [*Solomon et al.*, 2007]. Second, since N₂O is relatively long-lived, it is mixed upward to the stratosphere, where it is a major contributor to the production of ozone depleting substances (NO and NO₂) [WMO, 2011; Wuebbles, 2009]. Global-mean atmospheric N₂O concentrations have increased markedly from preindustrial levels, around 270 ppb, to near 330 ppb in 2017, mainly as a result of human activities [*Forster et al.*,

1095 2007, NOAA ESRL Global Monitoring Division, Boulder, Colorado, USA]. N₂O is pro-
1096 duced naturally in soils and the ocean; agricultural, land use change, and industrial activi-
1097 ties account for anthropogenic sources [Denman *et al.*, 2007]. The IPCC Fourth Assess-
1098 ment Report estimated that the ocean accounts for about 35% of the natural sources of
1099 N₂O to the atmosphere [Denman *et al.*, 2007].

1100 N₂O is produced by two microbially-mediated processes in the ocean: (1) under
1101 well-oxygenated conditions, microbes produce N₂O as a byproduct of nitrification (NH₄⁺ →
1102 NO₂⁻ + NO₃⁻); and (2) at suboxic concentrations, denitrification produces N₂O as an inter-
1103 mediate during the conversion of nitrate to N₂ (NO₃⁻ → NO₂⁻ → N₂O → N₂) [Bange
1104 *et al.*, 2010]. When oxygen concentrations are very near zero, there is net consumption
1105 of N₂O during denitrification and little N₂O accumulation [Bange *et al.*, 2010]. The N₂O
1106 yield of nitrification is sensitive to oxygen levels, however, increasing significantly as oxy-
1107 gen declines [e.g., Löscher *et al.*, 2012; Santoro *et al.*, 2011]; thus, suboxic regions and
1108 surrounding hypoxic waters account for a substantial fraction of marine N₂O production
1109 [Codispoti, 2010].

1110 The expansion of suboxic and hypoxic waters (i.e., Figure 12) is very likely to im-
1111 pact the production and decomposition of N₂O. Enhanced denitrification will lead to
1112 greater rates of fixed nitrogen loss from the ocean, with unknown implications on primary
1113 productivity. The role of increasing denitrification on N₂O production remains even less
1114 clear; however, it is likely that N₂O yields from nitrification will increase, on average, as
1115 oxygen levels decline. Moreover, oxygen loss in relatively shallow waters might enhance
1116 N₂O production because respiration rates are higher near the sunlit surface where primary
1117 productivity generates sinking organic matter [Codispoti, 2010]. Our understanding of the
1118 collection of processes driving N₂O production, however, is insufficient to make definitive
1119 predictions. Indeed, ocean warming may drive shifts in bacterial community composition,
1120 potentially impacting N₂O production [Freing *et al.*, 2012]. Nitrification has been shown
1121 to decrease at low pH, thus suggesting the potential for ocean acidification to impact N₂O
1122 production [Beman *et al.*, 2010]. Modeling studies have projected decreased global N₂O
1123 emissions from the ocean, driven by reductions in primary productivity, which limits ni-
1124 trification, and the direct effects of stratification, which traps N₂O at depth [Martinez-Rey
1125 *et al.*, 2015]. These projections are highly uncertain, however, in part because models lack
1126 fully mechanistic representations of the processes mediating microbial transformations in

1127 the nitrogen cycle and the resultant N₂O yields; indeed, our empirical understanding of
1128 these processes is still developing [Codispoti, 2010].

1129 **4.3 Coastal deoxygenation**

1130 Coastal ocean hypoxia has emerged as a growing threat to marine ecosystems and
1131 fisheries with high economic and societal value [Diaz and Rosenberg, 2008; McClatchie
1132 *et al.*, 2010]. Oxygen decline in many coastal waters is driven by nutrient pollution. The
1133 widespread use of chemical fertilizers and discharge of waste waters increases the nutri-
1134 ent content of surface waters on land; as these waters are discharged into coastal systems,
1135 elevated nutrient loads stimulate productivity [Rabalais *et al.*, 2010]. Additionally, fossil
1136 fuel combustion and agricultural activities are associated with increases in atmospheric
1137 deposition of nutrients to the ocean. In particular, reactive nitrogen loads have increased
1138 substantially over the last century, enabled by industrial-scale artificial nitrogen fixation via
1139 the Haber-Bosch process [e.g., Gruber and Galloway, 2008]. Nutrient pollution drives “eu-
1140 trophication”, wherein primary productivity increases, leading to oxygen declines as excess
1141 organic matter decomposes in subsurface waters.

1142 Coastal habitats can be particularly vulnerable to future deoxygenation because of
1143 the compounding effects of nutrient runoff from the land and the large-scale ocean de-
1144 oxygenation from the open ocean. A major concern is that ocean deoxygenation drives
1145 declines in the oxygen content of offshore waters, lowering the baseline concentrations
1146 from which coastal eutrophication causes further oxygen depletion. The CCS, for instance,
1147 is one of the most productive and biodiverse marine systems in the world [Block *et al.*,
1148 2011; Carr, 2001]. In the CCS, like other coastal ocean upwelling systems, changes in
1149 the oxygen content are controlled by complex interactions between circulation and biogeo-
1150 chemistry, and show prominent fluctuations on interannual and decadal timescales both
1151 in observations and models [section 3.5; Bograd *et al.*, 2008; Deutsch *et al.*, 2011]. Over
1152 the continental shelf region, where the marine ecosystem is most sensitive to low oxy-
1153 gen conditions, natural oxygen variations are associated with fluctuations in the strength
1154 of the coastal upwelling [Chan *et al.*, 2008; Connolly *et al.*, 2010]. The subsurface wa-
1155 ters in the offshore CCS region are charged with nutrient-rich, low-O₂ waters, which can
1156 trigger high production of new organic matter as water upwells onto the continental shelf.
1157 Coastal upwelling is driven by winds, which vary in intensity and seasonality due to both
1158 natural variability and anthropogenic climate warming. The seasonal timing of upwelling-

favorable winds has strong impact on the CCS system; for instance, *Barth et al.* [2007] demonstrated that delayed upwelling strongly impacted net primary productivity and food web structure in the CCS. Theory suggests that the seasonal timing and intensity of upwelling-favorable winds is likely to change significantly in a warmer climate [*Bakun*, 1990]. Indeed, consistent with this, a collection of the CMIP5 models suggest that upwelling-favorable winds in the CCS system will occur over a prolonged seasonal duration and become more intense at high latitudes [*Wang et al.*, 2015]. The likely impacts of these changes on coastal ecosystems and marine biodiversity are not well-understood and merits further study. It is clear, however, that changes in the properties of offshore source waters has a significant impact on hypoxia in the CCS system [*Bograd et al.*, 2008; *Grantham et al.*, 2004]. Moreover, the frequency of hypoxic events may be modulated by the slow, decadal changes in these subsurface water properties feeding the CCS upwelling. *Pozo Buil and Di Lorenzo* [2017], for instance, demonstrated that low-frequency changes in the oxygen levels of the CCS upwelling are driven by large-scale ocean circulation dynamics. Oxygen anomalies are generated in regions well offshore in the Subarctic North Pacific and are advected across the basin in the North Pacific Current; these anomalies contribute to variations in hypoxia within the CCS on decadal to multi-decadal timescales [*Pozo Buil and Di Lorenzo*, 2017]. Notably, the time required for the oxygen anomalies to cross the Pacific basin is about 10 years, indicating that with sufficiently robust observing capabilities, oxygen variability in the waters offshore the CCS might be predictable many years in advance.

In light of these dynamics, a major concern for the CCS and other similar coastal systems is the systematic and widespread depletion of oxygen in offshore waters. While there is limited research on the future of coastal hypoxia taking into account different scenarios of coastal eutrophication and emissions, it is reasonable to expect large-scale oxygen declines to propagate down to local scales [*Bianucci et al.*, 2015]. Oxygen depletion in coastal upwelling systems happens naturally; however, as the oxygen levels decline offshore, hypoxic and anoxic events may become much more frequent and severe. This is a critical consideration, especially since these coastal systems are profoundly important in both ecological and economic terms.

4.4 Habitat of the future

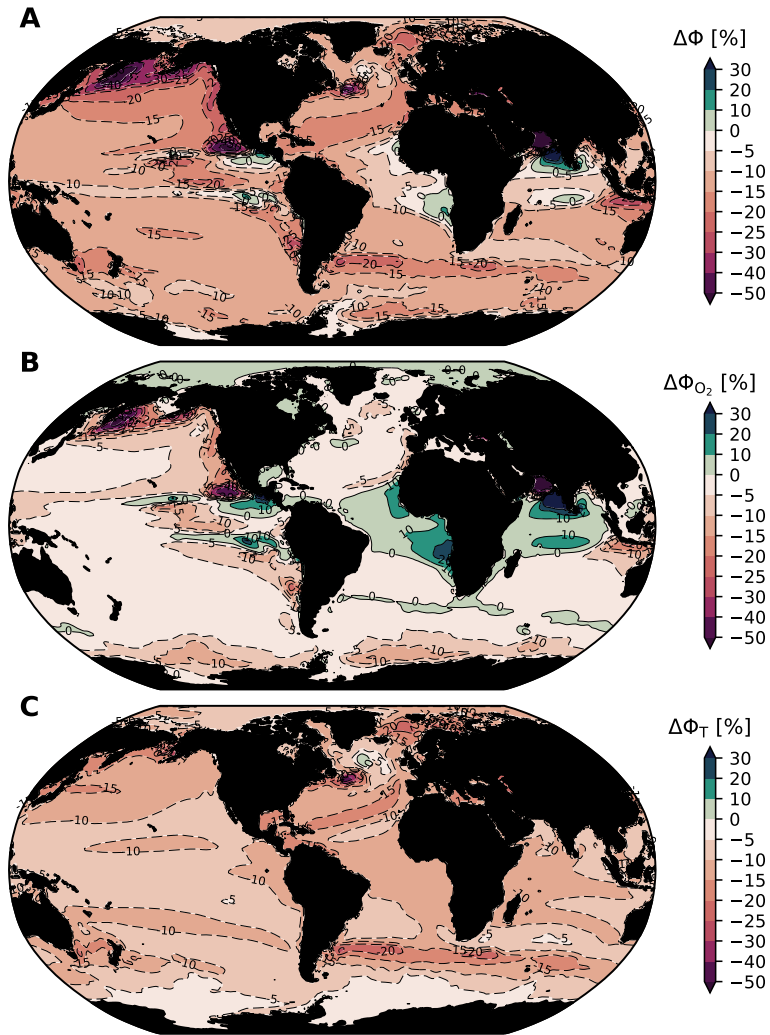
The impact of ocean deoxygenation on marine conservation goals depends on the number and ecological roles of the species for which the loss of dissolved O₂ crosses a

critical biological threshold. Based on compilations of lethal O₂ levels from laboratory studies and the distribution of O₂ in the ocean (i.e., Figure 1ab), it would appear that the impact of deoxygenation will be confined to those species residing in the relatively small volumes of the oceans already at or near O₂ levels below a nominal hypoxic level of ~60 mmol m⁻³. This view, however, neglects at least two critical facts about the provisioning of energy to aerobic marine organisms. First, the energetic demands of organism metabolism rise with temperature. Thus, as the oceans warms, even a constant O₂ may not suffice to meet organisms’ energetic demands. Second, lethal thresholds measured in laboratory studies are carried out under conditions designed to quantify oxygen demand at the minimum metabolic rate in a state of rest. Ecological survival in a realistic environments will typically require substantially more energy (and hence O₂ supply) than would be indicated by the physiological survival evaluated by laboratory studies. Indeed, among terrestrial taxa, active metabolic rates are found to be 1.5–7 times resting rates [Peterson *et al.*, 1990], suggesting that O₂ thresholds for ecological survival may be several times higher than lethal thresholds would imply.

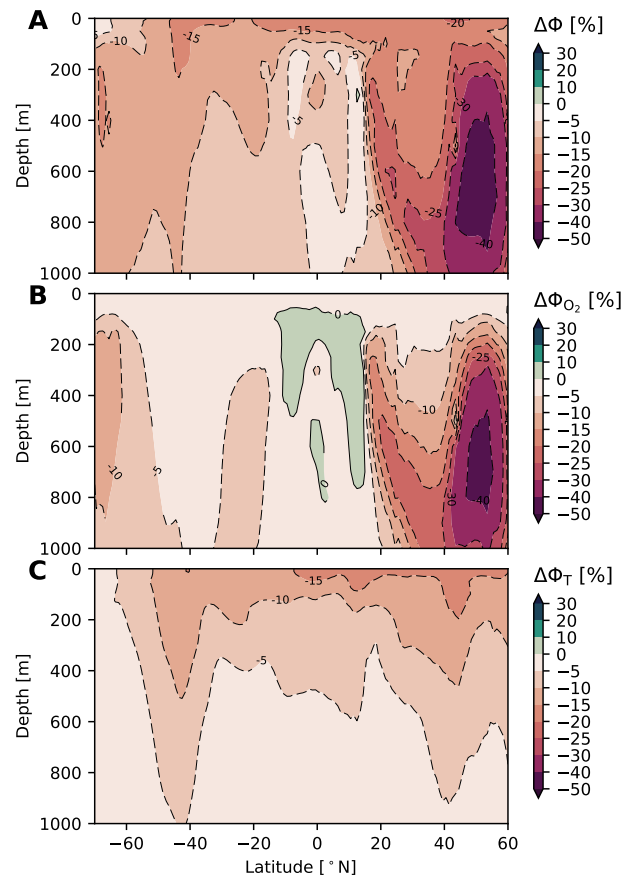
An ecophysiological framework has recently been developed to investigate metabolic habitat constraints in light of these factors, for the contemporary, past, and future oceans. The framework is built on a Metabolic Index (Φ), which can be calibrated with laboratory and biogeographic data [Deutsch *et al.*, 2015]. The Metabolic Index uses physiological data on hypoxia tolerance across a range of temperatures and body sizes to calibrate the ratio of oxygen supply (S) to an organism’s resting demand (D). The supply of oxygen is a function of the ambient partial pressure of oxygen (pO_2) and the efficiency with which an organism can acquire and utilize O₂. This can be written as $S = \alpha_S B^\delta pO_2$, where α_S is a mass-normalized coefficient expressing the rate of gas transfer between an organism and its environment and B^δ is the scaling of supply with biomass B [Piiper *et al.*, 1971]. Resting metabolic demand can be expressed as $D = \alpha_D B^\epsilon \exp(-E_o/k_B T)$, where α_D is a taxon-specific basal metabolic rate, B^ϵ is the scaling of this rate with biomass, E_o is the temperature dependence, and k_B is the Boltzmann constant [Gillooly *et al.*, 2001]. We construct the Metabolic Index as the ratio S/D :

$$\Phi = A_o B^n \frac{pO_2}{\exp(-E_o/k_B T)} \quad (2)$$

where $A_o = \alpha_S \alpha_D$ is the ratio of rate coefficients for gas exchange (O₂ supply) and minimum metabolic rate (O₂ demand) and n is the difference between the scaling exponents applied to body size (B) for O₂ supply and demand. If Φ falls below a critical threshold



1206 **Figure 22.** Relative change in the Metabolic Index (Φ ; equation 2) at year 2100 over the top 400 m of
 1207 the ocean according to the bias-corrected, CMIP5 ensemble mean: (A) the total relative change in Φ , i.e.
 1208 $\Delta\Phi = 100 \times (\Phi^{2100} - \Phi^{2000})/\Phi^{2000}$; (B) the relative change in Φ due purely to changes in O_2 ; (C) the rela-
 1209 tive change in Φ due purely to changes in temperature. The relative change has no dependence on A_o or B^n ;
 1210 the total and temperature-driven components of change depend on E_o . For this presentation, we have used
 1211 $E_o = 0.4$, which is the mean of the several taxa for which E_o has been characterized [Deutsch *et al.*, 2015].



1212 **Figure 23.** Zonal mean relative change in the Metabolic Index (Φ ; equation 2) at year 2100 according to the
 1213 bias-corrected, CMIP5 ensemble mean: (A) the total relative change in Φ ; (B) the relative change in Φ due
 1214 purely to changes in O_2 ; (C) the relative change in Φ due purely to changes in temperature. See the caption of
 1215 Figure 22 for further details.

1233 value of 1, organisms must either suppress aerobic activity or initiate anaerobic metabolism,
1234 conditions that are physiologically unsustainable. Conversely, values above 1 enable organ-
1235 ismal metabolic rates to increase by a factor of Φ above resting levels, permitting critical
1236 activities such as feeding, defense, growth, and reproduction. Thus for a given environ-
1237 ment, Φ estimates the ratio of maximum sustainable metabolic rate to the minimum rate
1238 necessary for maintenance for a given species.

1239 For marine animals, this ratio of active to resting energetic demand can be inferred
1240 by mapping Φ alongside the species biogeographic distribution [Deutsch *et al.*, 2015].
1241 Among all taxa studied to date ($n \approx 20$), species geographic range boundaries are found
1242 to coincide with Metabolic Index values of between 1.5–7, identical to the range predicted
1243 by terrestrial energetic demands. Where the ocean’s supply of O₂ falls below this criti-
1244 cal threshold, termed Φ_{crit} , the Metabolic Index acts as a fundamental energetic barrier
1245 for species habitat. In other words, if climate warming and O₂ loss reduce the Metabolic
1246 Index for an organism below its species-specific Φ_{crit} , the environment would no longer
1247 have the aerobic capacity to support the organism’s energetic requirements. The Metabolic
1248 Index can therefore be used to quantify the loss of aerobically viable habitat for marine
1249 animals due to the combined effects of climate warming and attendant O₂ loss. It can also
1250 be used to track the relative role of each stressor in governing viable habitat across space
1251 and depth. This is particularly useful as the magnitudes of warming and deoxygenation
1252 can differ dramatically among regions of the ocean (Figures 6 and 14).

1253 Figure 22 shows the relative change in Φ over the top 400 m of the ocean for an or-
1254 ganism with an average metabolic temperature sensitivity ($E_o = 0.4$). There are widespread
1255 declines in Φ over most of the ocean; only in small pockets in the tropics does Φ mod-
1256 estly increase. Relative changes in Φ in excess of 40% are found in the Subarctic North
1257 Pacific, suggesting that this region may be particularly impacted by climate change and
1258 deoxygenation. Figures 22b and 22c demonstrate why it is important to consider changes
1259 in temperature and oxygen together. Figure 22b shows the change in Φ that would be re-
1260 alized if oxygen was changed in isolation. The subarctic North Pacific stands out again in
1261 this field, but much of the tropics where models simulate oxygen increases show improve-
1262 ments in Φ . Temperature-driven reductions in Φ , however, are nearly ubiquitous, which we
1263 might expect from the distribution of surface warming (Figure 6). The fact that metabolic
1264 rates scale with temperature means that even present-day distributions of oxygen may not
1265 be sufficient to meet metabolic demands in some regions in the future. The depth struc-

ture of changes in Φ are shown in Figure 23. Strong reductions in Φ are predicted for the upper 1000 m of ocean over much of the high-latitude northern hemisphere (Figure 23a). The oxygen-driven and temperature-driven changes in the zonal-mean Φ have a fundamentally different structure (Figure 23bc). Oxygen-driven changes are most intense below 200 m, which is where oxygen depletion is most pronounced (Figure 11). The modest increases in oxygen in the tropical thermocline yield oxygen-driven increases in Φ locally.

The restrictions of habitat imposed by the need to balance O₂ supply and demand vary across species, and the tightening of those constraints during ocean warming will depend critically on the relative magnitude and patterns of ocean warming and deoxygenation. Thus, a generalized prediction of the responses of marine species to ongoing global change must rely on an adequate characterizations of species diversity with respect to Metabolic Index traits, and on a regional basis, since temperatures and O₂ levels can operate in both synergistic and counteracting directions.

5 Action

Ocean oxygen concentrations are strongly linked to ocean heat content (Figure 13); therefore, substantial deoxygenation is unavoidable without mitigating climate change. Even in the best circumstances, some degree of continued ocean warming is unavoidable and, given the longevity of perturbations to atmospheric CO₂ [Archer *et al.*, 1997], current emissions commit the climate system to sustained alteration. Efforts to conserve marine ecosystems must account for the synergistic effects of multiple variables changing simultaneously [e.g., Boyd *et al.*, 2014; Brewer and Peltzer, 2009; Deutsch *et al.*, 2015; Portner, 2010]. Indeed, ocean warming, acidification, oxygen loss, and reductions in primary productivity are key components of a suite of multiple stressors effecting ecosystem change. Specifically in the context of ocean deoxygenation, we can frame our discussion about mitigation actions around two questions. (1) What are the consequences if nothing is done to mitigate climate warming? (2) What are the benefits of mitigation actions?

Perspective on the risks of inaction is provided by considering what happens after 2100. Warming over the 21st century is very likely to lead to disruptive consequences; an examination of model projections under extended RCP8.5 scenarios out to 2300, however, suggest that long-term effects of unmitigated human-driven climate change could be catastrophic. Figure 24 presents a zonal-mean view of oxygen and phosphate in the present-day

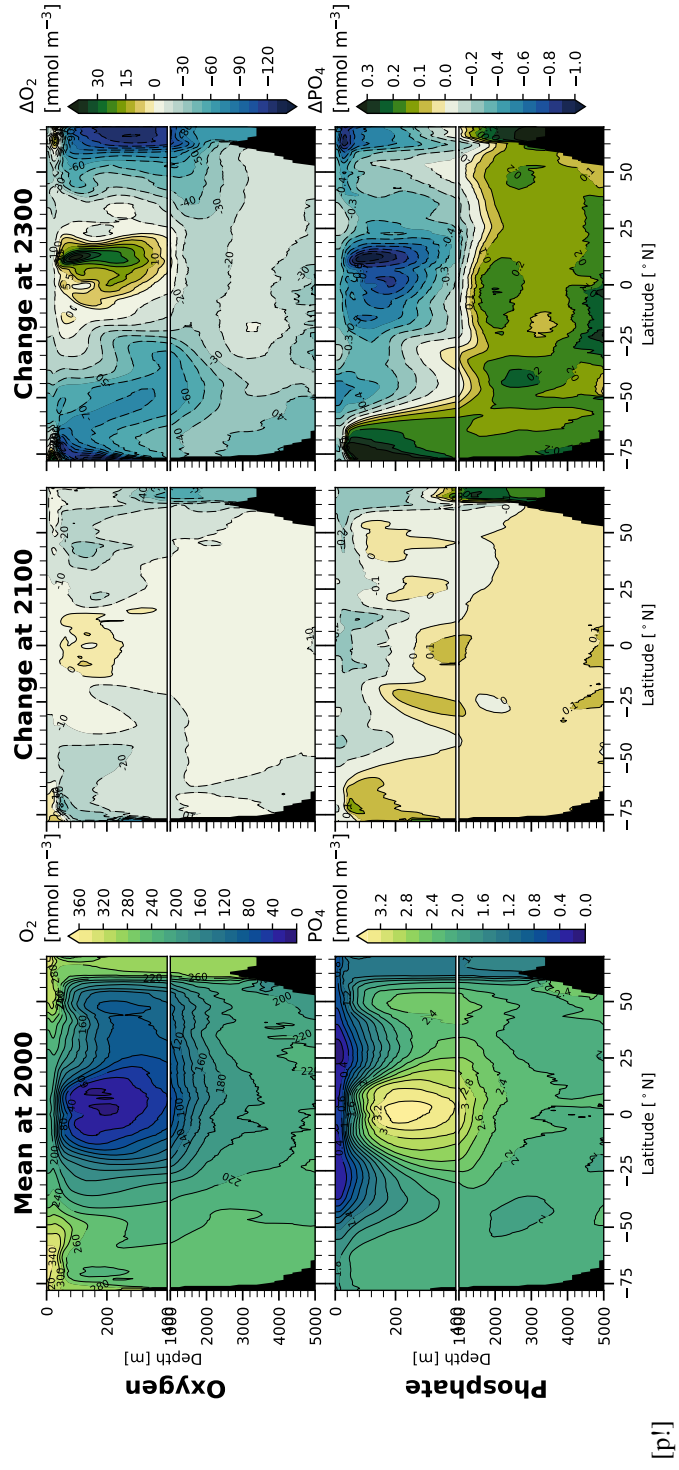


Figure 24. Zonal mean oxygen (top) and phosphate (bottom) in a CESM1-BGC simulation, averaged over 1995–2005 (left column). The middle column shows the change in zonal mean oxygen and phosphate at 2100 (2090–2100 minus 1995–2005); the right column shows the change at 2300 (2280–2300 minus 1995–2005).

climate as well as changes to these fields at 2100 and 2300. The scenario used to integrate the model out to 2300 follows historical and then the RCP8.5 forcing out to 2100; this entails an increase of atmospheric CO₂ from 285 ppm at 1850 to about 940 ppm at 2100—CO₂ then continues to increase to 1962 ppm at 2300. The impacts on ocean oxygen involve a strong amplification of the pattern of change at 2100: high latitude regions show substantial oxygen declines. While there are increases in oxygen within the tropical thermocline, those regions remain below the biological thresholds of habitability for many species. The magnitude of these changes is shocking: the zonal-mean changes in oxygen concentrations at high latitudes approach and even exceed 100 mmol m⁻³; the entire deep ocean substantially deoxygenates (Figure 24, top right).

The changes in oxygen at 2300 are associated with a massive redistribution of nutrients. The surface ocean becomes strongly depleted in phosphate, whereas the deep ocean phosphate inventory increases; this increase is consistent with growth of the remineralized nutrient inventory and thus AOU. Stratification reduces the vertical fluxes of phosphate from depth into the surface ocean over much of globe; however, reductions in sea ice and changes in upwelling in the Antarctic Zone of the Southern Ocean promote high productivity there, which effects a more complete transfer of nutrients from the upper ocean to deep waters [Primeau *et al.*, 2013]. The surface depletion of nutrients will drive declines in primary productivity, dramatically reducing the flow of energy into marine ecosystems. This is likely to strongly reduce potential fisheries yields [Pauly and Christensen, 1995; Stock *et al.*, 2017] and may lead to a fundamental reorganization of ocean food webs [Hoegh-Guldberg and Bruno, 2010].

The depletion of oxygen at 2300 represents a severe contraction of viable habitat on the basis of the metabolic constraints discussed in section 4.4. Indeed, these changes are similar in structure to simulations conducted with CESM of ocean climate change at the end-Permian extinction event (~252 million years ago); analysis of these simulations indicates that warming and deoxygenation can account for extinction patterns (unpublished), leading to a haunting conclusion: human-induced warming is driving patterns of change that are consistent with those of the most severe crisis in the history of life on Earth.

A comparison between 2100 and 2300 confirms that the severity of deoxygenation and its consequences will grow in the absence of efforts to mitigate climate change. However, it is also important to consider that climate change is essentially irreversible on hu-

man timescales. *Solomon et al.* [2009] demonstrated this using an Earth System Models of Intermediate Complexity; they conducted idealized forcing scenarios, wherein emissions were instantaneously ceased following a period of increase similar to that in RCP8.5. Carbon dioxide concentrations begin to decline following the cessation of emissions, but the carbon perturbation requires several centuries to fully dissipate [*Archer and Brovkin*, 2008; *Archer et al.*, 1997]. Moreover, even as radiative forcing due to CO₂ begins to decline, the ocean continues to warm, but at a slower rate; thus surface temperatures remain elevated for more than 1,000 years following an abrupt stop in emissions [*Solomon et al.*, 2009]. Few studies have explicitly examined irreversibility in the context of ocean biogeochemistry and ecology; this is an important area for further research.

The long persistence timescales of ocean deoxygenation drivers suggests that early action to mitigate climate change will maximize benefit. The benefits of mitigation can be quantified in terms of the reduced magnitude of change in some state variable (i.e., preserving oxygen content) or in delaying impacts, providing time for adaptation. *Henson et al.* [2017], for instance, examined the ToE of anthropogenic signals in sea surface temperature, pH, primary productivity, and interior oxygen distributions; by comparing RCP8.5 to a “mitigation scenario” (RCP4.5); they demonstrate benefits of mitigation in terms of reduced areal extent and delayed emergence of stressors. The benefits of delayed impacts can include time for organisms to adapt or migrate to avoid impacts [*Henson et al.*, 2017]. Understanding how delayed emergence will effect the structure and function of marine ecosystems is very complicated, however; thus, it is not clear whether the difference between RCP8.5 and RCP4.5 is a meaningful one from an ecological perspective. Moreover, in cases where species are already living near the edge of their ecophysiological-viable envelop, such as at high latitudes, there may be no refuge from which to avoid climate change impacts. These considerations are critical to developing better quantifications of the avoided impacts of climate change associated with mitigation efforts. A few studies have framed analyses of ESMs in this context [e.g., *Krumhardt et al.*, 2016], but this is an area where much more additional research is needed.

Finally, while climate change mitigation is critical to avoiding deoxygenation, investments in observing systems and modeling capabilities may help provide adaptive capacity. There is good reason to believe, for instance, that oxygen distributions can be forecast years in ahead in some regions [e.g., *Pozo Buil and Di Lorenzo*, 2017], possibly enabling advanced warming of especially low-oxygen periods. Humanity is changing marine

1362 ecosystems faster than we can understand them; there is strong role for science in enabling
1363 informed decisions about managing this global-scale impact.

1364 **6 Conclusions**

1365 Ocean deoxygenation presents a compelling case-study demonstrating the intricate
1366 interrelationships characterizing Earth system function. The planetary energy balance is
1367 determined by the composition of the atmosphere, including, most importantly, carbon
1368 dioxide. Carbon is the primary currency of life on Earth; the flow of energy and material
1369 through the biosphere plays a role in regulating atmospheric composition and the radia-
1370 tive balance controlling climate. Humans, however, have released massive quantities of
1371 geologically-sequestered CO₂, disrupting this balance, trapping more heat and warming the
1372 planet. The ocean is the dominant heat reservoir in the climate system and thus absorbs
1373 most of this anomalous heat. Ocean warming drives deoxygenation by directly impact-
1374 ing the gas solubility: warmer waters hold less oxygen. Furthermore, warming causes the
1375 ocean to become more stratified, inhibiting vertical exchange between surface and deep
1376 waters—and thereby reducing the supply of oxygen to the ocean interior.

1377 Ocean ecosystem are built on the energy harvested from the sun during photosynthesis—
1378 the same process that contributes to regulation of the carbon cycle and produces most
1379 of the oxygen in the Earth system. The flow of energy contained in photosynthetically-
1380 produced organic matter and the oxygen necessary to respire it have enabled the wide di-
1381 versity of animal life on the planet. The carbon cycle is coupled to the cycles of nutri-
1382 ents such as nitrogen and phosphorus, required building blocks of organic matter. Oxygen
1383 mediates the return of these nutrients from their organic forms to those that refuel pho-
1384 tosynthesis. In this manner, the global biosphere consists of an interconnected, metabolic
1385 network in which many of the key linkages are mediated by microbial transformations.
1386 Oxygen exerts strong control across two critical components of this network. It is a funda-
1387 mental requirement for animal life and it regulates microbial metabolism, affecting which
1388 transformations take place.

1389 Earth system models predict substantial deoxygenation over the 21st century, with a
1390 rapid acceleration in oxygen loss expected in the coming decades. These models suggest
1391 that deoxygenation will be strongest at high latitudes, where the effects of solubility and
1392 stratification are reinforcing. The loss of oxygen in the tropics, according to these mod-

els, is tempered by opposing drivers: reductions in solubility are projected to be offset somewhat by reductions in respiration, the latter caused primarily by changes in circulation. Most ESMs project increases in oxygen in the tropical thermocline over the 21st century. These increases occur in regions where oxygen is already very low in the present climate—and the models also tend to predict increases in hypoxic and suboxic water volumes, suggesting that while oxygen concentrations may increase in the core of oxygen minimum zones, these zones will still expand. However, ESMs struggle to accurately simulate present-day oxygen distributions in the tropics; thus, the future of oxygen in these regions of the ocean is somewhat uncertain. Moreover, an observationally-based relationship between oxygen loss and ocean heat content anomaly suggests that the model projections may be too conservative: the observed relationship would suggest greater rates of oxygen loss than simulated by the models.

The changes projected in dissolved oxygen over the next century are likely to force dramatic changes in marine ecosystems. Simulations of the “deep future” (out to 2300) project changes to oxygen and nutrient distributions that would yield catastrophic consequences for marine life. More research is needed to fully quantify how climate change mitigation can benefit conservation. However, there is virtually no uncertainty that the present climate trajectory will lead to substantial oxygen loss from the oceans, resulting in profound impacts to ocean ecosystems and biogeochemistry. Animals reliant on aerobic metabolisms will experience habitat contraction as regions with oxygen below hypoxic limits expand. Ocean microbial communities will be affected, leading to altered nutrients cycles: rates of fixed nitrogen loss from the ocean will increase; N₂O production and release is likely to change, though by how much is substantially uncertain.

The scale of the deoxygenation problem is truly planetary: the ocean occupies ~70% of the Earth’s surface; as anthropogenic warming proceeds, oxygen concentrations will decline—leaving a nearly ubiquitous imprint of human-activity on this vast ecosystem. The potentially profound changes in ocean habits and biogeochemical cycles associated with deoxygenation provide dramatic illustration of the degree to which humanity is a dominant influence on Earth’s ecosystems [Vitousek *et al.*, 1997].

1422 References

- 1423 Abraham, J. P., M. Baringer, N. Bindoff, T. Boyer, L. Cheng, J. Church, J. Conroy,
1424 C. Domingues, J. Fasullo, and J. Gilson (2013), A review of global ocean temperature
1425 observations: Implications for ocean heat content estimates and climate change, *Rev.
1426 Geophys.*, 51(3), 450–483, doi:10.1002/rog.20022.
- 1427 Anderson, L., and J. Sarmiento (1994), Redfield ratios of remineralization determined by
1428 nutrient data analysis, *Global Biogeochem. Cycles*, doi:10.1029/93GB03318.
- 1429 Andreev, A. G., and V. I. Baturina (2006), Impacts of tides and atmospheric forcing vari-
1430 ability on dissolved oxygen in the subarctic North Pacific, *J. Geophys. Res.*, 111(C7),
1431 C07S10, doi:10.1029/2005JC003103.
- 1432 Archer, D., and V. Brovkin (2008), The millennial atmospheric lifetime of anthropogenic
1433 CO₂, *Clim. Change*, 90(3), 283–297, doi:10.1007/s10584-008-9413-1.
- 1434 Archer, D., H. Kheshgi, and E. Reimer (1997), Multiple timescales for neutralization of
1435 fossil fuel CO₂, *Geophys. Res. Lett.*, 24(4), 405–408, doi:10.1029/97GL00168.
- 1436 Armour, K., J. Marshall, J. Scott, and A. Donohoe (2016), Southern ocean warm-
1437 ing delayed by circumpolar upwelling and equatorward transport, *Nat. Geosci.*, doi:
1438 10.1038/ngeo2731.
- 1439 Armstrong, R., C. Lee, J. Hedges, S. Honjo, and S. Wakeham (2002), A new, mechanis-
1440 tic model for organic carbon fluxes in the ocean based on the quantitative association
1441 of POC with ballast minerals, *Deep-Sea Res.*, 49(1–3), 219–236, doi:10.1016/S0967-
1442 0645(01)00101-1.
- 1443 Bakun, A. (1990), Global climate change and intensification of coastal ocean upwelling,
1444 *Science*, 247(4939), 198–201, doi:10.1126/science.247.4939.198.
- 1445 Balmaseda, M., K. Trenberth, and E. Källén (2013), Distinctive climate signals in re-
1446 analysis of global ocean heat content, *Geophys. Res. Lett.*, 40(9), 1754–1759, doi:
1447 10.1002/grl.50382.
- 1448 Bange, H., A. Freing, A. Kock, and C. Löscher (2010), Marine pathways to nitrous oxide,
1449 in *Nitrous oxide and climate change*, pp. 36–62, Routledge, doi:10.4324/9781849775113.
- 1450 Barnosky, A. D., N. Matzke, S. Tomiya, G. O. U. Wogan, B. Swartz, T. B. Quental,
1451 C. Marshall, J. L. McGuire, E. L. Lindsey, K. C. Maguire, and et al. (2011), Has
1452 the earth’s sixth mass extinction already arrived?, *Nature*, 471(7336), 51–57, doi:
1453 10.1038/nature09678.

- 1454 Barth, J. A., B. A. Menge, J. Lubchenco, F. Chan, J. M. Bane, A. R. Kirincich, M. A.
1455 McManus, K. J. Nielsen, S. D. Pierce, and L. Washburn (2007), Delayed upwelling al-
1456 ters nearshore coastal ocean ecosystems in the northern California current, *Proc. Natl.*
1457 *Acad. Sci. U.S.A.*, 104(10), 3719–3724, doi:10.1073/pnas.0700462104.
- 1458 Beman, J. M., C.-E. Chow, A. L. King, Y. Feng, J. A. Fuhrman, A. Andersson, N. R.
1459 Bates, B. N. Popp, and D. A. Hutchins (2010), Global declines in oceanic nitrification
1460 rates as a consequence of ocean acidification, *Proc. Natl. Acad. Sci. U.S.A.*, 108(1), 208–
1461 213, doi:10.1073/pnas.1011053108.
- 1462 Bianucci, L., K. Fennel, D. Chabot, N. Shackell, and D. Lavoie (2015), Ocean bioge-
1463 chemical models as management tools: a case study for atlantic wolffish and declining
1464 oxygen, *ICES J. Mar. Sci.*, 73(2), 263–274, doi:10.1093/icesjms/fsv220.
- 1465 Block, B. A., I. D. Jonsen, S. J. Jorgensen, A. J. Winship, S. A. Shaffer, S. J. Bograd,
1466 E. L. Hazen, D. G. Foley, G. A. Breed, A.-L. Harrison, and et al. (2011), Tracking
1467 apex marine predator movements in a dynamic ocean, *Nature*, 475(7354), 86–90, doi:
1468 10.1038/nature10082.
- 1469 Bograd, S. J., C. G. Castro, E. Di Lorenzo, D. M. Palacios, H. Bailey, W. Gilly, and F. P.
1470 Chavez (2008), Oxygen declines and the shoaling of the hypoxic boundary in the Cali-
1471 fornia Current, *Geophys. Res. Lett.*, 35, L12607, doi:10.1029/2008GL034185.
- 1472 Bopp, L., C. Quéré, M. Heimann, A. C. Manning, and P. Monfray (2002), Climate-
1473 induced oceanic oxygen fluxes: Implications for the contemporary carbon budget,
1474 *Global Biogeochem. Cycles*, 16(2), doi:10.1029/2001gb001445.
- 1475 Bopp, L., L. Resplandy, J. Orr, S. Doney, J. Dunne, M. Gehlen, P. Halloran, C. Heinze,
1476 T. Ilyina, R. Séférian, J. Tjiputra, and M. Vichi (2013), Multiple stressors of ocean
1477 ecosystems in the 21st century: projections with CMIP5 models, *Biogeosci.*, 10(10),
1478 6225–6245, doi:10.5194/bg-10-6225-2013.
- 1479 Boyd, P. W., S. T. Lennartz, D. M. Glover, and S. C. Doney (2014), Biological ramifi-
1480 cations of climate-change-mediated oceanic multi-stressors, *Nat. Clim. Change*, 5(1),
1481 71–79, doi:10.1038/nclimate2441.
- 1482 Brandt, P., V. Hormann, B. BourlèS, J. Fischer, F. A. Schott, L. Stramma, and M. Dengler
1483 (2008), Oxygen tongues and zonal currents in the equatorial Atlantic, *J. Geophys. Res.*,
1484 113, C04012, doi:10.1029/2007JC004435.
- 1485 Brandt, P., R. J. Greatbatch, M. Claus, S.-H. Didwischus, V. Hormann, A. Funk,
1486 J. Hahn, G. Krahmann, J. Fischer, and A. Körtzinger (2012), Ventilation of the equa-

- 1487 torial Atlantic by the equatorial deep jets, *J. Geophys. Res.*, 117(C16), C12015, doi:
1488 10.1029/2012JC008118.
- 1489 Brewer, P. G., and E. T. Peltzer (2009), Oceans: Limits to marine life, *Science*, 324(5925),
1490 347–348, doi:10.1126/science.1170756.
- 1491 Broecker, W. S. (1991), The great ocean conveyor, *Oceanography*, 4(2), 79–89, doi:
1492 10.5670/oceanog.1991.07.
- 1493 Buesseler, K. O., and P. W. Boyd (2009), Shedding light on processes that control particle
1494 export and flux attenuation in the twilight zone of the open ocean, *Limnol. Oceanogr.*,
1495 54(4), 1210–1232, doi:10.4319/lo.2009.54.4.1210.
- 1496 Burd, A. B., and G. A. Jackson (2009), Particle aggregation, *Ann. Rev. Mar. Sci.*, 1(1), 65–
1497 90, doi:10.1146/annurev.marine.010908.163904.
- 1498 Carr, M.-E. (2001), Estimation of potential productivity in eastern boundary currents using
1499 remote sensing, *Deep-Sea Res.*, 49(1-3), 59–80, doi:10.1016/s0967-0645(01)00094-7.
- 1500 Chan, F., J. A. Barth, J. Lubchenco, A. Kirincich, H. Weeks, W. T. Peterson, and B. A.
1501 Menge (2008), Emergence of anoxia in the California current large marine ecosystem,
1502 *Science*, 319(5865), 920–920, doi:10.1126/science.1149016.
- 1503 Cheng, L., K. E. Trenberth, M. D. Palmer, J. Zhu, and J. P. Abraham (2016), Observed
1504 and simulated full-depth ocean heat-content changes for 1970–2005, *Ocean Sci.*, 12(4),
1505 925–935, doi:10.5194/os-12-925-2016.
- 1506 Christian, J. R. (2014), Timing of the Departure of Ocean Biogeochemical Cycles from
1507 the Preindustrial State, *PLoS ONE*, 9(11), e109820, doi:10.1371/journal.pone.0109820.
- 1508 Cocco, V., F. Joos, M. Steinacher, T. L. Frölicher, L. Bopp, J. Dunne, M. Gehlen,
1509 C. Heinze, J. Orr, A. Oschlies, B. Schneider, J. Segschneider, and J. Tjiputra (2013),
1510 Oxygen and indicators of stress for marine life in multi-model global warming projec-
1511 tions, *Biogeosci.*, 10, 1849–1868, doi:10.5194/bg-10-1849-2013.
- 1512 Codispoti, L. A. (2010), Interesting times for marine N₂O, *Science*, 327(5971), 1339–
1513 1340, doi:10.1126/science.1184945.
- 1514 Collins, M., R. Knutti, J. Arblaster, J.-L. Dufresne, T. Fichefet, P. Friedlingstein,
1515 X. Gao, W. Gutowski, T. Johns, G. Krinner, M. Shongwe, C. Tebaldi, A. Weaver, and
1516 M. Wehner (2013), Long-term climate change: Projections, commitments and irre-
1517 versibility, in *Climate Change 2013: The Physical Science Basis. Contribution of Work-
1518 ing Group I to the Fifth Assessment Report of the Intergovernmental Panel on Climate
1519 Change*, edited by T. Stocker, D. Qin, G.-K. Plattner, M. Tignor, S. Allen, J. Boschung,

- 1520 A. Nauels, Y. Xia, V. Bex, and P. Midgley, Cambridge University Press, Cambridge,
1521 United Kingdom and New York, NY, USA.
- 1522 Collins, W. J., N. Bellouin, M. Doutriaux-Boucher, N. Gedney, P. Halloran, T. Hinton,
1523 J. Hughes, C. D. Jones, M. Joshi, S. Liddicoat, G. Martin, F. O’Connor, J. Rae, C. Se-
1524 nior, S. Sitch, I. Totterdell, A. Wiltshire, and S. Woodward (2011), Development and
1525 evaluation of an Earth-System model – HadGEM2, *Geosci. Model Dev.*, 4(4), 1051–
1526 1075, doi:10.5194/gmd-4-1051-2011.
- 1527 Connolly, T. P., B. M. Hickey, S. L. Geier, and W. P. Cochlan (2010), Processes influ-
1528 encing seasonal hypoxia in the northern California current system, *J. Geophys. Res.*,
1529 115(C3), doi:10.1029/2009JC005283, c03021.
- 1530 Cravatte, S., W. S. Kessler, and F. Marin (2012), Intermediate zonal jets in the tropi-
1531 cal Pacific ocean observed by Argo floats, *J. Phys. Oceanogr.*, 42(9), 1475–1485, doi:
1532 10.1175/JPO-D-11-0206.1.
- 1533 Denman, K., G. Brasseur, A. Chidthaisong, P. . Ciais, P. M. Cox, R. Dickinson,
1534 D. Hauglustaine, C. Heinze, E. Holland, D. Jacob, U. Lohmann, S. Ramachandran, P. L.
1535 da Silva Dias, S. Wofsy, and X. Zhang (2007), Couplings between changes in the cli-
1536 mate system and biogeochemistry, in *Climate Change 2007: The Physical Science Ba-
1537 sis. Contribution of Working Group I to the Fourth Assessment Report of the Intergovern-
1538 mental Panel on Climate Change*, edited by S. Solomon, D. Qin, M. Manning, Z. Chen,
1539 M. Marquis, K. Averyt, M. Tignor, and H. Miller, Cambridge University Press, Cam-
1540 bridge, United Kingdom and New York, NY , USA.
- 1541 Deser, C., A. Phillips, V. Bourdette, and H. Teng (2012), Uncertainty in climate change
1542 projections: the role of internal variability, *Clim. Dyn.*, 38(3-4), 527–546, doi:
1543 10.1007/s00382-010-0977-x.
- 1544 Deutsch, C., S. Emerson, and L. Thompson (2006), Physical-biological interac-
1545 tions in North Pacific oxygen variability, *J. Geophys. Res.*, 111, C09S90, doi:
1546 10.1029/2005JC003179.
- 1547 Deutsch, C., H. Brix, T. Ito, H. Frenzel, and L. Thompson (2011), Climate-Forced Vari-
1548 ability of Ocean Hypoxia, *Science*, 333, 336–339, doi:10.1126/science.1202422.
- 1549 Deutsch, C., W. Berelson, R. Thunell, T. Weber, C. Tems, J. McManus, J. Crusius,
1550 T. Ito, T. Baumgartner, V. Ferreira, and et al. (2014), Centennial changes in North
1551 Pacific anoxia linked to tropical trade winds, *Science*, 345(6197), 665–668, doi:
1552 10.1126/science.1252332.

- 1553 Deutsch, C., A. Ferrel, B. Seibel, H.-O. Pörtner, and R. B. Huey (2015), Climate change
1554 tightens a metabolic constraint on marine habitats, *Science*, 348(6239), 1132–1135, doi:
1555 10.1126/science.aaa1605.
- 1556 Devries, T., and C. Deutsch (2014), Large-scale variations in the stoichiometry of marine
1557 organic matter respiration, *Nat. Geosci.*, 7, 890–894, doi:10.1038/ngeo2300.
- 1558 Diaz, R. J., and R. Rosenberg (2008), Spreading dead zones and consequences for marine
1559 ecosystems, *Science*, 321(5891), 926–929, doi:10.1126/science.1156401.
- 1560 Dietze, H., and U. Loeptien (2013), Revisiting “nutrient trapping” in global coupled bio-
1561 geochemical ocean circulation models, *Global Biogeochem. Cycles*, 27, 265–284, doi:
1562 10.1002/gbc.20029.
- 1563 Drijfhout, S., G. van Oldenborgh, and A. Cimatoribus (2012), Is a decline of AMOC
1564 causing the warming hole above the north atlantic in observed and modeled warming
1565 patterns?, *J. Clim.*, 25(24), 8373–8379, doi:10.1175/jcli-d-12-00490.1.
- 1566 Dufresne, J. L., M. A. Foujols, S. Denvil, A. Caubel, O. Marti, O. Aumont, Y. Balka-
1567 nski, S. Bekki, H. Bellenger, R. Benshila, S. Bony, L. Bopp, P. Braconnot, P. Brock-
1568 mann, P. Cadule, F. Cheruy, F. Codron, A. Cozic, D. Cugnet, N. de Noblet, J. P. Duvel,
1569 C. Ethé, L. Fairhead, T. Fichefet, S. Flavoni, P. Friedlingstein, J. Y. Grandpeix, L. Guez,
1570 E. Guilyardi, D. Hauglustaine, F. Hourdin, A. Idelkadi, J. Ghattas, S. Joussaume,
1571 M. Kageyama, G. Krinner, S. Labeyrie, A. Lahellec, M. P. Lefebvre, F. Lefevre,
1572 C. Levy, Z. X. Li, J. Lloyd, F. Lott, G. Madec, M. Mancip, M. Marchand, S. Mas-
1573 son, Y. Meurdesoif, J. Mignot, I. Musat, S. Parouty, J. Polcher, C. Rio, M. Schulz,
1574 D. Swingedouw, S. Szopa, C. Talandier, P. Terray, N. Viovy, and N. Vuichard (2013),
1575 Climate change projections using the IPSL-CM5 Earth System Model: from CMIP3 to
1576 CMIP5, *Clim. Dyn.*, 40(9-10), 2123–2165, doi:10.1007/s00382-012-1636-1.
- 1577 Dunne, J. P., J. G. John, A. J. Adcroft, S. M. Griffies, R. W. Hallberg, E. Shevliakova,
1578 R. J. Stouffer, W. Cooke, K. A. Dunne, M. J. Harrison, J. P. Krasting, S. L. Malyshev,
1579 P. C. D. Milly, P. J. Phillipps, L. T. Sentman, B. L. Samuels, M. J. Spelman, M. Win-
1580 ton, A. T. Wittenberg, and N. Zadeh (2012), GFDL’s ESM2 Global Coupled Climate-
1581 Carbon Earth System Models. Part I: Physical Formulation and Baseline Simulation
1582 Characteristics, *J. Clim.*, 25, 6646–6665, doi:10.1175/JCLI-D-11-00560.1.
- 1583 Dunne, J. P., J. G. John, E. Shevliakova, R. J. Stouffer, J. P. Krasting, S. L. Malyshev,
1584 P. C. D. Milly, L. T. Sentman, A. J. Adcroft, W. Cooke, K. A. Dunne, S. M. Griffies,
1585 R. W. Hallberg, M. J. Harrison, H. Levy, A. T. Wittenberg, P. J. Phillips, and N. Zadeh

- 1586 (2013), GFDL’s ESM2 Global Coupled Climate-Carbon Earth System Models. Part
1587 II: Carbon System Formulation and Baseline Simulation Characteristics, *J. Clim.*, 26,
1588 2247–2267, doi:10.1175/JCLI-D-12-00150.1.
- 1589 Duteil, O., F. U. Schwarzkopf, C. W. Böning, and A. Oschlies (2014), Major role of
1590 the equatorial current system in setting oxygen levels in the eastern tropical Atlantic
1591 Ocean: A high-resolution model study, *Geophys. Res. Lett.*, 41, 2033–2040, doi:
1592 10.1002/2013GL058888.
- 1593 Emerson, S., Y. Watanabe, T. Ono, and S. Mecking (2004), Temporal Trends in Appar-
1594 ent Oxygen Utilization in the Upper Pycnocline of the North Pacific: 1980–2000, *J.*
1595 *Oceanogr.*, 60(1), 139–147, doi:10.1023/B:JOCE.0000038323.62130.a0.
- 1596 Erwin, D. H. (1993), *The great Paleozoic crisis: life and death in the Permian*, Columbia
1597 University Press.
- 1598 Forster, P. ., V. . Ramaswamy, P. . Artaxo, T. Berntsen, R. Betts, D. Fahey, J. Haywood,
1599 J. Lean, D. Lowe, G. Myhre, J. Nganga, R. Prinn, G. Raga, M. Schulz, and R. V. Dor-
1600 land (2007), Changes in atmospheric constituents and in radiative forcing. chapter 2, in
1601 *Climate Change 2007: The Physical Science Basis. Contribution of Working Group I to*
1602 *the Fourth Assessment Report of the Intergovernmental Panel on Climate Change*, edited
1603 by S. Solomon, D. Qin, M. Manning, Z. Chen, M. Marquis, K. Averyt, M.Tignor, and
1604 H. Miller, Cambridge University Press, Cambridge, United Kingdom and New York,
1605 NY , USA.
- 1606 Freing, A., D. W. Wallace, and H. W. Bange (2012), Global oceanic production of nitrous
1607 oxide, *Phil. Trans. R. Soc.*, 367(1593), 1245–1255, doi:10.1098/rstb.2011.0360.
- 1608 Frölicher, T. L., J. L. Sarmiento, D. J. Paynter, J. P. Dunne, J. P. Krasting, and M. Winton
1609 (2015), Dominance of the Southern Ocean in anthropogenic carbon and heat uptake in
1610 CMIP5 models, *J. Clim.*, 28(2), 862–886, doi:10.1175/JCLI-D-14-00117.1.
- 1611 Garcia, H. E., and L. I. Gordon (1992), Oxygen solubility in seawater: Better fitting equa-
1612 tions, *Limnol. Oceanogr.*, 37, 1307–1312.
- 1613 Garcia, H. E., T. P. Boyer, S. Levitus, R. A. Locarnini, and J. Antonov (2005),
1614 On the variability of dissolved oxygen and apparent oxygen utilization content
1615 for the upper world ocean: 1955 to 1998, *Geophys. Res. Lett.*, 32, L09604, doi:
1616 10.1029/2004GL022286.
- 1617 Garcia, H. E., R. A. Locarnini, T. P. Boyer, J. I. Antonov, A. V. Mishonov, O. K. Bara-
1618 nova, M. M. Zweng, J. R. Reagan, and D. R. Johnson (2014), World Ocean Atlas 2013,

- 1619 Volume 3: Dissolved Oxygen, Apparent Oxygen Utilization, and Oxygen Saturation, in
1620 *NOAA Atlas NESDIS 75*, edited by S. Levitus and A. Mishonov, p. 27 pp.
- 1621 Gattuso, J.-P., A. Magnan, R. Bille, W. W. L. Cheung, E. L. Howes, F. Joos, D. Allemand,
1622 L. Bopp, S. R. Cooley, C. M. Eakin, and et al. (2015), Contrasting futures for ocean
1623 and society from different anthropogenic co₂ emissions scenarios, *Science*, 349(6243),
1624 doi:10.1126/science.aac4722.
- 1625 Gent, P., and J. McWilliams (1990), Isopycnal mixing in ocean circula-
1626 tion models, *J. Phys. Oceanogr.*, 20(1), 150–155, doi:10.1175/1520-
1627 0485(2003)033<2341:RSFTAC>2.0.CO;2.
- 1628 Getzlaff, J., and H. Dietze (2013), Effects of increased isopycnal diffusivity mimicking
1629 the unresolved equatorial intermediate current system in an earth system climate model,
1630 *Geophys. Res. Lett.*, 40, 2166–2170, doi:10.1002/grl.50419.
- 1631 Gillooly, J. F., J. H. Brown, G. B. West, V. M. Savage, and E. L. Charnov (2001), Ef-
1632 fects of size and temperature on metabolic rate, *Science*, 293(5538), 2248–2251, doi:
1633 10.1126/science.1061967.
- 1634 Giorgetta, M. A., J. Jungclaus, C. H. Reick, S. Legutke, J. Bader, M. Böttinger,
1635 V. Brovkin, T. Crueger, M. Esch, K. Fieg, K. Glushak, V. Gayler, H. Haak, H.-D.
1636 Hollweg, T. Ilyina, S. Kinne, L. Kornblueh, D. Matei, T. Mauritsen, U. Mikolajew-
1637 icz, W. Mueller, D. Notz, F. Pithan, T. Raddatz, S. Rast, R. Redler, E. Roeckner,
1638 H. Schmidt, R. Schnur, J. Segschneider, K. D. Six, M. Stockhouse, C. Timmreck,
1639 J. Wegner, H. Widmann, K.-H. Wieners, M. Claussen, J. Marotzke, and B. Stevens
1640 (2013), Climate and carbon cycle changes from 1850 to 2100 in MPI-ESM simulations
1641 for the Coupled Model Intercomparison Project phase 5, *J. Adv. Model. Earth Syst.*, 5(3),
1642 572–597, doi:10.1002/jame.20038.
- 1643 Gnanadesikan, A., J. Russell, and F. Zeng (2007), How does ocean ventilation change un-
1644 der global warming?, *Ocean Sci.*, 3(1), 43–53, doi:10.5194/os-3-43-2007.
- 1645 Grantham, B. A., F. Chan, K. J. Nielsen, D. S. Fox, J. A. Barth, A. Huyer, J. Lubchenco,
1646 and B. A. Menge (2004), Upwelling-driven nearshore hypoxia signals ecosystem and
1647 oceanographic changes in the northeast pacific, *Nature*, 429(6993), nature02605, doi:
1648 10.1038/nature02605.
- 1649 Gruber, N. (2004), The dynamics of the marine nitrogen cycle and its influence on atmo-
1650 spheric CO₂ variations, in *The Ocean Carbon Cycle and Climate, NATO Science Se-*
1651 *ries (Series IV: Earth and Environmental Sciences)*, vol. 40, edited by M. Follows and

- 1652 T. Oguz, pp. 97–148, Springer, Dordrecht, doi:10.1007/978-1-4020-2087-2_4.
- 1653 Gruber, N. (2011), Warming up, turning sour, losing breath: ocean biogeochemistry under
1654 global change, *Phil. Trans. R. Soc.*, 369(1943), 1980–1996, doi:10.1098/rsta.2011.0003.
- 1655 Gruber, N., and J. N. Galloway (2008), An Earth-system perspective of the global nitrogen
1656 cycle, *Nature*, 451(7176), 293–296, doi:10.1038/nature06592.
- 1657 Gruber, N., and J. L. Sarmiento (1997), Global patterns of marine nitrogen fixation and
1658 denitrification, *Global Biogeochem. Cycles*, 11(2), 235–266, doi:10.1029/97GB00077.
- 1659 HadGEM2 Development Team (2011), The HadGEM2 family of Met Office Unified
1660 Model climate configurations, *Geosci. Model Dev.*, 4(3), 723–757, doi:10.5194/gmd-
1661 4-723-2011.
- 1662 Hansen, J., M. Sato, and P. Kharecha (2011), Earth’s energy imbalance and implications,
1663 *Atmos. Chem. Phys.*, doi:10.5194/acp-11-13421-2011.
- 1664 Hasselmann, K. (1976), Stochastic climate models part I. Theory, *Tellus*, 28(6), 473–485,
1665 doi:10.1111/j.2153-3490.1976.tb00696.x.
- 1666 Hasselmann, K. (1993), Optimal Fingerprints for the Detection of Time-
1667 dependent Climate Change, *J. Clim.*, 6(10), 1957–1971, doi:10.1175/1520-
1668 0442(1993)006<1957:OFFTDO>2.0.CO;2.
- 1669 Hawkins, E., and R. Sutton (2009), The potential to narrow uncertainty in regional climate
1670 predictions, *Bull. Am. Meteorol. Soc.*, 90(8), 1095–1107, doi:10.1175/2009BAMS2607.1.
- 1671 Held, I., M. Winton, K. Takahashi, and T. Delworth (2010), Probing the fast and slow
1672 components of global warming by returning abruptly to preindustrial forcing, *J. Clim.*,
1673 doi:10.1175/2009JCLI3466.1.
- 1674 Helm, K. P., N. L. Bindoff, and J. A. Church (2011), Observed decreases in oxygen con-
1675 tent of the global ocean, *Geophys. Res. Lett.*, 38, L23602, doi:10.1029/2011GL049513.
- 1676 Henson, S. A., C. Beaulieu, T. Ilyina, J. G. John, M. Long, R. Séférian, J. Tjiputra, and
1677 J. L. Sarmiento (2017), Rapid emergence of climate change in environmental drivers of
1678 marine ecosystems, *Nat. Commun.*, 8, 14,682, doi:10.1038/ncomms14682.
- 1679 Hoegh-Guldberg, O., and J. F. Bruno (2010), The impact of climate change on the world’s
1680 marine ecosystems, *Science*, 328(5985), 1523–1528, doi:10.1126/science.1189930.
- 1681 Hurrell, J. W., M. M. Holland, P. R. Gent, S. Ghan, J. E. Kay, P. J. Kushner, J. F. Lamar-
1682 que, W. G. Large, D. Lawrence, K. Lindsay, W. H. Lipscomb, M. C. Long, N. Ma-
1683 howald, D. R. Marsh, R. B. Neale, P. Rasch, S. Vavrus, M. Vertenstein, D. Bader,
1684 W. D. Collins, J. J. Hack, J. Kiehl, and S. Marshall (2013), The Community Earth Sys-

- tem Model: A Framework for Collaborative Research, *Bull. Am. Meteorol. Soc.*, doi:
10.1175/BAMS-D-12-00121.1.
- Ito, T., and C. Deutsch (2010), A conceptual model for the temporal spectrum of oceanic
oxygen variability, *Geophys. Res. Lett.*, 37, L03601, doi:10.1029/2009GL041595.
- Ito, T., M. Follows, and E. Boyle (2004), Is AOU a good measure of respiration in the
oceans?, *Geophys. Res. Lett.*, 31(17), doi:10.1029/2004GL020900.
- Ito, T., A. Nenes, M. S. Johnson, N. Meskhidze, and C. Deutsch (2016), Acceleration of
oxygen decline in the tropical Pacific over the past decades by aerosol pollutants, *Nat.
Geosci.*, 9(6), 443–447, doi:10.1038/ngeo2717.
- Ito, T., S. Minobe, M. C. Long, and C. Deutsch (2017), Upper ocean o₂ trends: 1958–
2015, *Geophys. Res. Lett.*, 44(9), 4214–4223, doi:10.1002/2017gl073613.
- Johnson, G. C., and N. Gruber (2007), Decadal water mass variations along
20°W in the Northeastern Atlantic Ocean, *Prog. Oceanogr.*, 73, 277–295, doi:
10.1016/j.pocean.2006.03.022.
- Kay, J., C. Deser, A. Phillips, A. Mai, C. Hannay, G. Strand, J. Arblaster, S. Bates,
G. Danabasoglu, and J. Edwards (2015), The community earth system model (CESM)
large ensemble project: A community resource for studying climate change in the pres-
ence of internal climate variability, *Bull. Am. Meteorol. Soc.*, 96(8), 1333–1349, doi:
10.1175/BAMS-D-13-00255.1.
- Keeling, R., A. Körtzinger, and N. Gruber (2010), Ocean deoxygenation in a warming
world, *Ann. Rev. Mar. Sci.*, 2(1), 199–229, doi:10.1146/annurev.marine.010908.163855.
- Key, R. M., A. Kozyr, C. L. Sabine, K. Lee, R. Wanninkhof, J. L. Bullister, R. A. Feely,
F. J. Millero, C. Mordy, and T. H. Peng (2004), A global ocean carbon climatology:
Results from Global Data Analysis Project (GLODAP), *Global Biogeochem. Cycles*,
18(4), GB4031, doi:10.1029/2004GB002247.
- Klaas, C., and D. Archer (2002), Association of sinking organic matter with various types
of mineral ballast in the deep sea: Implications for the rain ratio, *Global Biogeochem.
Cycles*, 16(4), 1116.
- Koslow, J., R. Goericke, A. Lara-Lopez, and W. Watson (2011), Impact of declining
intermediate-water oxygen on deepwater fishes in the California current, *Mar. Ecol.
Progr. Ser.*, 436, 207–218, doi:10.3354/meps09270.
- Krumhardt, K. M., N. S. Lovenduski, M. C. Long, and K. Lindsay (2016), Avoidable im-
pacts of ocean warming on marine primary production: Insights from the CESM en-

- 1718 sembles, *Global Biogeochem. Cycles*, 30, doi:10.1002/2016GB005528.
- 1719 Kwon, E. Y., C. Deutsch, S.-P. Xie, S. Schmidtko, and Y.-K. Cho (2016), The North
1720 Pacific Oxygen Uptake Rates over the Past Half Century, *J. Clim.*, 29(1), 61–76, doi:
1721 10.1175/jcli-d-14-00157.1.
- 1722 Laufkötter, C., M. Vogt, N. Gruber, M. Aita-Noguchi, O. Aumont, L. Bopp, E. Buitenhuis,
1723 S. C. Doney, J. Dunne, T. Hashioka, and et al. (2015), Drivers and uncertainties of fu-
1724 ture global marine primary production in marine ecosystem models, *Biogeosci.*, 12(23),
1725 6955–6984, doi:10.5194/bg-12-6955-2015.
- 1726 Levitus, S., J. Antonov, and T. Boyer (2012), World ocean heat content and ther-
1727 mosteric sea level change (0–2000 m), 1955–2010, *Geophys. Res. Lett.*, doi:
1728 10.1029/2012GL051106.
- 1729 Li, C., J. von Storch, and J. Marotzke (2013), Deep-ocean heat uptake and equilibrium
1730 climate response, *Clim. Dyn.*, doi:10.1007/s00382-012-1350-z.
- 1731 Loeb, N., J. Lyman, G. Johnson, and R. Allan (2012), Observed changes in top-of-
1732 the-atmosphere radiation and upper-ocean heating consistent within uncertainty, *Nat.*
1733 *Geosci.*, 5, doi:10.1038/NGEO1375.
- 1734 Long, M., C. Deutsch, and T. Ito (2016), Finding forced trends in oceanic oxygen, *Global*
1735 *Biogeochem. Cycles*, 30(2), 381–397, doi:10.1002/2015GB005310.
- 1736 Löscher, C. R., A. Kock, M. Könneke, J. LaRoche, H. W. Bange, and R. A. Schmitz
1737 (2012), Production of oceanic nitrous oxide by ammonia-oxidizing archaea, *Biogeosci.*,
1738 9(7), 2419–2429, doi:10.5194/bg-9-2419-2012.
- 1739 Lovenduski, N. S., G. A. McKinley, A. R. Fay, K. Lindsay, and M. C. Long (2016), Par-
1740 titioning uncertainty in ocean carbon uptake projections: Internal variability, emis-
1741 sion scenario, and model structure, *Global Biogeochem. Cycles*, 30, 1276–1287, doi:
1742 10.1002/2016GB005426.
- 1743 Lyons, T. W., C. T. Reinhard, and N. J. Planavsky (2014), The rise of oxygen in earth’s
1744 early ocean and atmosphere, *Nature*, 506(7488), 307–315, doi:10.1038/nature13068.
- 1745 Manning, A., and R. F. Keeling (2006), Global oceanic and land biotic carbon sinks from
1746 the Scripps atmospheric oxygen flask sampling network, *Tellus B*, 58(2), 95–116, doi:
1747 10.1111/j.1600-0889.2006.00175.x.
- 1748 Martinez-Rey, J., L. Bopp, M. Gehlen, A. Tagliabue, and N. Gruber (2015), Projections
1749 of oceanic N₂O emissions in the 21st century using the IPSL earth system model, *Bio-*
1750 *geosci.*, 12(13), 4133–4148, doi:10.5194/bg-12-4133-2015.

- 1751 Matear, R. J., and A. C. Hirst (2003), Long-term changes in dissolved oxygen concentra-
1752 tions in the ocean caused by protracted global warming, *Global Biogeochem. Cycles*,
1753 17(4), n/a–n/a, doi:10.1029/2002gb001997.
- 1754 McClatchie, S., R. Goericke, R. Cosgrove, G. Auad, and R. Vetter (2010), Oxygen in the
1755 southern California bight: Multidecadal trends and implications for demersal fisheries,
1756 *Geophys. Res. Lett.*, 37(19), n/a–n/a, doi:10.1029/2010GL044497, 119602.
- 1757 McKinley, G. A., D. J. Pilcher, A. R. Fay, K. Lindsay, M. C. Long, and N. Lovenduski
1758 (2016), Timescales for detection of trends in the ocean carbon sink, *Nature*, 530, 469–
1759 472, doi:10.1038/nature16958.
- 1760 Mecking, S., C. Langdon, R. A. Feely, C. L. Sabine, C. A. Deutsch, and D.-H. Min
1761 (2008), Climate variability in the North Pacific thermocline diagnosed from oxy-
1762 gen measurements: An update based on the U.S. CLIVAR/CO₂ Repeat Hydrography
1763 cruises, *Global Biogeochem. Cycles*, 22, GB3015, doi:10.1029/2007GB003101.
- 1764 Meinshausen, M., S. Smith, K. Calvin, J. Daniel, M. Kainuma, J.-F. Lamarque, K. Mat-
1765 sumoto, S. Montzka, S. Raper, K. Riahi, A. Thomson, G. Velders, and D. Vuuren
1766 (2011), The RCP greenhouse gas concentrations and their extensions from 1765 to
1767 2300, *Clim. Change*, 109, 213–241, doi:10.1007/s10584-011-0156-z.
- 1768 Najjar, R. G., and R. F. Keeling (2000), Mean annual cycle of the air–sea
1769 oxygen flux: A global view, *Global Biogeochem. Cycles*, 14(2), 573–584, doi:
1770 10.1029/1999GB900086.
- 1771 Nakamura, T., T. Toyoda, Y. Ishikawa, and T. Awaji (2006), Effects of tidal mixing at
1772 the Kuril Straits on North Pacific ventilation: Adjustment of the intermediate layer
1773 revealed from numerical experiments, *J. Geophys. Res.*, 111(C10), C04003, doi:
1774 10.1029/2005JC003142.
- 1775 Nevison, C., J. H. Butler, and J. W. Elkins (2003), Global distribution of n₂O and the
1776 $\delta^{15}\text{N}_{\text{NO}_x}$ yield in the subsurface ocean, *Global Biogeochem. Cycles*, 17(4), doi:
1777 10.1029/2003gb002068.
- 1778 Ono, T., T. Midorikawa, Y. W. Watanabe, K. Tadokoro, and T. Saino (2001), Temporal
1779 increases of phosphate and apparent oxygen utilization in the subsurface waters of west-
1780 ern subarctic Pacific from 1968 to 1998, *Geophys. Res. Lett.*, 28(17), 3285–3288, doi:
1781 10.1029/2001GL012948.
- 1782 Oschlies, A., O. Duteil, J. Getzlaff, W. Koeve, A. Landolfi, and S. Schmidtko (2017), Pat-
1783 terns of deoxygenation: sensitivity to natural and anthropogenic drivers, *Phil. Trans. R.*

- 1784 *Soc.*, 375(2102), doi:10.1098/rsta.2016.0325.
- 1785 Passow, U. (2002), Transparent exopolymer particles (tep) in aquatic environments, *Prog.*
1786 *Oceanogr.*, 55(3-4), 287–333, doi:10.1016/s0079-6611(02)00138-6.
- 1787 Pauly, D., and V. Christensen (1995), Primary production required to sustain global fish-
1788 eries, *Nature*, 374(6519), 255–257, doi:10.1038/374255a0.
- 1789 Payne, J. L., and M. E. Clapham (2012), End-Permian mass extinction in the oceans: an
1790 ancient analog for the twenty-first century?, *Ann. Rev. Earth Planet. Sci.*, 40, 89–111,
1791 doi:10.1146/annurev-earth-042711-105329.
- 1792 Penn, J., T. Weber, and C. Deutsch (2016), Microbial functional diversity alters the struc-
1793 ture and sensitivity of oxygen deficient zones, *Geophys. Res. Lett.*, 43(18), 9773–9780,
1794 doi:10.1002/2016gl070438.
- 1795 Peterson, C., K. Nagy, and J. Diamond (1990), Sustained metabolic scope, *Proc. Natl.*
1796 *Acad. Sci. U.S.A.*, 87(6), 2324–2328, doi:10.1073/pnas.87.6.2324.
- 1797 Piiper, J., P. Dejours, P. Haab, and H. Rahn (1971), Concepts and basic quantities
1798 in gas exchange physiology, *Respir. Physiol.*, 13(3), 292–304, doi:10.1016/0034-
1799 5687(71)90034-X.
- 1800 Plattner, G., F. Joos, and T. Stocker (2002), Revision of the global carbon budget due to
1801 changing air–sea oxygen fluxes, *Global Biogeochem. Cycles*, 16(4), 43–1–43–12, doi:
1802 10.1029/2001GB001746.
- 1803 Portner, H.-O. (2010), Oxygen- and capacity-limitation of thermal tolerance: a matrix for
1804 integrating climate-related stressor effects in marine ecosystems, *J. Exp. Bio.*, 213(6),
1805 881–893, doi:10.1242/jeb.037523.
- 1806 Pörtner, H. O., and A. P. Farrell (2008), Ecology: Physiology and climate change, *Science*,
1807 322(5902), 690–692, doi:10.1126/science.1163156.
- 1808 Pozo Buil, M., and E. Di Lorenzo (2017), Decadal dynamics and predictability of oxygen
1809 and subsurface tracers in the California current system, *Geophys. Res. Lett.*, 44(9), 4204–
1810 4213, doi:10.1002/2017GL072931, 2017GL072931.
- 1811 Primeau, F. W., M. Holzer, and T. DeVries (2013), Southern Ocean nutrient trapping
1812 and the efficiency of the biological pump, *J. Geophys. Res.*, 118(5), 2547–2564, doi:
1813 10.1002/jgrc.20181.
- 1814 Rabalais, N., R. Díaz, L. Levin, R. Turner, D. Gilbert, and J. Zhang (2010), Dynamics
1815 and distribution of natural and human-caused hypoxia, *Biogeosci.*, 7(2), 585–619, doi:
1816 10.5194/bg-7-585-2010.

- 1817 Rabalais, N. N., R. E. Turner, and W. J. Wiseman (2002), Gulf of mexico hy-
1818 poxia, a.k.a. “the dead zone”, *Ann. Rev. Ecol. System.*, 33(1), 235–263, doi:
1819 10.1146/annurev.ecolsys.33.010802.150513.
- 1820 Raup, D. M. (1979), Size of the permo-triassic bottleneck and its evolutionary implica-
1821 tions, *Science*, 206(4415), 217–218, doi:10.1126/science.206.4415.217.
- 1822 Rhein, M., S. Rintoul, S. Aoki, E. Campos, D. Chambers, R. Feely, S. Gulev, G. Johnson,
1823 S. Josey, M. C. Kostianoy, D. Roemmich, L. Talley, and F. Wang (2013), Observations:
1824 ocean, in *Climate Change 2013: The Physical Science Basis. Contribution of Work-
1825 ing Group I to the Fifth Assessment Report of the Intergovernmental Panel on Climate
1826 Change*, edited by T. Stocker, D. Qin, G. Plattner, M. Tignor, S. Allen, J. Boschung,
1827 A. Nauels, Y. Xia, V. Bex, and P. Midgley, Cambridge University Press, Cambridge,
1828 United Kingdom and New York, NY, USA.
- 1829 Rodgers, K., J. Lin, and T. Frölicher (2015), Emergence of multiple ocean ecosys-
1830 tem drivers in a large ensemble suite with an earth system model, *Biogeosci.*, doi:
1831 10.5194/bg-12-3301-2015.
- 1832 Santer, B. D., W. Brüggemann, U. Cubasch, K. Hasselmann, H. Höck, E. Maier-Reimer,
1833 and U. Mikolajewica (1994), Signal-to-noise analysis of time-dependent greenhouse
1834 warming experiments, *Clim. Dyn.*, 9, 267–285, doi:10.1007/BF00204743.
- 1835 Santer, B. D., C. Mears, C. Doutriaux, P. Caldwell, P. J. Gleckler, T. M. L. Wigley,
1836 S. Solomon, N. P. Gillett, D. Ivanova, T. R. Karl, J. R. Lanzante, G. A. Meehl, P. A.
1837 Stott, K. E. Taylor, P. W. Thorne, M. F. Wehner, and F. J. Wentz (2011), Separating
1838 signal and noise in atmospheric temperature changes: The importance of timescale, *J.
1839 Geophys. Res.*, 116(D15), D22105, doi:10.1029/2011JD016263.
- 1840 Santoro, A. E., C. Buchwald, M. R. McIlvin, and K. L. Casciotti (2011), Isotopic signa-
1841 ture of n₂O produced by marine ammonia-oxidizing archaea, *Science*, 333(6047), 1282–
1842 1285, doi:10.1126/science.1208239.
- 1843 Sasano, D., Y. Takatani, N. Kosugi, T. Nakano, T. Midorikawa, and M. Ishii (2015), Mul-
1844 tidecadal trends of oxygen and their controlling factors in the western North Pacific,
1845 *Global Biogeochem. Cycles*, 29, 935–956, doi:10.1002/2014GB005065.
- 1846 Schmidtko, S., L. Stramma, and M. Visbeck (2017), Decline in global oceanic
1847 oxygen content during the past five decades, *Nature*, 542(7641), 335–339, doi:
1848 10.1038/nature21399.

- Screen, J. A., and I. Simmonds (2010), The central role of diminishing sea ice in recent Arctic temperature amplification, *Nature*, 464(7293), 1334–1337, doi: 10.1038/nature09051.
- Solomon, S., D. Qin, M. Manning, Z. Chen, M. Marquis, K. Averyt, M. Tignor, and H. Miller (Eds.) (2007), *Climate Change 2007: The Physical Science Basis. Contribution of Working Group I to the Fourth Assessment Report of the Intergovernmental Panel on Climate Change*, Cambridge University Press, Cambridge, U. K.
- Solomon, S., G.-K. Plattner, R. Knutti, and P. Friedlingstein (2009), Irreversible climate change due to carbon dioxide emissions, *Proc. Natl. Acad. Sci. U.S.A.*, 106(6), 1704–1709, doi:10.1073/pnas.0812721106.
- Song, H., P. B. Wignall, D. Chu, J. Tong, Y. Sun, H. Song, W. He, and L. Tian (2014), Anoxia/high temperature double whammy during the permian-triassic marine crisis and its aftermath, *Scientific Reports*, 4(1), doi:10.1038/srep04132.
- Stammer, D. (1997), Global characteristics of ocean variability estimated from regional TOPEX/POSEIDON altimeter measurements, *J. Phys. Oceanogr.*, 27(8), 1743–1769, doi:10.1175/1520-0485(1997)027<1743:GCOOVE>2.0.CO;2.
- Steinacher, M., F. Joos, T. Frölicher, L. Bopp, P. Cadule, V. Cocco, S. Doney, M. Gehlen, K. Lindsay, J. Moore, B. Schneider, and J. Segschneider (2010), Projected 21st century decrease in marine productivity: a multi-model analysis, *Biogeosci.*, 7(3), 979–1005, doi:10.5194/bg-7-979-2010.
- Stendardo, I., and N. Gruber (2012), Oxygen trends over five decades in the north atlantic, *J. Geophys. Res.*, 117(C11), doi:10.1029/2012JC007909.
- Stock, C., J. John, R. Rykaczewski, R. Asch, W. Cheung, J. Dunne, K. Friedland, V. Lam, J. Sarmiento, and R. Watson (2017), Reconciling fisheries catch and ocean productivity, *Proc. Natl. Acad. Sci. U.S.A.*, 114(8), E1441–E1449, doi:10.1073/pnas.1610238114.
- Stouffer, R. (2004), Time scales of climate response, *J. Clim.*, 17(1), 209–217, doi: 10.1175/1520-0442(2004)017<0209:TSOCR>2.0.CO;2.
- Stramma, L., G. Johnson, J. Sprintall, and V. Mohrholz (2008), Expanding oxygen-minimum zones in the tropical oceans, *Science*, doi:10.1126/science.1153847.
- Stramma, L., E. D. Prince, S. Schmidtko, J. Luo, J. P. Hoolihan, M. Visbeck, D. W. R. Wallace, P. Brandt, and A. Körtzinger (2011), Expansion of oxygen minimum zones may reduce available habitat for tropical pelagic fishes, *Nat. Clim. Change*, 2(1), 33–37, doi:10.1038/nclimate1304.

- 1882 Stramma, L., A. Oschlies, and S. Schmidtko (2012), Mismatch between observed and
1883 modeled trends in dissolved upper-ocean oxygen over the last 50 yr, *Biogeosci.*, 9(10),
1884 4045–4057, doi:10.5194/bg-9-4045-2012.
- 1885 Tagklis, F., A. Bracco, and T. Ito (2017), Physically driven patchy O₂ changes in the north
1886 atlantic ocean simulated by the CMIP5 earth system models, *Global Biogeochem. Cy-*
1887 *cles*, 31(8), 1218–1235, doi:10.1002/2016GB005617, 2016GB005617.
- 1888 Talley, L., R. Feely, B. Sloyan, R. Wanninkhof, M. Baringer, J. Bullister, C. Carlson,
1889 S. Doney, R. Fine, E. Firing, N. Gruber, D. Hansell, M. Ishii, G. Johnson, K. Kat-
1890 sumata, R. Key, M. Kramp, C. Langdon, A. Macdonald, J. Mathis, M. E.L., S. Meck-
1891 ing, F. Millero, C. Mordy, T. Nakano, C. Sabine, W. Smethie, J. Swift, T. Tanhua,
1892 A. Thurnherr, M. Warner, and J. Zhang (2015), Changes in ocean heat, carbon content,
1893 and ventilation: A review of the first decade of GO-SHIP global repeat hydrography,
1894 *Ann. Rev. Mar. Sci.*, 8(1), 1–31, doi:10.1146/annurev-marine-052915-100829.
- 1895 Taylor, K. E., R. J. Stouffer, and G. A. Meehl (2012), An Overview of CMIP5 and the
1896 Experiment Design, *Bull. Am. Meteorol. Soc.*, 93, 485–498, doi:10.1175/BAMS-D-11-
1897 00094.1.
- 1898 Trenberth, K., J. Fasullo, and M. Balmaseda (2014), Earth’s energy imbalance, *J. Clim.*,
1899 doi:10.1175/JCLI-D-13-00294.1.
- 1900 van Aken, H. M., M. Femke de Jong, and I. Yashayaev (2011), Decadal and multi-decadal
1901 variability of Labrador Sea Water in the north-western North Atlantic Ocean derived
1902 from tracer distributions: Heat budget, ventilation, and advection, *Deep-Sea Res.*, 58,
1903 505–523, doi:10.1016/j.dsr.2011.02.008.
- 1904 Vaquer-Sunyer, R., and C. Duarte (2008), Thresholds of hypoxia for marine biodiversity,
1905 *Proc. Natl. Acad. Sci. U.S.A.*, 105(40), doi:10.1073/pnas.0803833105.
- 1906 Vitousek, P. M., H. A. Mooney, J. Lubchenco, and J. M. Melillo (1997), Hu-
1907 man domination of Earth’s ecosystems, *Science*, 277(5325), 494–499, doi:
1908 10.1126/science.277.5325.494.
- 1909 Volk, T., and M. I. Hoffert (1985), Ocean carbon pumps - Analysis of relative strengths
1910 and efficiencies in ocean-driven atmospheric CO₂ changes, in *The Carbon Cycle and*
1911 *Atmospheric CO₂: Natural Variations Archean to Present*, edited by E. T. Sundquist &
1912 W. S. Broecker, pp. 99–110.
- 1913 Wang, D., T. C. Gouhier, B. A. Menge, and A. R. Ganguly (2015), Intensification and
1914 spatial homogenization of coastal upwelling under climate change, *Nature*, 518(7539),

- 1915 390–394, doi:10.1038/nature14235.
- 1916 Watson, A. J., T. M. Lenton, and B. J. Mills (2017), Ocean deoxygenation, the global
1917 phosphorus cycle and the possibility of human-caused large-scale ocean anoxia, *Phil.
1918 Trans. R. Soc.*, 375(2102), 20160,318, doi:10.1098/rsta.2016.0318.
- 1919 Weber, T., J. A. Cram, S. W. Leung, T. DeVries, and C. Deutsch (2016), Deep ocean nu-
1920 trients imply large latitudinal variation in particle transfer efficiency, *Proc. Natl. Acad.
1921 Sci. U.S.A.*, 113(31), 8606–8611, doi:10.1073/pnas.1604414113.
- 1922 Whitney, F. A., H. J. Freeland, and M. Robert (2007), Persistently declining oxygen levels
1923 in the interior waters of the eastern subarctic Pacific, *Prog. Oceanogr.*, 75, 179–199,
1924 doi:10.1016/j.pocean.2007.08.007.
- 1925 Wilson, S., and D. Steinberg (2010), Autotrophic picoplankton in mesozooplankton guts:
1926 evidence of aggregate feeding in the mesopelagic zone and export of small phytoplank-
1927 ton, *Mar. Ecol. Progr. Ser.*, 412, 11–27, doi:10.3354/meps08648.
- 1928 WMO (2011), *Scientific assessment of ozone depletion: 2010*, Global Ozone Research
1929 and Monitoring Project-Report No. 51, World Meteorological Organization, Geneva,
1930 Switzerland.
- 1931 Wuebbles, D. J. (2009), Nitrous oxide: No laughing matter, *Science*, 326(5949), 56–57,
1932 doi:10.1126/science.1179571.
- 1933 Xu, L., S.-P. Xie, and Q. Liu (2012), Mode water ventilation and subtropical countercur-
1934 rent over the North Pacific in CMIP5 simulations and future projections, *J. Geophys.
1935 Res.*, 117(C16), C12009, doi:10.1029/2012JC008377.
- 1936 Xu, L., S.-P. Xie, and Q. Liu (2013), Fast and slow responses of the North Pacific mode
1937 water and Subtropical Countercurrent to global warming, *J. Ocean Univ. China*, 12,
1938 216–221, doi:10.1007/s11802-013-2189-6.
- 1939 Yang, S., N. Gruber, M. C. Long, and M. Vogt (2016), ENSO driven variability of den-
1940 itrification and suboxia in the Eastern Pacific Ocean, *Global Biogeochem. Cycles*,
1941 GBC20591, doi:10.1002/2016GB005596.
- 1942 Zamora, L., A. Oschlies, H. Bange, K. Huebert, J. Craig, A. Kock, and C. Löscher (2012),
1943 Nitrous oxide dynamics in low oxygen regions of the Pacific: insights from the ME-
1944 MENTO database, *Biogeosci.*, 9(12), 5007–5022, doi:10.5194/bg-9-5007-2012.